Dissertation zur Erlangung des Doktorgrades
der Fakultät für Chemie und Pharmazie
der Ludwig-Maximilians-Universität München

Functional characterization of rabies virus in mouse embryonic stem cell-derived neurons

Maximilian Ferdinand Eizinger
aus
München, Deutschland
2018

Erklärung

Diese Dissertation wurde im Sinne von § 7 der Promotionsordnung vom 28. November 2011 von Herrn Prof. Dr. Karl-Klaus Conzelmann betreut und von Herrn Prof. Dr. Klaus Förstemann von der Fakultät für Chemie und Pharmazie vertreten.

Eidesstattliche Versicherung

Diese Dissertation wurde eigenständig und ohne unerlaubte Hilfe erarbeitet.

München, den 28.05.2018

Max Eizinger
(Unterschrift des Autors)

Dissertation eingereicht am:	26.02.2018
1. Gutachter:	Prof. Dr. Klaus Förstemann
2. Gutachter:	Prof. Dr. Karl-Klaus Conzelmann
Tag der mündlichen Prüfung:	02.05.2018

“Science is the process that brings us from confusion to understanding…”

Brian Greene

This thesis has been prepared in the laboratory of Prof. Dr. Karl-Klaus Conzelmann at the Max von Pettenkofer-Institute and Gene Center of the Ludwig-Maximilians-University Munich

Danksagung

Ich möchte mich sehr herzlich bei allen bedanken, die mich während dieser sehr interessanten, anspruchsvollen und schöne Zeit begleitet und unterstützt haben.

An aller erste Stelle möchte ich mich bei **Prof. Dr. Karl-Klaus Conzelmann** bedanken, der mir das Vertrauen gab in seiner Arbeitsgruppe meine Doktorarbeit anzufertigen. Ich möchte mich dafür bedanken, dass ich an diesem höchst interessanten und herausvordernden Themen arbeiten durfte. Indem er mir die Freiheiten gab meinen eingenen Ideen nachzugehen und seine Türe für Fragen und Diskussion immer offen stand, kreierte Prof. Dr. Karl-Klaus Conzelmann hervorragende fachliche sowie menschliche Rahmenbedingungen. Des Weiteren möchte ich mich bei **Prof. Dr. Klaus Förstemann** bedanken, der sich freundlicherweise bereit erklärt hat diese Arbeit als Fachvertreter der Biochemie zu betreuen. Zudem möchte ich den Mitgliedern der Prüfungskomission **Prof. Dr. Christian Wahl-Schott**, **PD Dr. Dietmar Martin**, **PD Dr. Barbara Adler** und **Prof. Dr. Karl-Peter Hopfner** für Ihre Mühen bedanken.

Ein ganz besonderer Dank gilt meinen lieben Arbeitskollegen, die diese aussergewöhnlich gute Arbeitsatmosphere ermöglicht haben. Allen voran möchte ich mich bei **Alex** bedanken der mir bereits während der Bachelorarbeit die ersten Schritten in der Laborwelt beigebracht hat und sich während der Doktorarbeit für Fragen, Diskussionen und hilfreiche Tipps immer zeitgenommen hat. Merci beaucoup **Chloé** für das hervorragende Teamwork bei der Stammzellenkultur. Mein Dank gilt selbstverständlich auch **Blex**, **Verena** und **Johanna** für ihre Unterstützung im Laboralltag, wenn nötig die passenden aufmunternden Worte und die vielen lustigen Kaffeepausen. Vielen Dank auch an **Doro** die mich über all die Jahre immer wieder mit sehr feinen Kuchen versorgt hat. Auch den Alumnis möchte ich ganz herzlich danken. **Marco** für die vielen spannenden Diskussionen; **Daniel** für die vielen Stunden beim „soggen“; **Konstantin**, **Kerstin**, **Tobi**, **Nadin** und **Martina** für ihre große Hilfsbereitschaft am Anfang meiner Doktorarbeit.

Mit der größte Dank gilt meinen **Eltern** für ihre großartige Unterstützung und ihren Zuspruch. Selbsvertändlich möchte ich mich auch bei **Susi**, **Luki**, **Isabell** und **Jürgen** für ihre Unterstützung bedanken.

Mein größter Dank gilt **Judith** für ihre unendliche Geduld mit mir und meiner Arbeit.

Contents

1 Summary

While rabies virus (RABV) is the causative agent of the rabies disease that kills approximately 59,000 people per year, RABV is also a superb tool to reveal neural circuits due to its exclusive spread to presynaptically connected neurons. Since the mechanism behind the anterograde transport of RABV to dendrites and the exclusive retrograde transsynaptic spread of RABV in the CNS are still poorly understood, this thesis aimed to provide an insight into the molecular mechanism of the neuronal virus transmission, which would have a tremendous impact in terms of improving RABV as a neuronal tracer, understanding the RABV pathology and developing therapeutic strategies to fight RABV infection.

The first and overarching aim of this thesis was the introduction of a high quality, feeder-free mESC culture system, followed by the establishment of a highly reliable differentiation protocol of mESCs into a nearly homogenous neuronal cell population of glutamatergic pyramidal neurons, forming chemical synapses. Further, by generating a neuronal mix population, which contains a small portion of mESC-derived neurons that enable the primary infection of this neuron with an EnvA pseudotyped G-gene deficient RABV and the *in situ* trans-complementation of the G-gene deficient RABV, an *in vitro* model to investigate the mono- transsynaptic spread of RABV ΔG was established.

Using the mESC-derived neurons and reverse genetics to generate a recombinant RABV encoding for a mutated late domain within the matrix protein (M) it was shown that the ESCRT system is involved in the neuronal transfer of RABV. Further, this thesis provides some evidence that ^{34}PPPEYVPL^{41} represents rather an extended motif of the PPEY late domain, than overlapping late domains consisting of PPEY and YVPL. In a second approach, which included recombinant RABVs encoding for dominant-negative syntaxins and the transduction of mESC-derived neurons with lentiviral vectors encoding for neurotoxin light chains a participation of SNARE proteins in the transsynaptic spread of RABV was illustrated.

Since the retrograde axonal transport of RABV is G-dependent, an insertion site for external trafficking signals within G should be identified in order to change G trafficking and thereby the subcellular localization of G. While modifications of the ectodomain destroyed the functionality of G, the insertion of the kinesin light-chain binding sequence (KBS) downstream of the transmembrane domain resulted in infectious virus particles. Further, the recombinant SAD G-TM-3xKBS-RT virus was able to infect and spread in mESC-derived neurons. Remarkably, G-TM-3xKBS-

RT exhibited a homogeneous distribution, which differed clearly from granular, probably PSD-associated distribution of G wildtype. Thus, G-TM-3xKBS-RT might be the first step to generate an redirected anterograde transsynaptic tracer.

In order to evolve a less cytotoxic SAD virus for long-term studies of infected neurons, a persistent infection model for SAD in HEK293T cells, which usually succumb to viral infection, was generated. The following analysis of the virus pool produced by the surviving HEK293T cells by NGS revealed only six notable mutations that occur in different frequencies, reflecting the existence of a mixed virus population. Interestingly, two point mutations within the non-coding leader region were sufficient to turn SAD eGFP into a non-cytotoxic virus, not only in HEK293T cells but also in mESC-derived neurons.

In summary, this thesis provides an insight into the molecular mechanism behind the transsynaptic spread of RABV, creates first hints for generating an anterograde transsynaptic tracing model, and generates a less-cytotoxic RABV.

2 Introduction

2.1 Rabies virus

2.1.1 Rabies disease

Numerous writings which date back until the antique describe dogs and humans suffering from rabies disease, most likely due to its disturbing symptoms, its long period of suffering and its fatality after the onset of symptoms (Wilkinson, 1977). Already Hippocrates described supposedly human rabies as he wrote, “persons in a frenzy drink very little, are disturbed and frightened, tremble at the least noise, or are seized by convulsion” (Jackson, 2013). Aristotle wrote that the disease drives the dog mad, is fatal to the afflicted dog itself and any animal, which was bitten by the dog. Wrongly, Aristotle wrote that humans are not affected by the disease (Jackson, 2013; Wilkinson, 1977). Celsus already introduced the term hydrophobia as a symptom of rabies in humans and he identified that the causative agent of rabies is in the saliva of the biting animal (Jackson, 2013).

Nowadays it is well-known, that rabies is a viral zoonotic disease caused by RABV, which still kills approximately 59000 people per year according to the center of disease control and prevention (CDC.) With the exception of the Antarctica, rabies is distributed all over the world. Whereas all mammals are susceptible to RABV infection, Carnivora and Chiroptera represent the main reservoirs of the virus (reviewed in (Rupprecht et al., 2002)).

In most cases, humans are infected with RABV through an animal bite or scratch, which leads to the exposure of muscle cells with the RABV containing saliva (Davis et al., 2015). After the exposure to RABV, rabies exhibits a mean incubation period of one up to two months. However, extreme incubation periods of as short as seven days (after a dog bite into the brachial plexus) up to more than six years (after ABLV infection) are documented (Hemachudha et al., 2002). The incubation period depends probably on the virus load, virus type and the site of infection. Nevertheless, incubation times of up to six years are still puzzling.

The pre-exposure vaccination (an active immunization) or the post-exposure prophylaxis (PEP), which consists of wound cleansing, passive vaccination with human rabies immune globulin and active vaccination with cell culture rabies vaccine, protects efficiently against RABV (Manning et al., 2008). However, if RABV exposed humans are not vaccinated and the PEP is not carried out before the virus enters the central nervous system (CNS), which comes along with the onset of

symptoms, rabies proceeds to almost 100 % fatal (Koyuncu et al., 2013). Until now, only a single patient, which had neither a pre-exposure vaccination nor a PEP, survived a RABV infection after the onset of symptoms (Willoughby et al., 2005).

According to the progression of the acute neurological phase, rabies is grouped into classic rabies and non-classic rabies. The classic human rabies is subdivided into furious (encephalitic) rabies and paralytic (dumb) rabies (Hemachudha et al., 2002). Two-thirds of the classic human rabies cases are furious rabies cases, which lead to death within seven days after the onset of symptoms. The symptoms of the furious rabies start with hyperactivity, which is intensified by thirst, fear, light, noise and other stimuli (Hemachudha et al., 2002). The disease progresses with the onset of fluctuating consciousness, phobic or inspiratory spasm (hydrophobia, aerophobia), and autonomic dysfunction (hypersalivation, sweating) (Hemachudha et al., 2002). The victims die because of cardiac arrest, circulatory insufficiency, or respiratory failure (Davis et al., 2015). The paralytic rabies kills the patients within 14 days on average (Hemachudha et al., 2002). It causes an ascending paralysis, followed by coma and death (Davis et al., 2015).

The non-classic rabies occurs in patients, which were infected by bats or in patients, which were infected by a dog-bite in Thailand. The non-classic rabies has no characteristic features, however observed clinical features include neuropathic pain and radicular pain (reviewed in (Hemachudha et al., 2002)).

2.1.2 Taxonomy of RABV

The RABV genome is a single stranded, non-segmented, negative-sense ribonucleic acid (RNA) genome. RABV belongs to the order *Mononegavirales*, which is also designated as non-segmented negative strand RNA viruses (NNSV), and is a prototype of the *Rhabdoviridae* family. However, recently the family *Rhabdoviridae* was expanded by genera *Dichorhavirus* and *Varicosavirus*, which are bi-segmented plant viruses (Afonso et al., 2016; Shi et al., 2018).

The order *Mononegavirales* is subdivided into the families *Bornaviridae, Filoviridae, Mymonaviridae, Nyamiviridae, Paramyxoviridae*, *Pneumoviridae*, and *Rhabdoviridae* (International Committee on Taxonomy of Viruses (ICTV) 28.11.2017). Since RABV virions have a bullet-/rod-shaped structure (Figure 1C) it is grouped into the family *Rhabdoviridae*, deduced from the greek word *rhabdos*, meaning rod (Wunner and Conzelmann, 2013).

The family *Rhabdoviridae* is subdivided into 18 genera named *Almendravirus, Curiovirus, Cytorhabdovirus, Dichorhavirus, Ephemerovirus, Hapavirus, Ledantevirus, Lyssavirus, Novirhabdovirus, Nucleorhabdovirus, Perhabdovirus, Sigmavirus, Sprivivirus, Sripuvirus, Tibrovirus, Tupavirus, Varicosavirus and Vesiculovirus* (ICTV 28.11.2017). RABV is the prototype of

the genus *Lyssavirus.* This name has its origin in the greek mythology since *Lyssa* (meaning “rage”) was the goddess of madness (reviewed in (Wunner and Conzelmann, 2013)).

Dependent on the passaging history, RABV strains are subdivided into street strains (wildtype) and fixed strains. Street strains are isolated directly out of infected animals or humans, whereas fixed strains were generated by passaging the viruses repeatedly in cell culture or in animals (Davis et al., 2015).

In this thesis, all RABV constructs are based on the fixed Street Alabama Dufferin (SAD) L16 strain, which was the first negative-sensed RNA virus generated by reverse genetics. Indeed, SAD L16 virus emerges from the cDNA encoding for SAD B19 (Schnell et al., 1994). SAD virus was isolated from a rabid dog, passaged on mouse brain cells, and adapted on BHK-21 cells. The passaging of SAD, which was initially passaged on mouse brain cells, on a cloned BSR cell line resulted in SAD B19, which is used as a live vaccine virus (Vos et al., 1999). Another fixed RABV strain, which was used in this work is CVS-N2c. CVS-N2c was generated by passaging the mouse adapted fixed strain CVS-24 (challenged virus standard) on a mouse neuroblastoma cell line. CVS-N2c exhibits a higher neurotropism as well as a reduced cytotoxicity compared to SAD B19 (Morimoto et al., 1998; Reardon et al., 2016). Another strain used in this thesis, is the street strain THA, which was isolated from a human bitten by a rabid dog, and passaged only for a few times on a mouse neuroblastoma cell line (Thongcharoen et al., 1990).

2.1.3 Route of RABV infection

In most of the human rabies cases, people are exposed to RABV by a bite or scratch of a rabid animal (Davis et al., 2015). Thereby, RABV containing saliva gets in contact with the peripheral muscle tissue. RABV can bind to the muscular nicotinic acetylcholin receptor (nAChR), which is located at the postsynaptic membrane of a neuron muscular junction (NMJ), and enter the muscle cell via a receptor-mediated endocytosis (Kalamida et al., 2007; Lafon, 2005). The presence of the nAChR at the postsynaptic membrane of the NMJ indicates that not motor neurons, but muscle cells are the primarily infected cells. Presumably, the infection of muscle cells enables the amplification of RABV. The additional replication cycle might increase the probability for a successful infection of the motor neuron (Lafon, 2005). After virus transcription and replication, RABV is released into the synaptic cleft of a NMJ, binds to the p75 nerve growth factor receptor (p75NTR) or the neuronal cell adhesion molecule (NCAM) on the surface of the presynaptic motor neuron and internalizes via receptor-mediated endocytosis into the first order neuron (Ugolini, 2011). In the motor neuron, the entire enveloped virus travels within an endosomal vesicle along microtubules by a directed retrograde axonal transport to the cell body (Klingen et al., 2008). Remarkably, the p75NTR-dependent retrograde axonal transport of RABV loaded vesicles is faster

than the transport of a standard p75NTR-vesicle. Further, a p75NTR-knockdown in dorsal root ganglions suggested that the p75NTR-dependent RABV transport is faster and more directed than the p75NTR-independent axonal transport of RABV (Gluska et al., 2014).

The acidification of the endosomal lumen causes the glycoprotein-dependent fusion of the viral membrane with the endosomal membrane and results in the release of the ribonucleoprotein (RNP) complex into the cytoplasm of the host cell (Gaudin, 2000; Roche and Gaudin, 2004). After the release of the RNP into the cytoplasm, viral transcription and replication takes place within spherical cytoplasmic inclusion bodies named Negri bodies (Lahaye et al., 2009; Nikolic et al., 2017). Finally, new RABV particles assemble and spread to presynaptically connected neurons. The retrograde transport directs RABV directly to the CNS. After the invasion of the CNS, at late stage of disease, RABV spreads centrifugally from the CNS to extraneuronal organs like the heart or salivary glands (Jackson et al., 1999; Ugolini, 2011).

2.1.4 Virion structure and protein function

RABV virions have an average length of 180 nm, an average diameter of 75 nm and form a bullet-shaped structure (Figure 1C). The genome is a single-stranded, non-segmented, negative-sense RNA genome. It is 12 kb long and has an unmodified 3´-hydroxyl end and a 5´-triphosphate end (Wunner and Conzelmann, 2013). The genome encodes for five monocistronic genes in the following order: nucleoprotein (N), phosphoprotein (P), matrix protein (M), glycoprotein (G) and the RNA-dependent RNA polymerase, also named large protein (L). The 3´-end of the viral genome is flanked by a non-coding leader (Le) RNA region and the 5´-end is flanked by a non-coding trailer (Tr) RNA region.

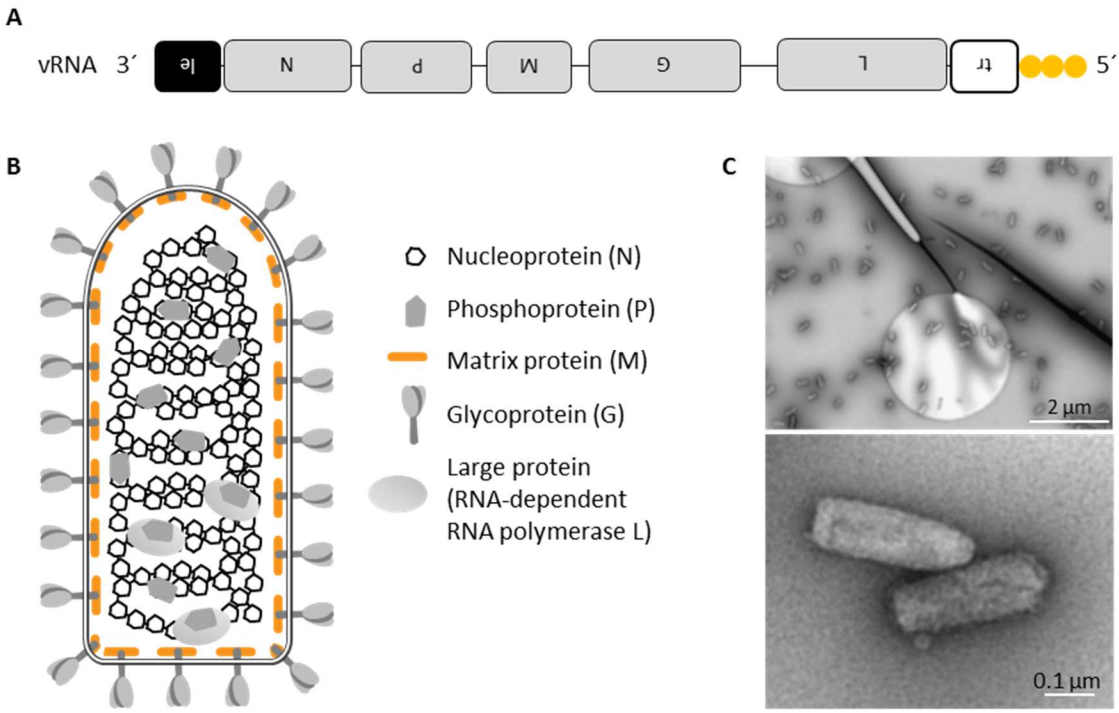

Figure 1: Organization of a Rabies virus particle.

A, Schematic representation of the 12 kb long, negative-sense RNA genome with its triphosphorylated 5´-end (adapted from (Ghanem and Conzelmann, 2016)). **B,** Schematic representation of the bullet-shaped RABV virion (adapted from dissertation of Marco Wachowius, 2016). **C,** SAD L16 virions were purified via sucrose cushion centrifugation and were subjected to uranyl acetate negative staining, followed by transmission electron microscopy. The pictures were taken together with Daniel Aberle in collaboration with Otto Beringhausen (LMU, Gene Center).

The RABV genome organization

The RABV genome order 3´-Le-N-P-M-G-L-Tr-5´ is conserved in the family *Rhabdoviridae* and in the order of *Mononegavirales* (reviewed in (Pfaller et al., 2015)). However, many rhabdoviruses and other virus families of the *Mononegavirales* can encode for accessory genes (Davis et al., 2015; Pfaller et al., 2015). Within the RABV genome, the five monocistronic genes are separated by conserved gene border signals, which encode for a transcription stop signal, a polyadenylation signal for the upstream gene, an intergenic sequence (IGS) and a transcription restart signal for the downstream gene (reviewed in (Wunner and Conzelmann, 2013)).

The nucleoprotein (RABV N)

The nucleoprotein is 450 amino acids long and has a molecular weight of about 57 kDa (Wunner and Conzelmann, 2013). RABV N enwraps the viral genome into a permanent, helical nucleocapsid and thereby shields the viral RNA from nucleases and the recognition by the immune system, e.g. the Toll-like receptors and RIG-I like receptors during the virus entry (Albertini et al., 2006). Additionally, exclusively the N-RNA complex serves as template for the viral transcription and

replication by the viral RNA-dependent-RNA polymerase, which is a complex of RABV L and its cofactor RABV P. Moreover, the amount of RABV N plays an important role in the transition from viral transcription to replication (reviewed in (Albertini et al., 2008)).

The phosphoprotein (RABV P)

The phosphoprotein is 297 amino acids in size, exhibits in SDS-PAGE a molecular weight of 37 kDa and fulfills multiple functions. First, RABV P is the noncatalytic cofactor of the RNA-dependent RNA Polymerase RABV L. Second, RABV P binds freshly synthesized RABV N (N^0), prevents RABV N polymerization and unspecific binding to cellular RNA. Thus, RABV P enables the interaction of N^0 with the freshly transcribed viral RNA (reviewed in (Wunner and Conzelmann, 2013)). Third, RABV P suppresses innate immune signaling in infected cells by interfering with the induction of interferon and by the inhibition of interferon signaling. The current model is that RABV P blocks on the one hand the phosphorylation of the transcription factor IRF-3 by TBK1 and IKKε, thereby inhibiting the transcription of type I interferon genes (Brzozka et al., 2005; Marschalek et al., 2009). On the other hand, RABV P blocks the interferon signaling by retaining the activated STATs in the cytoplasm. Thus, P inhibits the transcription of the antiviral interferon-stimulated genes (ISGs) (Brzozka et al., 2006).

The large protein (RABV L)

RABV L is 2127 amino acids long and exhibits a molecular weight of 244 kDa. Together with its noncatalytic cofactor P, RABV L forms the active RNA-dependent RNA polymerase, which is responsible for the viral transcription, the cotranscriptional modifications (5´-capping, methylation and 3´-polyadenylation of the mRNA) and the viral replication (reviewed in (Wunner and Conzelmann, 2013)).

The matrix protein (RABV M)

The matrix protein is 202 amino acids in size and has a molecular weight of 25 kDa. RABV M is a peripheral membrane protein, which is located under the lipid bilayer envelope and bridges G with the RNP complex. It is a multifunctional viral protein. Its tasks include the regulation of viral RNA synthesis, virus assembly, formation of the typical bullet-shape structure, virus budding and interaction with cellular proteins like Nedd4 (neuronal precursor cell-expressed developmentally gene 4) (Finke et al., 2003; Harty et al., 1999; Mebatsion et al., 1999). See below for a more detailed description of RABV M.

The glycoprotein (RABV G)

The mature RABV G is 505 amino acids long, highly glycosylated and has a molecular weight of 65 kDa in SDS-PAGE. RABV G is a type I transmembrane protein, which enables receptor binding and pH-dependent fusion of viral membrane with endosomal membrane. See below for a more detailed description of the functions of RABV G.

2.1.5 RABV transcription and replication

Negri bodies are spherical cytoplasmic inclusion bodies that resemble liquid organelles (Nikolic et al., 2017). They contain, next to cellular proteins, particularly the viral proteins N, P, L, all five viral messenger RNAs (mRNAs), genomic RNA and antigenomic RNA. The presence of these viral components indicate that Negri bodies represent the site of viral transcription and replication (Lahaye et al., 2009).

As mentioned above, the RNP complex represents the template for viral transcription and replication. The 3´-end leader region represents the genomic promoter for the transcription of monocistronic mRNAs and the replication of the antigenome/complementary RNA (cRNA). However, in the antigenome the 3´-end trailer region acts as the antigenomic promoter that directs exclusively the replication of the full-length vRNA (reviewed in (Wunner and Conzelmann, 2013)). The primary transcription starts by binding of the RNA-dependent RNA polymerase complex (L-P complex) to the genomic promoter, followed by the transcription of the 58 nucleotides (nts) long, non-coding, 5´-triphosphorylated, non-polyadenylated leader RNA. Subsequently, the monocistronic mRNAs of N, P, M, G and L are transcribed into 5´-end capped and 3´-end polyadenylated mRNAs (reviewed in (Wunner and Conzelmann, 2013)). The transcription of the genes downstream of N (P, M, G and L) depend on the reinitiation of the transcriptase after the IGS at the transcription restart signal. The decreasing probability for the transcriptional reinitiation results in a gradient of viral mRNA transcripts, according to the gene order in the genome. The steepness in mRNA levels in RABV is more striking than in other *Rhabdoviridae* (e.g. vesicular stomatitis virus), since the length of IGS increase in RABV from a dinucleotide in between N-P, to pentanucleotides between P-M and M-G, up to 19-28 nucleotides between G-L. This causes a steeper mRNA gradient compared to VSV, which has only two nucleotides long IGSs in each gene border (reviewed in (Wunner and Conzelmann, 2013)).

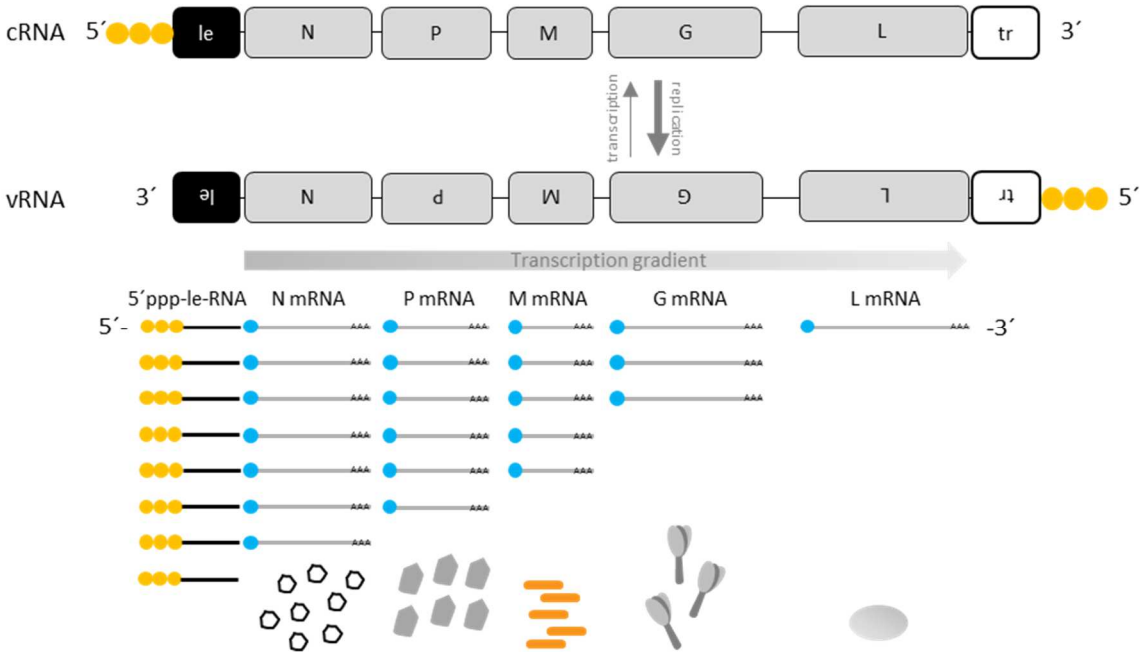

Figure 2: Rabies virus replication cycle.

The schematic representation of the RABV transcription and replication cycle was adapted from the dissertations of Alexander Ghanem (2012) and Marco Wachowius (2016). First, the non-segmented negative-sense genomic vRNA is transcribed. The transcription starts at the 3´-end of the vRNA and generates a non-coding, 5´-end triphosphorylated, non-polyadenylated leader RNA, followed by the transcription of five monocistronic 5´-end capped and 3´-end polyadenylated mRNAs. In between the viral genes are non-coding regions, which encode for a transcriptional stop signal, a polyadenylation signal, an IGS and a transcription restart signal. The decreasing chance of reinitiation of the L-P complex at the transcription restart signal, in combination with the increasing length of IGSs results in a transcriptional gradient. RABV N and RABV M concentrations regulate the transition from transcription to replication, which results in the antigenome (cRNA). The stronger antigenomic promoter in the trailer leads to a more efficient replication of the cRNA, leading to a vRNA/cRNA ratio of 49:1 that is indicated by the bold replication arrow.

The transition from transcription to replication, in which the cis-acting elements in the gene borders must be skipped, is still topic of ongoing research and the gained knowledge bases especially on the vesicular stomatitis virus (VSV). The nucleoprotein concentration seems to play an important role in the regulation of the transition from transcription to replication. The binding of nucleoproteins to the nascent leader RNA results in a skipping of the transcriptional stop and start signals and an N-encapsidation of the nascent cRNA (Blumberg et al., 1981). Furthermore, the existence of a tripartite replicase complex is discussed, consisting of N, P and L, which initiates the replication at the genome 3´-end (Banerjee, 2008; Curran and Kolakofsky, 2008; Whelan, 2008). Next to the nucleoprotein concentration, Finke and colleagues demonstrated that the increasing concentrations of matrix protein causes a downregulation of the transcription and promotes the viral replication (Finke et al., 2003).

In the cRNA, the antigenomic promoter is located within the trailer region. Interestingly, the antigenomic promoter exhibits a much stronger signal for replication than the genomic promoter of the vRNA. That leads to a ratio of genome to antigenome of 49:1 (Finke and Conzelmann, 1997). In turn, the vRNA is used for further transcription, replication, and virus assembly. In Figure 2, the RABV replication cycle is schematically illustrated.

2.1.6 The envelope proteins

The matrix protein and the glycoprotein form together with the host cell derived double membrane the envelope of RABV. Both proteins are multifunctional. In the following, the functions of M and G, especially concerning budding and transsynaptic spread, are explained in more detail.

2.1.6.1 The matrix protein

RABV M is 202 amino acids long and has a molecular weight of about 25 kDa. The matrix protein is located on the cytoplasmic site of the viral envelope (Mebatsion et al., 1999). For VSV M, the binding of the matrix protein to the lipid bilayer bases on electrostatic as well as hydrophobic interactions (Ye et al., 1994). In the case of RABV M, an additional palmitoylation anchor might contribute to the binding of M to the membrane (Gaudin et al., 1991).

Cryo-electron microscopy studies of VSV virions have shown that the matrix protein forms a helical mesh, in which a matrix protein is located within a groove of the helical nucleocapsid. Inside of that groove, the matrix protein interacts with nucleoproteins of the upper and lower helical turn and thereby stabilizes the RNP. Additional homotypic interactions between the matrix protein and its lateral neighbor as well as with the matrix protein of the upper helical turn have stabilizing effects for the condensed RNP complex (Ge et al., 2010). Furthermore, RABV M interacts with the cytoplasmic tail of the glycoprotein and thus links the glycoprotein with the RNP complex (Mebatsion et al., 1999).

As already mentioned above, RABV M regulates the transition of viral transcription to replication. Finke and colleagues showed that the transcription rate is enhanced in M gene-deletion mutants and that the transcription rate is regulated in an M dose-dependent manner (Finke et al., 2003). Furthermore, they identified aa R58 as a critical residue concerning the downregulation of viral transcription and activation of viral replication (Finke and Conzelmann, 2003). Remarkably, the ability of supporting virus assembly and budding is not impaired by a R58G mutation, indicating that the regulation of viral RNA synthesis and the support of virus assembly and budding are two independent functions of RABV M (Finke and Conzelmann, 2003).

Mebatsion and colleagues demonstrated that the deletion of the M gene (SAD ΔM) results in a 500.000-fold reduction of virus titers in the supernatant of infected BSR cells. In addition, the few released SAD ΔM virions do not exhibit the normal bullet-shape structure, but a long rod-shape structure, which could be compensated by the trans-complementation with M, pointing out the important role of the matrix protein in the condensation of the RNP complex (Mebatsion et al., 1999). Interestingly, the deletion of the glycoprotein (SAD ΔG) caused only a 30-fold reduction in virus titers and the virions exhibited the typical bullet-shape structure (Mebatsion et al., 1996). These findings emphasize the central role of RABV M in virus assembly and budding.

With PPxY and YxxL, two late domain (L-domain) motifs could be identified in the matrix protein, which overlap as followed: ^{35}PPEYVPL^{41} (Okumura and Harty, 2011). The PPxY motif interacts with the HECT E3 ubiquitin ligase Nedd4 and the YxxL motif usually mediates an interaction with the ESCRT-III associated adaptor protein ALIX (apoptosis-linked gene 2-interacting protein X) (Chen and Lamb, 2008). However, Wirblich et al. 2008 suggested that exclusively the PPxY motif plays a crucial role in the RABV release (Wirblich et al., 2008).

2.1.6.2 The glycoprotein

The RABV glycoprotein is translated as a 524 aa long precursor protein, which comprises a 19 aa long signal peptide (SP) that is cleaved off in the ER lumen. Further, the ectodomain is N-glycosylated depending on the RABV strain on one up to three sites, followed by oligomerization to a homotrimer in the Golgi apparatus. The final mature glycoprotein is a type I transmembrane protein, consisting of an N-terminal, highly glycosylated ectodomain (aa 1 -439), a hydrophobic 22 aa long transmembrane domain that anchors the trimeric spikes in the plasma membrane and after budding in the virion envelope, and a 44 aa long cytoplasmic domain (Conzelmann et al., 1990; Tordo et al., 1986; Whitt et al., 1991; Wunner and Conzelmann, 2013).

The correct folding and thereby the functionality and stability of the RABV G is dependent on the correct glycosylation. Especially the N-glycosylation of Asparagine 319, which is conserved among all Lyssaviruses is essential for correct folding and the transport to the plasma membrane (Wojczyk et al., 2005; Wunner and Conzelmann, 2013).

During the entry process, three different RABV G conformations have been identified. First, RABV G binds to one of its cell receptors in its native pre-fusion conformation (pH 7). After receptor-mediated endocytosis, the acidification in the early endosome leads to the transition of RABV G into the activated conformation, in which a hydrophobic part in the glycoprotein is able to interact with the host cell membrane. During the endosomal maturation, the endosome lumen gets more acidic causing the transition from the active conformation to the post-fusion conformation,

resulting in the G-mediated fusion of the virus membrane with the endosomal membrane. Remarkably, by incubation of the post-fusion state glycoprotein at a pH above 7, G can revert into the pre-fusion conformation of the glycoprotein. That is a unique feature of the rhabdoviral glycoproteins (reviewed (Albertini et al., 2012)).

Ectodomain of RABV G

As mentioned above, the N-glycosylated ectodomain is responsible for receptor binding, low pH-dependent fusion of the viral membrane with the endosomal membrane, the retrograde axonal transport and the transsynaptic spread of RABV (Etessami et al., 2000; Mazarakis et al., 2001; Wunner and Conzelmann, 2013)

Until now, the muscular nicotinic acetylcholine receptor (nAChR) (Lentz et al., 1983), the neural cell adhesion molecule (NCAM) (Thoulouze et al., 1998) and the p75 neurotrophin receptor (p75NTR) (Tuffereau et al., 1998) have been described as RABV receptors (Lafon 2005). However, the role of each single receptor in the RABV life cycle is still highly controversially discussed. The muscle-type nAChRs are located almost exclusively at the postsynaptic membrane of neuromuscular junctions (NMJ) (Kalamida et al., 2007; Lentz et al., 1983). However, in the brain the neuronal nAChRs are located in presynaptic, perisynaptic and postsynaptic areas (Kalamida et al., 2007). NCAM is concentrated in synaptic regions and at the NMJs (Lafon, 2005), where it is located at the presynaptic membrane as well as at postsynaptic membranes within junctional folds of NMJ (reviewed in (Lafon, 2005)). It plays a central role in the invasion of the nervous system through RABV. p75NTR is expressed in neuronal tissues, is located at the presynaptic membrane and is suggested to be involved in the trafficking of RABV (reviewed in (Lafon, 2005). Furthermore, highly sialylated gangliosides, phospholipids, glycolipids and glycoproteins might play a role in the attachment and entry of RABV in fibroblasts (Lafon, 2005; Superti et al., 1984; Superti et al., 1986; Wunner et al., 1984).

The ectodomain comprises two major so called “antigenic sites”, which are the main targets for virus neutralizing antibodies. Antigenic site II is a discontinuous epitope that is composed out of two clusters. The first cluster is located between aa 34-42 and the second cluster between aa 198-200 (Prehaud et al., 1988). Antigenic site III is a continuous epitope, which is located between aa 330 and aa 338 (Seif et al., 1985). Interestingly, substitution experiments have shown that R333 of the antigenic site III is responsible for the pathogenicity of RABV (Coulon et al., 1998; Seif et al., 1985). Another noteworthy prominent site in the RABV G is the nAChR binding site. The nAChR binding site was identified with help of an alignment with snake venom curaremimetic neurotoxins - a potent nAChR antagonist – and an antagonist assay of the binding of α-bungarotoxin (a snake venom neurotoxin) to nAChR. The 29-mer of RABV G (aa 175- 203) inhibits

competitively the binding of α-bungarotoxin to nAChR and therefore might represent the nAChR binding site of RABV G (Lentz, 1990; Lentz et al., 1983; Lentz et al., 1987; Lentz et al., 1984)

Transmembrane domain and C-tail of RABV G

The 22 aa long hydrophobic, single alpha-helical transmembrane (TM) domain contains a palmitoylation site at Cys 461 that most likely stabilizes the trimeric anchor. It is also discussed that the palmitic acid might support virus budding by enabling the interaction of the C-tail with the matrix protein (reviewed in (Wunner and Conzelmann, 2013)).

The C-terminal, cytoplasmic domain (C-tail) interacts with the M mesh and supports the virion assembly (Mebatsion et al., 1999). Nevertheless, Mebatsion et al. demonstrated that a recombinant virus lacking the glycoprotein C-tail was still able to spread (Mebatsion et al., 1996). However, the C-tail contains a specific signal that is crucial for efficient G-incorporation and therefore used for pseudotyping of RABV with chimeric glycoproteins e.g. HIV-1 Env with RABV C-tail (Mebatsion and Conzelmann, 1996).

2.1.7 Retrograde axonal transport, transsynaptic spread and monosynaptic tracing of RABV

The first hint for a microtubule dependent axonal transport of RABV was the observation that colchicine blocks the axonal transport of RABV (Ceccaldi et al., 1989). Interestingly, a direct interaction of RABV P and LC8 dynein light chain– a component of the dynein motor protein complex, which moves along microtubules to the minus end – was detected (Raux et al., 2000). However, closer examinations revealed that the deletion of the LC8 binding site in the phosphoprotein had no effect on retrograde axonal transport of the virus, rather on attenuation of primary transcription and replication in neurons (Mebatsion, 2001; Tan et al., 2007). Pseudotyping of lentiviral vectors with RABV G resulted in a retrograde axonal transport of the lentiviral vectors, demonstrating that RABV G is responsible and sufficient for the retrograde axonal transport (Mazarakis et al., 2001). Further analyses showed that the complete RABV particle is transported within an endosomal vesicle along microtubules in the retrograde direction, although this does not exclude the transport of single viral components along the axon (Klingen et al., 2008).

Next to the active axonal transport, the glycoprotein is essential for the transsynaptic spread of RABV, which occurs exclusively at chemical synapses and not at electrical synapses via gap junctions (Ugolini, 2011). However, the exact molecular mechanism of the transsynaptic spread of RABV is still puzzling.

The specific unidirectional retrograde transsynaptic spread of RABV via exclusively chemical synapses make RABV to an ideal tool for neuronal tracing.

The major problem of the usage of non-modified RABV as a transsynaptic tracer is its capability of unlimited transsynaptic spread (Ghanem and Conzelmann, 2016).

In 2007 Wickersham and colleagues established a system for mono-transsynaptic (also termed monosynaptic) tracing, which has become the gold standard for mapping direct synaptic connections. The system is based on an EnvA pseudotyped G gene-deficient RABV virus and a starter cell that expresses the EnvA receptor TVA (tumor virus A), the RABV glycoprotein and the red fluorescent protein (DsRed2) (Wickersham et al., 2007b). EnvA is the glycoprotein of the avian sarcoma leucosis virus (ASLV) that infects avian cells via its receptor TVA. Pseudotyping of SAD ΔG eGFP (EnvA) guarantees the specific targeting of the TVA-expressing mammalian neuronal starter cells, as TVA is naturally not expressed in mammals (Wickersham et al., 2007b). After the primary infection, the starter neuron expresses next to DsRed2 also the virus encoded eGFP, which enables an identification of the starter cell. The G gene-deficient virus is trans-complemented within the starter cell and infects presynaptically connected neurons of the starter cell. The monosynaptically connected neurons can be identified by the eGFP fluorescence and the absence of the DsRed2 fluorescence. Since the secondary infected neurons do not express the glycoprotein, which is essential for the transsynaptic spread of SAD ΔG eGFP, no further round of transsynaptic spread occurs, resulting in a retrograde monosynaptic tracing system (Wickersham et al., 2007b) (reviewed in (Ghanem and Conzelmann, 2016)).

2.2 Membrane scission and fusion machineries

2.2.1 The ESCRT machinery

The endosomal sorting complex required for transport (ESCRT) complex regulates budding events away from the cytoplasm. Its most prominent functions are in the biogenesis of multivesicular bodies (MVBs), the cell abscission during cytokinesis and the budding of enveloped viruses like HIV-1 (Hurley, 2015). The ESCRT machinery, which is responsible for the MVB biogenesis is composed of the peripheral membrane protein complexes ESCRT-0,-I, -II and –III, ALIX and the AAA+ ATPase vacuolar protein-sorting associated protein 4 (VPS4) (reviewed in (Hurley and Hanson, 2010)).

ESCRT-0 is responsible for the clustering of ubiquitinated cargos, ESCRT-I and ESCRT-II are responsible for budding (meaning vesicle is still attached to the membrane) and ESCRT-III is essential for membrane scission (reviewed in (Hurley and Hanson, 2010)).

During MVB biogenesis the heterotetramers ESCRT-0, ESCRT-I and ESCRT-II bind monoubiquitinated membrane proteins at the endosomal membrane. ESCRT-I and ESCRT-II form a bud neck, followed by recruitment of ESCRT-III. ESCRT-III in turn recruits deubiquitinases and catalyzes the scission of the vesicle (reviewed in (Hurley and Hanson, 2010; Schmidt and Teis, 2012)). Additionally, ESCRT-III recruits VPS4, which disassembles the ESCRT-III complex by ATP hydrolysis, releases ESCRT subunits into the cytoplasm, and thereby recovers the ESCRT machinery for further budding and scission events (Hurley and Hanson, 2010).

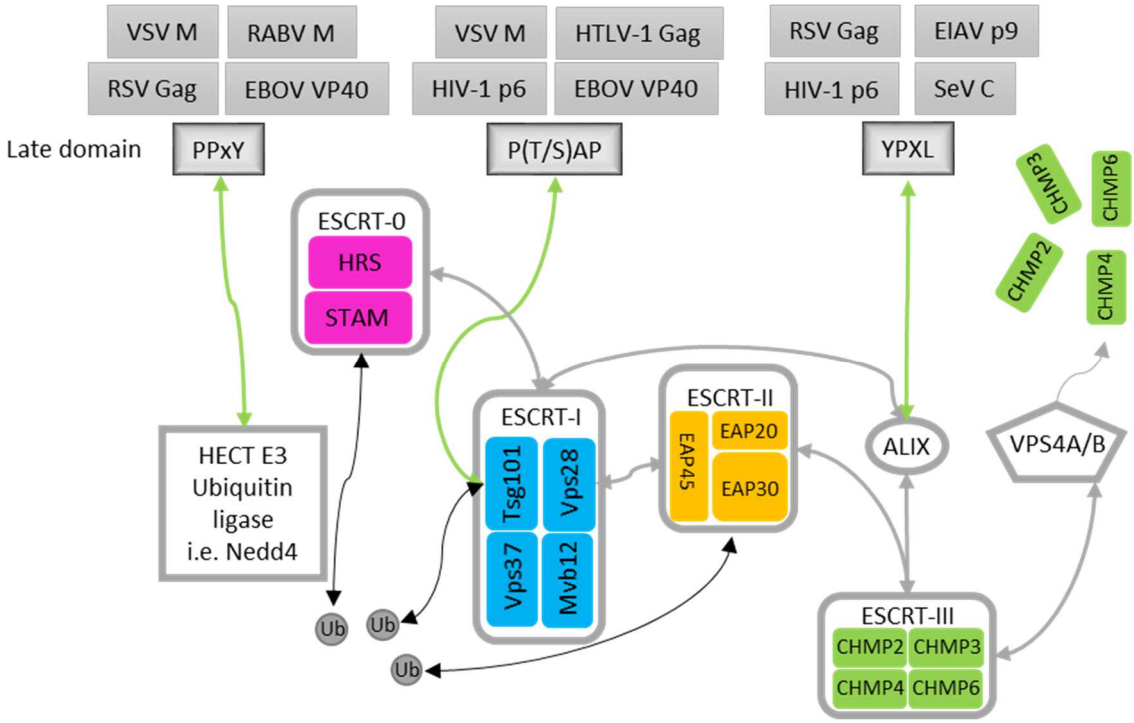

Figure 3: The ESCRT machinery

The illustration above was adapted form (Bieniasz, 2006; Chen and Lamb, 2008) and the dissertation of Anika Kern (2011). Schematic representation of the ESCRT components, which are involved in the MVB biogenesis and which are hijacked by the late domain of multiple enveloped viruses. Grey arrows indicate interactions of ESCRT components, green arrows indicate the interaction between the respective late domain and its ESCRT component, and black arrows indicate the interaction of ubiquitinated cargos and the ESCRT machinery. See text above for a detailed description of the illustration.

Interestingly, only for the MVB formation all five ESCRT complexes are necessary, while for the separation of two daughter cells or the egress of HIV ESCRT-I, ESCRT-III, VPS4 and ALIX are sufficient (Hurley and Hanson, 2010).

As already mentioned, many enveloped viruses use the ESCRT machinery for viral budding. It was shown that four peptide motifs (P(S/T)AP, YP(x)$_n$L, PPxY and FPIV) can mediate the interaction with specific components of the ESCRT machinery and thereby support the ESCRT-dependent virus budding (Figure 3). As these motifs play a role in the late stage of the virus life cycle, they are named late (L) domains (reviewed in (Chen and Lamb, 2008; Freed, 2002; Votteler and Sundquist, 2013)). Interestingly, some viruses like EBOV encode for overlapping late domains (PTAPPEY) (Chen and Lamb, 2008). It is also suggested that RABV with PPEYVPL encodes for an overlapping late domain, which is composed of PPxY that binds Nedd4 and YxxL that binds ALIX (Okumura and Harty, 2011). Another interesting feature of late domains is that some of them are exchangeable. Parent et al. demonstrated that the late domains of the retroviruses RSV and HIV are exchangeable (Parent et al., 1995).

The late domain PTAP of HIV-1 is located in the p6 region of the precursor polyprotein Gag (Gottlinger et al., 1991; Huang et al., 1995). It was shown that PTAP binds Tsg101 (a subunit of ESCRT-I), thereby recruits ESCRT-I, ESCRT-III and VPS4 to the site of viral budding at the plasma membrane, followed by the release of the HIV virions (Pornillos et al., 2003) (reviewed in (Chen and Lamb, 2008; Votteler and Sundquist, 2013). The tetrapeptide FPIV was identified in the matrix protein of the parainfluenza virus-5. It was demonstrated that FPIV can replace PTAP in HIV-1 (Schmitt et al., 2005). However, the cellular interaction partner of FPIV motif is unknown (Chen and Lamb, 2008). The $YP(x)_nL$ motif was identified by Puffer and colleagues in the Gag p9 region of the equine infectious anemia virus (EIAV), which is the only lentivirus that does not contain the P(S/T)AP motif (Puffer et al., 1997; Strack et al., 2003). $YP(x)_nL$ binds ALIX/AIP1, which in turn interacts with Tsg101 (ESCRT-I subunit) and CHMP4 (ESCRT-III subunit) and thereby enables the EIAV budding (Strack et al., 2003). The PPxY late domain was first described in the Gag p2 region of the rous sarcoma virus (RSV) (Xiang et al., 1996). PPxY interacts with the membrane-localized Nedd4, a HECT E3 ubiquitin ligase. Nedd4 ubiquitinates cargo proteins and thereby directs them to the MVB sorting pathway (Sette et al., 2010). The binding of Nedd4 to the viral matrix protein via the PPxY late domain, causes the mono-ubiquitination of the viral matrix proteins, as well as the recruitment of the ESCRT machinery and the virus release (Han et al., 2014; Harty et al., 2001). Like the majority of the *Retroviridae*, also matrix proteins of the *Filoviridae* and *Rhabdoviridae* contain the PPxY late domain. Interestingly, the EBOV VP40 matrix protein contains overlapping late domain sequences, consisting of PTAP and PPxY (PTAPPxY). In 2004, Irie and colleagues demonstrated that the VSV (PPPY) late domain can be replaced by the overlapping EBOV late domains (PTAPPEY), resulting in an 11-fold higher budding of VSV virus-like particles (VLPs), indicating that L domains are exchangeable in terms of the efficiency to hijack the cellular ESCRT machinery (Irie et al., 2004). The knockdown of Tsg101 and the overexpression of a dominant-negative VPS4A, which does not bind and does not hydrolyze ATP, reduced the budding efficiency of VSV VLPs with the EBOV late domain. However, neither the knockdown of Tsg101 nor the overexpression of the dominant-negative VPS4A resulted in a reduction of VSV VLPs with its natural PPxY late domain (Irie et al., 2004).

In contrast, Kielian and colleagues suggested that dominant-negative VPS4, in this approach expressed by an inducible cell line, inhibits the viral budding of the VSV (30-fold). Additionally, they showed that the proteasome inhibitor MG-132 that decreases the level of free ubiquitin in the cell causes a 300-fold reduced budding of VSV, which indicates that VSV buds in an ubiquitin-dependent way (Taylor et al., 2007). The effect of MG-132 is in agreement with previous observations by Harty et. al., who also detected a 20 –fold reduction of VSV titers and a 16-fold reduction of RABV viral titers after MG-132 treatment (Harty et al., 2001).

RABV contains an overlapping late domain near the N-terminus, which is composed of the PPxY (interacts with Nedd4) motif and the YxxL (interacts with ALIX/AP1) motif. The entire overlapping late domain is the heptapeptide ^{35}PPEYVPL^{41}. Wirblich and colleagues demonstrated that aa P35 is the most important residue for the late domain activity since mutation of this residue caused a nearly 100-fold reduction in infectious viral titers, whereas the point mutations of P36, Y38, L41A, and the mutations of all four aa in one construct caused at the most a 10-fold reduction. Additionally, these data point out that the YxxL motif has no beneficial effect for RABV budding (Wirblich et al., 2008). In summary, regardless of the conflicting findings of Harty and Kilian with respect to the participation of VPS4 in RABV budding, Wirblich demonstrated an important role of the PPEY motif in RABV budding.

2.2.2 SNARE proteins

Cellular soluble N-ethylmaleimide-sensitive factor attachment protein receptor (SNARE) proteins are essential for the attachment and fusion of vesicles in general. In neurons, SNARE proteins are essential for the presynaptic vesicle fusion and therewith e.g. the neurotransmitter release as well as postsynaptic vesicle fusion, which is important for the postsynaptic plasticity (Harris et al., 2016; Jurado et al., 2013).

Until now, the human SNARE protein superfamily consists of 38 members (Hong and Lev, 2014). Interestingly, 31 out of the 38 SNARE proteins have a C-terminal transmembrane domain, while the remaining SNARE proteins are located to the membrane by a palmitoylation (SNAP25, Snap23, Stx9/19 and Stx11), prenylation (YKT6), or via interactions with other membrane bound SNARE proteins (SNAP29, SNAP47) (Hong, 2005; Hong and Lev, 2014). However, all SNARE proteins contain a 60-70 aa long, coiled-coil SNARE motif (Lou and Shin, 2016). A SNARE complex is composed of four SNARE motifs, which assemble to a four-helix bundle (Lou and Shin, 2016). The four-helix bundle is composed of 15 layers of interacting hydrophobic amino acids and a conserved hydrophilic layer (0-layer) in its center, which is composed of three glutamines (Q) and one arginine (R) residue (Lou and Shin, 2016; Sudhof and Rizo, 2011).

According to the presence of the hydrophilic residue of the SNARE motif in the center of the four-helix bundle, SNARE motifs are grouped into Qa-SNAREs, Qb-SNAREs, Qc-SNAREs, and R-SNAREs. The syntaxin family is specified as Qa-SNARE, the SNAP25 family is referred to as Qbc-SNARE, since it has two SNARE motifs, and the VAMP family is referred to as R-SNARE (Hong, 2005; Lou and Shin, 2016).

However, the SNARE proteins can be also functionally categorized into vesicular SNAREs (v-SNAREs) and target-membrane SNAREs (t-SNAREs) (Sudhof and Rizo, 2011). The v-SNARE

subfamily consists of VAMPs and its relatives. The t-SNAREs can be subdivided into the subfamily of syntaxins and the subfamily of SNAP25 (Hong, 2005).

The syntaxin family (t-SNAREs/Qa-SNAREs) consists of 15 members. Syntaxins are type II transmembrane proteins with the exception of syntaxin-19 and syntaxin-11, which have no transmembrane domain (Hong and Lev, 2014; Teng et al., 2001). All syntaxins exhibit a specific cellular localization, e.g. endosomes, TGN, plasma membrane. Syntaxin-1, -2, -3 and -4 are located at the plasma membrane (Bennett et al., 1993; Teng et al., 2001). Interestingly, in the peripheral nervous system (PNS) and CNS two isoforms of syntaxin-1 are coexpressed (syntaxin-1A and syntaxin-1B) (Bennett et al., 1992; Bennett et al., 1993). While syntaxin-1A knockout mouse exhibited a normal life span, the knockout of syntaxin-1B is lethal (Wu et al., 2015).

Whereas the presynaptic membrane of neurons is already well characterized with respect to the SNARE composition, very little is known about the postsynaptic membrane. However, during the last few years, postsynaptic functions for syntaxin-4 (Kennedy et al., 2010), syntaxin-3 (Jurado et al., 2013) and syntaxin-1 (Hussain et al., 2016) were documented.

The synaptosome-associated protein of 25 kDa (SNAP25) subfamily (t-SNAREs) is classified as Qbc-SNAREs since the family members have two SNARE motifs (Qb and Qc). The SNAP25 subfamily is composed of Snap23, -25, -29, and -47. As already mentioned, Snap25 and Snap23 are associated with the target membrane by multiple palmitoylations, whereas SNAP29 and SNAP47 have no palmitoylation site and bind by interactions with other SNARE proteins to the target membrane (Holt et al., 2006; Steegmaier et al., 1998).

The v-SNAREs (Vamp1, -2, -3, -4, -5, -7, -8) and the t-SNAREs YKT6 and Sec22b are structurally classified into R-SNAREs. Vamp1, -2, -3, -4, -5, -7, and -8 exhibit an N-terminal R-SNARE motif, a transmembrane domain and an intravesicular tail (Filippini et al., 2001). The Vamps can be subdivided into brevins and longins. Whereas brevins exhibit a short, non-conserved N-terminal region (Vamp1, -2, -3, -4, -5, -8), longins exhibit an approximately 110 aa long, highly conserved longin-domain. The longin Vamps can be subdivided into the three subfamilies Vamp7, Ykt6 and Sec22b (Daste et al., 2015; Filippini et al., 2001).

A SNARE complex assembly requires one of each structural SNARE motifs (R-, Qa-, Qb- and Qc-SNARE) for a heterotypic membrane fusion (Sudhof and Rothman, 2009). The first and best characterized SNARE complex is located at the presynaptic membrane, responsible for the neurotransmitter release into the synaptic cleft and consists of the R-SNARE Vamp2, the Qa-SNARE syntaxin-1 and the Qbc-SNARE Snap25. Briefly, the N-terminal end of the R-SNARE motif of Vamp2 interacts with the N-terminal end of the Qa-SNARE motif of syntaxin-1 and the two SNARE-motifs of the Qbc-SNARE Snap25, resulting in a trans-SNARE complex. The following zippering of the SNARE motifs from the N-terminus to the C-terminus pulls the opposing membranes together,

lower the energy barrier, and thereby enables the membrane fusion (van den Bogaart et al., 2013; Zhang, 2017). The membrane fusion transforms the trans-SNARE complex to a cis-SNARE complex, which in turn is disassembled by the ATPase NSF. R-SNAREs and Q-SNAREs are recycled and ready for a new membrane fusion cycle (reviewed in (Lou and Shin, 2016; Sudhof and Rizo, 2011; Sudhof and Rothman, 2009)). However, the fusion of synaptic vesicles with the membrane is a highly complex process in that is not only regulated by SNARE proteins, but also by SM proteins (Sec1/Munc18), Rab GTPases (Ras-related in brain GTPase), tethering factors, complexin and synaptotagmin to mention only the most prominent (Baker and Hughson, 2016; Baker et al., 2015; Stenmark and Olkkonen, 2001)

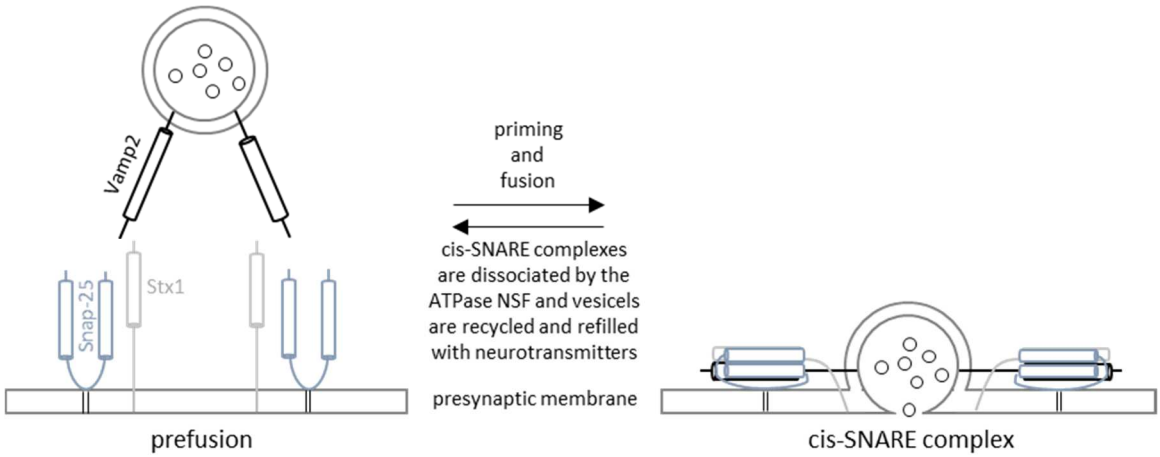

Figure 4: Illustration of the formation of a cis-SNARE complex.
Simplified illustration of the formation of a cis-SNARE complex at the presynaptic membrane adapted from (Dulubova et al., 2007). The cylinders represent the SNARE motifs. The synaptic vesicle interacts via the N-terminal end of the R-SNARE motif of Vamp2 with the N-terminus of the Qa-SNARE motif of Stx1 and the Qb,c-SNARE motifs of Snap25 resulting in a trans-SNARE complex (not depicted). The zippering of the four SNARE-motifs pulls the synaptic vesicle and the presynaptic membrane together, decreases the energy barrier and herewith drives the membrane fusion, resulting in a transformation of the trans-SNARE complex into a cis-SNARE complex. The components of the cis-SNARE complex are disassembled and recycled by the ATPase NSF and the vesicles are recycled and refilled with neurotransmitters(not depicted) (Sudhof and Rizo, 2011).

2.2.3 Neurotoxins

Clostridium botulinum toxins and tetanus toxin are bacterial neurotoxins that are described as powerful tools for studying synaptic vesicle exocytosis, as they inhibit the fusion of synaptic vesicles with the presynaptic membrane without changing the morphological structure of the synapse (Sudhof and Rizo, 2011). Additionally, studies using neurotoxins delivered the first hint that SNAREs are also located at the postsynaptic membrane since the toxins disrupted the

postsynaptic plasticity at excitatory synapses (Kennedy et al., 2010; Lledo et al., 1998; Lu et al., 2001).

The seven botulinum neurotoxins (BoNT/A-H) and the tetanus neurotoxin (TeNT) form the family of Clostridial neurotoxins (CNTs). With LD_{50} values between 0.1 up to 1 ng/kg body weight, CNTs represent the most toxic substances. CNTs are zinc metalloproteases, which hydrolyze specific peptide bonds of SNARE proteins and thereby causing a blockade of neurotransmission (Binz et al., 2010; Schiavo et al., 2000). CNTs are heterodimers consisting of a heavy chain (HC) and a light chain (LC), which are connected by a disulfide bond. The HC is responsible for receptor binding and translocation of the LC into the cytoplasm. The LC harbors the metalloprotease activity (Peng et al., 2013). TeNT-LC hydrolyses the peptide bond between Gln76 and Phe77 of Vamp1, -2, and -3, BoNT/A-LC cleaves Snap25 at position Gln197-Arg198 and BoNT/C-LC leads to the proteolysis of Snap25 at position Arg198-Ala199 as well as of syntaxin-1A and syntaxin-1B between amino acids Lys253-Ala254 and Lys252-Ala253, respectively (see Figure 5) (Schiavo et al., 1992; Wheeler and Smith, 2013).

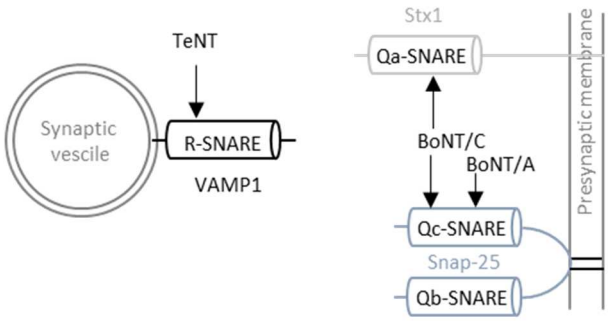

Figure 5: Cleavage site of CNTs at the neuronal SNARE complex.
Schematic representation of a synaptic vesicle at the presynaptic membrane and the cleavage sites of the CNTs TeNT, BoNT/A and BoNT/C (adapted from (Pirazzini et al., 2017)).

2.3 mESCs and mESC-derived neurons at a glance

2.3.1 mESCs at a glance

During the mouse embryogenesis, three different stages of potency are passed: totipotency, pluripotency and multipotency.

Totipotent stem cells can give rise to an entire functional organism. During mouse embryogenesis, cells are totipotent beginning with the fertilization of the oocyte, resulting in a zygote, up to the eight-cell stage of the morula. The morula evolves to a blastocyst, which consists of the outer trophoblast cells and undifferentiated, pluripotent inner cells, named the inner cell mass (ICM). The pluripotent mouse embryonic stem cells (mESCs) are isolated out of the ICM. Pluripotent stem cells can differentiate into the three primary germ layers (ectoderm, mesoderm, and endoderm) and into primordial germ cells. However, pluripotent stem cells cannot form an entire organism by themselves. Pluripotent stem cells differentiate into multipotent stem cells, which differentiate to more restricted specialized cells (reviewed in (Biehl and Russell, 2009)).

First, mESCs were cultured on mitotic inactivated mouse fibroblasts (feeder layer) in the presence of calf serum. However, this conditions are very different from the physiological environment of the cells. Further, nearly all pluripotent ES cell “lines”, which were derived by the cultivation on feeder cells in the presence of calf serum, derived from the mouse strain 129 or its hybrids (reviewed in (Martello and Smith, 2014)). Over the last decades, the requirements to keep pluripotent, self-renewing mESC in culture were revealed. The first discovered differentiation inhibitor was the leukemia inhibitor factor (LIF). LIF is produced by the feeder cells, where it is mainly located at the cell surface. It activates the transcription factor Stat3 and thereby promotes the mESC self-renewal property. However, in a feeder-free culture system with calf serum and LIF, the ES cell culture contains some differentiated cells, which were absent in the presence of feeder cells, indicating that feeder cells provided another important factor for the ES cell self-renewal. In addition, the withdraw of the calf serum results within six days in the differentiation of mostly neural precursors and neurons. A little bit conflicting seems the finding that LIF also activates Janus-associated kinases (JAKs), which activates the extracellular signal-related kinase (Erk) that is antagonistic to the ES self-renewal. Interestingly, the combination of LIF with the bone morphogenetic protein (BMP) was able to inhibit the differentiation of the self-renewal ES cells in absence of feeders and serum. Further investigations identified the fibroblast growth factor 4 (FGF4) as an autoinductive stimulation factor of the mitogen-activated protein kinase (ERK1/2). Furthermore, the Wnt signaling pathway plays an important role in the ES cell self-renewal as it enhances the ES cell growth, the ES cell viability and it suppresses the differentiation. Ying et al

demonstrated that ES cells could be cultivated in the absence of serum and LIF using two-small-molecule inhibitors (2i) (Ying et al., 2008). PD0325901 inhibits MEK1 and MEK2 of the MEK/ERK signaling pathway that would stimulate the differentiation of the ES cells. CHIR99021 inhibits the glycogen synthase kinase-3 (GSK3) of the Wnt signaling pathway, thereby prevents the phosphorylation of β-Catenin, which accumulates in the nucleus, binds the transcription repressor Tcf3 and dissociates it from its binding site and leads to the expression of pluripotency factors. The combination of LIF, PD0325901 and CHIR99021 (2i+LIF) results in a very robust cultivation of self-renewal, naive pluripotent mESCs (reviewed in (Martello and Smith, 2014; Nichols and Smith, 2012; Wray et al., 2010)).

2.3.2 Introduction of mESC-derived neurons

The chance to study RABV *in vitro* in immortalized cell lines enabled big achievements regarding the decipherment of the RABV biology. Fundamental insights into the RABV transcription, replication, the functional characterization of the viral proteins and the suppression of the innate immune system by RABV were gained. However, several specific aspects of the RABV biology, e.g neuronal transfer, can only be addressed in neurons, which represent the natural target cells of the neurotropic virus.

A difficulty in addressing neurobiological and neurovirological questions *in vitro* is the post-mitotic nature of neurons. That is the reason why people use undifferentiated or differentiated neuroblastoma cell lines (mouse N2A, human NS20Y), primary neuronal cells, or brain slices for their investigations *in vitro*.

In 1995, three groups independently of each other reported that cultured mESCs can be differentiated into neurons and glial cells (reviewed in (Wobus and Boheler, 2005)). Unfortunately, mESCs tend to differentiate spontaneously even in the presence of LIF, which makes it quite difficult to differentiation mESCs into a homogenous neuronal cell population (Bibel et al., 2007). In most cases, the differentiation of mESCs into neuronal cultures results in a heterogeneous cell population, which is composed of different neuronal subtypes and non-neuronal cells (Bibel et al., 2004). However, over the last years big achievements were made regarding the development of numerous *in vitro* differentiation protocols of mESC into distinct neuronal subtypes (reviewed in (Garcia et al., 2012b)). It is now possible to differentiate mESCs into GABAergic neurons, dopaminergic neurons, glutamatergic neurons, motor neurons, as well as non-neuronal cells. The characterization of the mESC-derived neurons with molecular markers and electrophysiological examinations demonstrated that the mESC-derived neurons resemble neurons of the intact brain tissues regarding its action potentials and neurochemical profiles. Further, it was shown that mESC-derived neurons are able to form functional synapses with primary neurons and slice

explants *in vitro* (Garcia et al., 2012a; Plachta et al., 2004) (reviewed in (Garcia et al., 2012b)). However, the *in vitro* differentiation of mESCs into neurons is still a delicate process.

Due to the similarity of mESC-derived neurons with neurons *in vivo*, mESC-derived neurons represent a powerful tool to investigate neurobiological questions in general as well as in this thesis particularly the biology of RABV in its natural target cells *in vitro*.

3 Material and Methods

3.1 Materials

3.1.1 Laboratory equipment

Equipment	Name	Manufacturer
Centrifuge	5418	Eppendorf
	5804 R	Eppendorf
	Varifuge 3.0R	Heraeus
	Allegra X-22R	Beckman Coulter
	Optima L-80 xp ultracentrifuge	Beckman Coulter
Microscope	Axiovert 200M	Zeiss
	Light microscope TMS	Nikon
	UV-Light microscope IX71	Olympus
Miscellaneous	T3 Thermocycler	Biometra
	Chemiluminescence developing system (Fusion FX7)	Vilber-Lourmat
	Luminometer Centro LB 960	Berthold
	Magnetic stirrer/heater	VELP Scientifica
	pH-meter	VWR International
	PIPETBOY acu	IBS
	Pipettes (2/10/200/1000 µL)	Eppendorf; Gilson
	Polyacrylamid gel electrophoresis system	Peqlab
	Agarose gel electrophoresis system	Peqlab
	Roller mixer SRT2	Stuart
	Semi-Dry blotting system	Peqlab
	Spectrophotometer Nanodrop ND-1000	Peqlab
	Thermocycler T3	Biometra
	Thermomixer 5436	Eppendorf

	Thermostated hot-block 5320	Eppendorf
	Horizontal shaker Swip SM-25	Edmund Bühler GmbH
	Digital Sonifier® Cell Disruptor	Branson
	GJ Balance	Kern
	LUNA Automated Cell Counter	Logos biosystems
	Cell Strainer 40 µM Nylon strainer	Corning

3.1.2 Dishes, well plates and miscellaneous

Miscellaneous	Manufacturer
Cell culture flasks (T25/T75)	Falcon
Cell culture plates (6-well, 12-well, 24-well, 96-well)	Sarstedt
Cryo tube 1.8 mL	Sarstedt
6-cm dish	Falcon
10-cm dish	Sarstedt
10-cm bacteriological petri dish	Greiner (cat. no. 633102)
1.5/2.0 mL reaction tube	Eppendorf
15/50 mL reaction tube	Sarstedt
Tube, Thinwall, Polypropylene, 17 mL/38.5 mL	Beckman coulter
µ-Dish 35mm, high, standard bottom	ibidi
µ-Dish 35 mm, high, glass Bottom	ibidi
Clarity Western ECL Blotting Substrats	Biorad
Microscope slides, frosted end	Roth
Microscope cover glasses, 12 mm Ø	Roth
Mr. Frosty Freezing Container	ThermoFisher
Vectashield HardSet Antifade Mounting Medium	Vector Laboratories
1 kb DNA ladder	New England Biolabs
PCR Marker	New England Biolabs

3.1.3 Cell lines and Bacteria strains

Cell line	Description	Medium	Source
BSR-T7/5	BHK-21-derived cells, stably expressing phage T7 RNA Polymerase	G-MEM 4+ Every 2nd passage, add 1 M G-418.	(Buchholz et al., 1999)
HEK 293T	HEK-293-derived cells stably expressing the simian virus 40 (SV40) large T antigen.	D-MEM 3+	ATCC
HeLa	Human cervix carcinoma cell line (epithelial cells)	D-MEM 3+	ATCC
N2A	Mouse neuroblastoma cell line	D-MEM 3+	ATCC
129/SvJ mESC	Stem cell line derived from 129/SvJ mouse.	LIF/2i medium	Benjamin R. Arenkiel
ROSA26-tomRITVA mESC	tdTomato, RABV G and TVA introduced into the ROSA26 locus of 129/SvJ mESC.	LIF/2i medium	(Garcia et al., 2012a)
$MG_{on}136$	BSR-derived cells, which express more SAD M as SAD G under control of Tetracycline inducible promoter. Induction with doxycyclin (1µg/mL).	G-MEM 4+ Every 2nd passage, add 1 M G-418 and 0.5 mg/mL hygromycin B	(Finke and Conzelmann, 2003)
$MG_{on}139$	BSR-derived cells, which express more RABV G as RABV M under control of Tetracycline inducible promoter. Induction with doxycyclin (1µg/mL).	G-MEM 4+	Stefan Finke (in house)
BHK EnvA	BSR-derived cells, stably expressing the avian sarcoma envelope protein (EnvA).	GMEM 4+	(Wickersham et al., 2007b)

3.1.4 Chemicals

Chemical	Manufacturer
Acetic acid, 100 %	Roth
Acetone, Rotipuran 99.8 %	Roth
Acrylamide Rotiphorese® Gel 30 (37.5 : 1)	Roth
Agar	BD
Agarose, UltraPure	Invitrogen
Ammonium chloride	Merck
Ammonium persulfate	Sigma-Aldrich
Ampicillin sodium salt	Roth
Bis-Tris	Santa Cruz Biotech.
Bromophenole blue	Sigma-Aldrich
Dimethyl sulfoxide	Roth
Dimethylformamide	Merck
Disodium hydrogen phosphate	Merck
Ethanol	Merck
Ethidium bromide solution 1 %	Roth
Ethylenediamine tetraacetic acid	Sigma
Geneticin (G418)	Roth
Glycerol , Rotipuran 99.5 %	Roth
HEPES	Roth
Hydrochloric acid, Rotipuran 37 %	Merck
Imidazole	Merck
Isopropanol	Merck
Kanamycin monofulfate	Sigma-Aldrich
Magnesium sulfate heptahydrate	Merck
Methanol	Roth
Milk powder, blotting grade	Roth
3-(N-morpholino)propanesulfonic acid	Roth
Orange G	Fluka
ortho-Phosphoric acid, 85 %	Merck
Paraformaldehyde	Merck
Poly-D-lysine hydrobromide	Sigma-Aldrich

Polyethylenimine, branched	Sigma-Aldrich
Potassium acetate, extra pure	Merck
Potassium chloride	Merck
Potassium dihydrogen phosphate	Merck
Sodium bisulfite	Sigma
Sodium chloride	Merck
Sodium dihydrogen phosphate	Merck
Sodium dodecyl sulfate	Serva
Sodium hydroxide	VWR Chemicals
Tetramethylethylenediamine	Roth
Tris, Pufferan 99.9 %	Roth
Triton X-100	Merck
Tryptone	BD
Tween-20	Roth
β-Mercaptoethanol	Sigma-Aldrich

3.1.5 Buffers and solutions

In the following, the different buffers and solutions, which were used in this thesis, are listed. If not specifically mentioned, all buffers and solutions were stored at RT.

Agarose gel electrophoresis	
10 x TAE	2 M Tris-HCl, (pH 7.8) 0.25 M Sodium acetate trihydrate 0.25 M EDTA
10 x TEN	50 mM Tris-HCl (pH 7.4) 1 mM EDTA 150 mM NaCl
1 x TAE + EtBr	200 mL 10 x TAE 1800 mL ddH2O 120 µL Ethidium bromide solution (1%)
OG loading buffer	50 % (v/v) 10x TAE 15 % (w/v) Ficoll 400 0.125 % (w/v) Orange G Store at -20°C, after thawing 4 °C

Immunofluorescence	
80 % Aceton	800 mL Aceton p.a. 200 mL ddH_2O Store at 4 °C
3 % PFA	1 x PBS 3 % (w/v) Paraformaldehyd
NH_4Cl in PBS	1x PBS 50 mM NH4Cl
0.1 % Triton X-100	1x PBS 0.1 % (v/v) Triton X-100
2.5 % milk in PBS	1x PBS 2.5 % (w/v) milk powder

Mini preparation	
Flexi I	100 mM Tris-HCl pH 7.5 10 mM EDTA 200 µg/mL RNase Stored at 4 °C
Flexi II	200 mM NaOH 1 % (w/v) SDS
Flexi III	3 M potassium acetate 2 M acetic acid, pH 5.75

SDS-PAGE	
APS	10 % APS (w/v) Appropriate volume ddH2O Store at -20 °C, after thawing at 4 °C
3.5 x Bis-Tris	1.25 M Bis-Tris HCl pH 6.8
20 x MOPS buffer	1 M Tris 1 M MOPS 20 mM EDTA 2 % SDS
1 x MOPS buffer (running buffer)	50 mL 20 x MOPS 2 mL 2.5 M Sodium Bisulfite

	948 mL ddH2O
SDS sample buffer	62 nm Tris/HCl pH 6.8 10 % SDS 15 % β-mercaptoethanol 30 % Glycerol 0.012 % Bromophenol blue
Separation gel mix (10 %)	1 x Bis-Tris 10 % acrylamide/bisacrylamide 37.5:1 ddH_2O appropriate volume
Separation gel	Separating gel mix (10 %) 1 % APS (v/v) 0.4 % TEMED (v/v)
Stacking gel mix (6 %)	1 x Bis-Tris 6 % acrylamide/bisacrylamide 37.5:1 ddH_2O appropriate volume
Stacking gel	Stacking gel mix (6 %) 1 % APS 0.1 % TEMED

Western blotting	
Extra-Dry blotting buffer	48 mM Tris 20 mM Hepes 1 mM EDTA 1.3 mM Sodium Bisulfite 1.3 mM Dimethylformamide
TBS	50 mM Tris 150 mM NaCl pH 7.4 (adjusted with HCl)
TBS-T	TBS 0.05 % Tween-20
2.5 % milk in TBS	1x TBS 2.5 % (w/v) milk powder

3.1.6 Medium and cell culture additives

Bacteria growth medium	
LB	85 mM NaCl 0.5 % (w/v) Bacto yeast extract 1 % (w/v) Bactotryptone 1 mM MgSO4 Stored at 4 °C
LB Amp	1 x LB 25 mg/mL Ampicillin Stored at 4 °C
LB ++	1 x LB 20 mM MgSO4 10 mM KCl

Components of cell culture medium	manufacturer
ara-C	Sigma-Aldrich
B27 supplement serum free (50x)	Gibco
D-MEM (L-Glutamine, high glucose)	Gibco
Knockout DMEM (No L-glutamine, high glucose)	Gibco
Pansera ES	PAN-Biotech
FBS Premium	PAN-Biotech
G-MEM (L-Glutamine, high glucose)	Gibco
DPBS (no calcium, no magnesium)	Gibco
L-Glutamine	Gibco
GlutaMAX	Gibco
Gentamicin (50mg/mL)	Gibco
MEM Amino Acids	Gibco
MEM NEAA	Gibco
Neurobasal medium (no Aspartic Acid, no Glutamic Acid, serum free)	Gibco
Tryptose Phosphate Broth	Gibco
Penicillin-Streptomycin	Gibco
Trypsin-EDTA 0.25 %	Gibco

Stem Pro Accutase	Gibco
PD0325901	Selleckchem
CHIR-99021	Selleckchem
Leukemia Inhibitory Factor	Merck Millipore

cell culture medium	Composition of media
D-MEM 3+	450 mL D-MEM 50 mL FBS 5 mL L-Glutamine 2 mL Pen-Strep Stored at 4 °C
G-MEM 4+	450 mL G-MEM (Invitrogen) 50 mL Fetal calf serum 4.5 mL Tryptose-phosphate (Invitrogen) 10 mL MEM amino acids (Invitrogen) 2 mL Pen-Strep (Invitrogen) Stored at 4 °C
EB medium	217 mL Knockout DMEM 125 mL Pansera ES 0.1 mM β-mercaptoethanol 2.5 mL NEAA 2.5 mL GlutaMAX 2.5 mL Pen/Strep Stored at 4 °C
mESC LIF/2i medium	mESC without LIF/2i 1 x 10^6 U/mL LIF 5 mM PD0325901 15 mM CHIR 99021 Stored at 4 °C
mESC LIF medium	mESC without LIF/2i 1 x 10^6 U/mL LIF Stored at 4 °C
Neuron medium	97 mL Neurobasal medium 2 mL B27

	1 mL GlutaMAX 1µL Gentamicin (50 mg/mL) Stored at 4 °C
Neuron medium +FBS	92 mL Neurobasal medium 5 mL Pansera ES 2 mL B27 1 mL GlutaMAX 1 µL Gentamicin (50 mg/mL) Stored at 4 °C

3.1.7 Kits

Purpose	Kit	Manufacturer
DNA purification	QIAquick PCR Purification Kit	QIAGEN
	QIAquick Gel Extraction Kit	QIAGEN
RNA isolation	RNeasy Mini Kit	QIAGEN
Transfection	Mammalian Transfection Kit	Stratagene
	Lipofectamine 2000	Invitrogen
	FuGene HD	Promega

3.1.8 Enzymes

Enzyme	Manufacturer
Restriction Enzymes	New England Biolabs
Phusion DNA Polymerase	NEB/Thermo Fisher Scientific
T4 DNA ligase	New England Biolabs
Alkaline Phosphatase, Calf Intestinal (CIAP)	New England Biolabs
Instant Sticky-End Ligase Master Mix	New England Biolabs
DNase, RNase-free	Qiagen
Transcriptor Reverse Transcriptase	Roche
RNase	Macherey-Nagel

3.1.9 Primary antibodies

Epitope	Host	Dilution	Manufacturer
Actin (20-33))	Rabbit	1/1000	Sigma-Aldrich
RABV P (160-5)	Rabbit	1/50000	In house

RABV G (HCA0501)	Rabbit	1/1000	In house
RABV M (M2D4)	Rabbit	1/1000	In house
RABV N (S50)	Rabbit	1/25000	In house
Oct4	Mouse	1/1000	Merck Millipore
Nestin	Mouse	1/1000	Santa-Cruz
β-III Tubulin	Mouse	1/1000	Merck Millipore
MAP2	Rabbit	1/1000	Synaptic Systems
MAP2	Mouse	1/1000	Sigma-Aldrich
NF H	Rabbit	1/1000	Synaptic Systems
PSD-95	Rabbit	1/1000	Synaptic Systems
Syntaxin-1	Mouse	1/1000	Santa Cruz
Syntaxin-3	Rabbit	1/1000	Abcam
Syntaxin-4	Mouse	1/1000	Abcam
VAMP1	Rabbit	1/1000	Abcam
VAMP2	Rabbit	1/1000	Abcam
VAMP3	Rabbit	1/1000	Novus
GFP	Rabbit	1/1000	Cell signaling
CytoPainter Phalloidin-iFluor 555		1/1000	Abcam
To-Pro3		1/1000	Invitrogen

3.1.10 Secondary antibodies

Horseradish-peroxidase (HRP) coupled secondary antibodies were used for Western blotting and Alex Fluor labeled secondary antibodies were used for immunostaining in confocal microscopy.

Epitope	Conjugate	Host	Dilution	Manufacturer
Rabbit IgG	HRP	Goat	1/20000	Jackson ImmuoResarch Laboratories
Mouse IgG	HRP	Goat	1/20000	Jackson ImmuoResarch Laboratories
Rabbit IgG	Alexa-488	Goat	1/200	Invitrogen
Rabbit IgG	Alexa-555	Goat	1/200	Invitrogen
Mouse IgG	Alexa-488	Goat	1/200	Invitrogen
Mouse IgG	Alexa-555	Goat	1/200	Invitrogen

3.1.11 Oligonucleotides

The DNA oligonucleotides used in this thesis were ordered from Eurofins Genomics. The sequences are listed in the appendix (see section 6.1).

3.1.12 Plasmids

Plasmid	Source if not this thesis	Description
eGFP Stx4 ΔTM	(Kennedy et al., 2010)	eGFP was fused to the N-terminus of the cytoplasmic domain of Stx4
mCherry Stx1 ΔTM	(Kennedy et al., 2010)	mCherry was fused to the N-terminus of the cytoplasmic domain of Stx1A
mCherry Stx3 ΔTM	(Kennedy et al., 2010)	mCherry was fused to the N-terminus of the cytoplasmic domain of Stx3
pCAGGS	(Niwa et al., 1991)	Eukaryotic expression vector with chicken-β-actin promoter
pCAGGS-G	Anika Kern	RABV G in pCAGGS vector
pCAGGS-M	Anika Kern	RABV M in pCAGGS vector
pCAGGS-M34AAA		RABV M with indicated mutated aa (^{34}PPP^{36} → AAA) in pCAGGS vector
pCAGGS-M35AA		RABV M with indicated mutated aa (^{34}PP^{35} → AAA) in pCAGGS vector
pCAGGS-SADG-ΔnAChbinding site		SAD G in which nAChR binding site is replaced by SP
pCAGGS-SADG-ΔnAChRbs-(SP)		SAD G with deleted nAChR binding site (Δaa194-204)
pCAGGS-SADG-Δ-siteIII		SAD G with antigenic site III (Δaa349-357)
pCAGGS-SADG-Δ-siteIII [(GS)2-SP-(GS)2]		SAD G in which antigenic site III is replaced by SP
pCAGGS-G-TM-3xKBS-RT		SAD G with three copies of KBS on the C-terminus of TM

pCAGGS-SADG 3xKBS		SAD G with three copies of KBS on the C-terminus of the C-tail
pCMV LC-A	Thomas Binz	Light chain of BoNT/A in CMV expression vector
pCMV LC-C	Thomas Binz	Light chain of BoNT/C in CMV expression vector
pCMV LC TeNT	Thomas Binz	Light chain of TeNT in CMV expression vector
pCR3-eGFP-BoNT/A-LC		Light chain of BoNT/A with an N-terminal eGFP tag
pCR3-eGFP-BoNT/C-LC		Light chain of BoNT/C with an N-terminal eGFP tag
pCR3-eGFP-TeNT/LC		Light chain of TeNT with an N-terminal eGFP tag
pTIT-G	(Finke et al., 2003)	T7-Pol and EMCV IRES dependent expression of RABV G
pTIT-L	(Buchholz et al., 1999)	T7-Pol and EMCV IRES dependent expression of RABV L
pTIT-M	(Finke et al., 2003)	T7-Pol and EMCV IRES dependent expression of RABV M
pTIT-N	(Buchholz et al., 1999)	T7-Pol and EMCV IRES dependent expression of RABV N
pTIT-P	(Buchholz et al., 1999)	T7-Pol and EMCV IRES dependent expression of RABV P
Full-length RABV constructs		
pCVS-N2c	Mathias Schnell	Full-length cDNA of RABV CVS-N2c strain
pSAD eGFP	Alexander Ghanem	Full-length cDNA of RABV SAD L16 in the T7-HHRz-SC with an extra transcription unit in between G and L with an N/P gene border followed by eGFP
pSAD eGFPStx4DN		Dominant-negative Stx4 with N-terminal eGFP-tag in an extra

		transcription unit in pSAD L16 (N/P gene border)
pSAD eGFPStx4DN/Stx3DN		Dominant-negative Stx4 with N-terminal eGFP-tag in an extra transcription unit in pSAD L16 (N/P gene border) followed by an additional M/G gene border and dominant-negative Stx3
pSAD G-TM-3xKBS-RTeGFP		pSAD with SADG-TM-3KBS-RT instead of SADG
pSAD L(I30T) eGFP		pSAD eGFP with point mutation in RABV L at the indicated aa.
pSAD L(stop) eGFP		pSAD eGFP with point mutation in RABV L introducing an in frame stop codon at aa 935
pSAD mchStx1ADN		Dominant-negative Stx1 with N-terminal mCherry-tag in an extra transcription unit in pSAD L16 (N/P gene border)
pSAD mChStx3DN		Dominant-negative Stx3 with N-terminal mCherry-tag in an extra transcription unit in pSAD L16 (N/P gene border)
pSAD M34AAA	Christine Schnellhammer	pSAD with mutations at the indicated positions of SAD M: ^{34}PPP^{36} → AAA
pSAD M35AA	Christine Schnellhammer	pSAD with mutations at the indicated positions of SAD M: ^{35}PP^{36} → AA
pSAD M34AAA eGFP		pSAD eGFP with mutations at the indicated positions of SAD M: ^{34}PPP^{36} → AAA
pSAD mut52/54 eGFP	Alexander Ghanem	pSAD eGFP with two mutations in the leader: A52T and A54G

pSAD mut52/54/12845 eGFP	Alexander Ghanem	pSAD eGFP with two mutations in the leader and one mutation in the trailer: A52T, A54G, A12845G
pSAD mut12845 eGFP	Alexander Ghanem	pSAD eGFP one mutation in the trailer: A12845G
pSAD N2CM		pSAD in which SAD M is replaced by N2C M
pSAD N2c M34AAA		pSAD N2C M with mutations at the indicated positions of N2C M: ^{34}PPP^{36} → AAA
pSAD P(M83R) eGFP		pSAD eGFP with point mutation in RABV P at the indicated aa, mutating the start codon of P4
pTHA	Hervé Bourhy	Plasmid encoding for THA strain
Recombinant SAD deletion mutants		
pSAD ΔG eGFP	Alexander Ghanem	G gene-deficient pSAD, in which the glycoprotein encoding gene is replaced by eGFP encoding gene
pSAD ΔG eGFP-TeNT-LC		G gene-deficient pSAD, in which the glycoprotein encoding gene is replaced by eGFP-TeNT-LC encoding gene
pSAD ΔM eGFP		M gene-deficient pSAD eGFP

The cloning strategies of the plasmids, which were cloned in this thesis are listed in section 6.2.

3.1.13 Recombinant viruses

The following recombinant viruses were generated from cDNA by reverse genetics (Ghanem et al., 2012; Schnell et al., 1994).

Virus	If not rescued in this thesis, nicely provided by
Recombinant full-length viruses	
CVS-N2c	Chloé Scordel
SAD eGFP	
SAD eGFPStx4DN	
SAD eGFPStx4DN/Stx3DN	
SAD G-TM-3xKBS-RTeGFP	
SAD L(I30T) eGFP	
SAD L(stop) eGFP	
SAD mchStx1ADN	
SAD mChStx3DN	
SAD M34AAA eGFP	
SAD mut52/54 eGFP	Alexander Ghanem
SAD mut52/54/12845 eGFP	Alexander Ghanem
SAD mut12845 eGFP	Alexander Ghanem
SAD N2CM	
SAD N2c M34AAA	
SAD P(M83R) eGFP	
THA	Chloé Scordel
Recombinant deletion-mutant viruses	
SAD ΔG eGFP	
SAD ΔG eGFP-TeNT-LC	
SAD ΔM eGFP	

3.2 Methods

3.2.1 Working with DNA

In the following, the methods for working with DNA are explained.

3.2.1.1 Polymerase Chain Reaction (PCR)

The PCR enables the amplification of a defined DNA fragment for cloning or alternatively for sequencing of cDNA. Therefore, template specific primers, which frame the 5´- and 3´-end of the DNA fragment of interest and prolong the amplicon with adequate restriction sites or insert the desired nucleotide sequence, were designed.
The standard PCR was prepared according to the instruction manual of the Phusion High-Fidelity PCR Kit from NEB.

Component	Amount	Final concentration
Template	1 µL	1 pg -10 ng
5x Phusion HF Buffer	10 µL	1 x
10 mM dNTPs	1 µL	200 µM
10µM forward Primer	2.5 µL	0.5 µM
10µM reverse Primer	2.5 µL	0.5 µM
DMSO	1.5 µL	3 %
Phusion DNA Polymerase	0.5 µL	1 units/50 µL PCR
H_2O_{dd}	31 µL	-

PCR reactions were performed in a T3 Thermocycler (Biometra). The lid was preheated up to 105 °C. The standard PCR-program was as follows.

Step	Temperature	Duration	
1. Denaturation	98°C	2 min	
2. Denaturation	98°C	30 sec	
3. Primer annealing	50°C -65°C (Mostly 5°C below the lowest T_m)	30sec	30x
4. Elongation	72°C	15sec/1000nt	
5. Final elongation	72°C	10 min	
6. End	4 °C	pause	

To confirm the correct size of the PCR product, 5 % of the sample were analyzed by agarose gel electrophoresis. The remaining 95 % of the PCR product were purified according to the QIAquick PCR Purification Kit (QIAGEN).

3.2.1.2 Agarose gel electrophoresis

The agarose gel electrophoresis was executed to analyze the length of PCR products (analytic gel) or to separate DNA fragments, which resulted from the digestion of DNA with restriction endonucleases (preparative gel).

Therefore, dependent on the size of the DNA fragment a 1 % - 2 % (w/v) agarose gel in 1 x TAE-buffer was prepared. After the gel was solid, it was placed into an agarose gel electrophoresis chamber. The running buffer composed of 1 x TAE and 0.075 % ethidium bromide, which enables the detection of nucleic acid under UV light. DNA samples were mixed with 5 x Orange G loading buffer and loaded into the pockets of the gel. The standard electrophoresis was performed for 30 – 60 min at 120 V and 400 mA. The gels were analyzed with the Biorad GelDoc System.

3.2.1.3 Restriction enzyme digestion

Restriction endonuclease digestion of DNA was used for analytic or preparative purpose.

The following digestions were prepared according to the suggestions of the enzyme supplier New England Biolab.

An analytic digestion was performed in a total volume of 20 µL containing up to 1 µg DNA, 5 U of each restriction enzyme, the corresponding 10 x NEB buffer and H_2O_{dd}. The reaction mix was incubated for 1 h at 37 °C. The product size was analyzed by agarose gel electrophoresis.
A preparative digestion was performed for 1.5 h at 37 °C in a total volume of 50 µL. The reaction mix contained three up to five µg DNA, 20 U of each restriction enzyme, the corresponding 10 x NEB buffer and H_2O_{dd}.
To prevent religation of a linearized vector, the 5´-end of the digested vector was dephosphorylated with the alkaline phosphatase Calf intestine phosphatase (CIP) immediately after the digestion. Therefore, 10 U CIP were added directly to the reaction mix and incubated for another 30 min at 37°C.
Finally, the products were purified via the agarose gel electrophoresis, followed by QIAquick Gel Extraction Kit (Qiagen).

3.2.1.4 Gel purification of DNA fragments

After PCR products and vectors were subject to a preparative digestion, they were undergone an agarose gel electrophoresis. The DNA fragment of the correct size was cut out from the agarose gel and the favored DNA was extracted out of the gel with the QIAquick Gel extraction kit (QIAGEN). The DNA extraction was performed according to the instruction manual of QIAGEN.

3.2.1.5 Ligation of DNA fragments

The T4 DNA Ligase was used to ligate a cohesive or blunt-ended DNA fragment with a linearized, cohesive, or blunt-ended vector. The T4 DNA Ligase catalyzes the formation of a phosphodiester bond between the hydroxyl group on the 3´-end and the phosphate group on the 5´-end, which leads to the formation of a circular plasmid. For the calculation of the molar ratios, the NEBiocalculator™ was used. The ratio of vector to insert was 1 to 3. As a control for vector religation, the insert was replaced by water.

Component	Volume
T4 DNA Ligase buffer 10x	2 µL
Vector	0.04 pmol
Insert	0.12 pmol
T4 DNA Ligase	1 µL
H_2O_{dd}	To 20 µL

The ligation reaction was incubated for 1 h at RT or overnight at 16 °C.

3.2.1.6 Transformation of plasmid DNA into competent bacteria

For transformation, 50 µL of the chemical-competent E. coli strain XL1-Blue were thawed on ice. Then 10 µL of the ligation mix or 100 ng of plasmid (retransformation) were added to the XL1-Blue bacteria. This mixture was incubated for 20 min on ice, followed by a 2 min heat shock at 42 °C and a 2 min cooling step on ice. Subsequently, 200 µL LB++ medium were added to the transformed XL1-Blue bacteria. The suspension was incubated on a Thermoshaker at 37 °C, 800 rpm for 45 min. Finally, the transformed bacteria were plated onto a LB-agar plate containing the appropriate antibiotic (ampicillin, kanamycin, streptomycin). The LB-agar plate was incubated overnight at 37 °C.

3.2.1.7 Mini preparation of plasmid DNA from bacteria

For DNA plasmid isolation out of bacteria, the alkaline lysis was used.
Single colonies, which were grown overnight on selective LB-plates, were picked and used to inoculate 1 mL selective LB-medium. Then the bacteria suspension was incubated on a shaker, overnight at 37 °C. The bacteria were pelleted by centrifugation for 1 min at 14000 rpm. The pellets were resuspended in 200 µL RNAse containing Flexi I. Afterwards, 200 µL Flexi II were added, to burst the bacteria and to denature the DNA. After 5 min 200 µL Flexi III were added to renature the plasmid by neutralizing the suspension. 5 min later, the cell debris and the bacterial DNA were pelleted by centrifugation for 7 min at 14000 rpm. The plasmid DNA containing supernatant was added to 400 µL isopropanol and centrifuged (RT, 10 min, 14000 rpm). The supernatant was discarded, the plasmid DNA pellets were air dried at RT and finally dissolved in 50 µL H_2O_{dd}.
Mini preparations were analyzed by an analytic digestion. The bacterial clones, which showed the correct DNA fragment pattern in the agarose gel, were used for retransformation.

3.2.1.8 Midi preparation of plasmid DNA from bacteria

After retransformation of a mini preparation, a single colony was picked and used to inoculate 50 mL selective LB-medium. The bacterial suspension was incubated in a rotary shaker, overnight at 37 °C and 800 rpm. The bacteria were harvested by centrifugation (RT, 20 min, 3500 rpm).
The plasmid DNA was extracted according to the instruction manual of the NucleoBond® Xtra Midi/Maxi Kit (Machery & Nagel).
The DNA concentration was measured with the UV-Vis Spectrophotometer Nanodrop ND-1000.

3.2.1.9 Sequencing of DNA

For sequencing, sequence specific primers, DNA plasmids and linear DNA fragments were diluted according to the guidelines of GATC Biotech, which performed a Sanger Sequencing. The resulting sequences were analyzed with the software SnapGene 2.6.2.

3.2.2 Cell culture

In the following, the cell culture of mammalian adherent cell lines and pluripotent mESC is listed.

3.2.2.1 Cultivation of mammalian adherent cell lines

The mammalian adherent cell lines were cultured under sterile conditions in T25 or T75 cell culture flasks, in the appropriate growth medium at 37 °C and at 5 % CO_2. Cells were passaged every three up to four days. First, the adherent cells were detached by trypsinization with Trypsin-EDTA 0.25% (Gibco). Dependent on the cell growth rate of each cell line, the cells were split 1/4 up to 1/12. If needed, antibiotics were added every second passage for selection.
To seed the correct amount of the cells for an experiment, the cell concentration (cells/mL) was determined with the LUNA™ Automated Cell Counter (logos Biosystems) or calculated based on the estimated number of cells in a T25 cell culture flask ($3.1x10^6$cells/T25). Afterwards, the appropriate number of cells was seeded per well or dish.

3.2.2.2 Cultivation of mESC in a feeder free culture

To keep mESC as long as possible pluripotent, a high quality mESC culture was performed. Therefore, mESC were cultured under sterile conditions, in mESC LIF/2i growth medium, in a freshly 0.1 % gelatine coated 6-well plate at 37 °C and 5 % CO_2. The basic medium (EB medium) and the mESC LIF/2i medium were stored at 4 °C for up to two weeks. Since the repeatedly warming of the inhibitor-containing LIF/2i medium turns the pH basic, only small volumes (25 mL - 50 mL) of the mESC LIF/2i medium were prepared.
For the *in vitro* cultivation of mESCs in a feeder-free systems, a 6-Well was coated with about 1.5 mL 0.1 % gelatine at 37 °C. After 20 min the gelatine solution was removed and 475000 mESCs were seeded per 6-Well (5×10^4 cells/cm^2). About 30 h post seeding, the medium was carefully replaced with chilled LIF/2i medium. Another 14 h post medium exchange, the mESCs were washed twice with PBS and enzymatically detached from the dish by incubating the cells for 5 min at 37 °C with Stem Pro Accutase (350 µL/6–Well). Subsequently, the Stem Pro Accutase was diluted with 1 mL chilled EB medium, the cell suspension was carefully resuspended, transferred into 1.5 mL reaction tube and pelleted by a centrifugation step (160 g, 5 min, RT). The cell pellet

was carefully resuspended to a single cell suspension and split 1/4 up to 1/6 (equates to 5 x 10^4 cells/cm^2) into a 0.1 % gelatine coated 6-Well. The mESCs were cultured as long as they formed the characteristic dome-shaped clusters.

3.2.3 Freezing and thawing of mESCs

Freezing of mESCs

To produce a lot of mESCs for freezing, the cells were expanded to 10-cm dishes. After the cells were dissociated into a single cell suspension, as described above, a cell suspension of 5.5 x 10^6 cells/mL was adjusted in chilled EB medium. Just before freezing, 10 % DMSO were slowly added to the cell suspension. Subsequent, 1 mL aliquots were transferred into the Mr. Frosty Freezing container and frozen at - 80 °C. After 24 h, the tubes were transferred to a liquid nitrogen tank.

Thawing of mESCs

The cryo tube was thawed in a water bath (37 °C). During the thawing, the tube was slewed to enable a homogenous warming of the cell suspension. To remove the DMSO containing medium, the cell suspension was diluted with 9 mL EB medium, centrifuged (160 g, 5 min, RT), carefully resuspended in LIF/2i medium and plated into a gelatine coated 6-Well.

3.2.4 Transfection

In this thesis, eukaryotic cells were transfected with plasmid DNA using Polyethylenimine (PEI), Lipofectamin™ 2000, FuGENE HD or Calcium Phosphate. In the following, the different transfection protocols are described.

Transfection with Polyethylimin (PEI)

PEI was used to transfect one plasmid per HEK293T cell. For a standard PEI transfection, HEK293T cells were seeded about 16 h prior to transfection into a 6-Well plate to have them to the time point of transfection about 75 % confluent. The used ratio of DNA to PEI was 1 µg DNA to 2.5 µL PEI (1 mg/mL). The DNA and the adequate volume of PEI were diluted separately in 100 µL DMEM per 6-well. After an incubation time of 5 min at RT, the two dilutions were mixed and incubated for another 20 min at RT. Finally, the transfection mix was added dropwise onto the cells. Dependent on the experiment, the medium was exchanged 6 h or 24 h post transfection.

Transfection with Lipofectamin 2000 (Invitrogen)

Lipofectamin 2000 was used transfect N2A cells, mESC-derived neurons or to cotransfect at least two plasmids per cell. The standard Lipofectamin 2000 transfection protocol followed the PEI transfection protocol.

Transfection with FuGENE HD (Promega)

In this thesis, FuGENE was exclusively used for the transfection of already Calcium Phosphate transfected BSR-T7 cells. The FuGENE HD transfection protocol followed the PEI transfection protocol.

Transfection with Calcium Phosphate (*Stratagene Mammalian Transfection Kit)*

The Calcium Phosphate transfection was performed in a 6-Well. About 3 x 10^5 BSR-T7 cells were seeded 16 h pre transfection to have them at a confluency of approximately 90 % to the time point of transfection. One hour prior transfection 2 mL GMEM 4+ were aspirated, the BSR-T7 cells were washed twice with DMEM and incubated for 1 h in DMEM in the incubator. During the incubation time, 20 µg DNA per 6-Well were in diluted in a total volume of 90 µL ddH_2O. After 30 min 10 µL of solution 1 from the Mammalian Transfection $CaPO_4$ Kit (Stratagene) were added to 90 µL DNA solution, mixed by pipetting thoroughly up and down, and incubated for 5 min on ice. Subsequently, 100 µL of solution 2 from the Mammalian Transfection $CaPO_4$ Kit (Stratagene) were added to DNA-solution 1 reaction mix. The transfection mix was incubated for 20 min at RT, before it was added dropwise onto the BSR-T7 cells. The cells with the transfection mix were put back into the incubator for 3.5 hours. Finally, the transfected cells were washed twice with 2 mL GMEM 4+, 2 mL GMEM 4+ were added onto the transfected cells and the plate was returned into the incubator.

3.2.5 Immunofluorescence imaging

Seeding of cells for immunofluorescence

The immunofluorescence of mESC-derived neurons was performed on ibidi µ-dishes, which were coated overnight at 37 °C with 0.1 mg/mL PDL, or on coverslips, which were coated overnight at 37 °C with 1 mg/mL PDL. On the following day, the dish was washed twice with H_2O and once with PBS. Subsequently, 1.5 x 10^5/cm^2 dissociated neurospheres were seeded and the last steps of the differentiation protocol were performed as described in section 4.1.1.5.

The immunofluorescence of naive pluripotent stem cells (mESCs), primed pluripotent stem cells (mEpiSCs), EBs and neurospheres was performed in ibidi µ-dish. To this, the ibidi µ-dish was coated

for 20 min with 0.1 mg/mL gelatine solution. For the IF of mESCs and mEpiSCs mESCs, 5 x 10^4 cells/cm^2 were seeded per dish. Two days post seeding the immunofluorescence protocol was executed. For the IF of the floating EBs and neurospheres, 500 µL of the respective cell suspension were seeded per dish. Then 1.5 mL of the respective medium was added. Three hours post seeding the EBs and neurospheres passively settled down, attached to the coated dish and it could be proceeded with the immunofluorescence protocol.

Fixation and immunofluorescence staining of the cells

After the cells were washed twice with PBS, the cells were fixed with 3 % PFA (RT, 20 min). Subsequently, the fixed cells were washed once with PBS, quenched with 50 mM NH_4Cl in PBS (RT, 10 min), permeablized with 0.5 % Triton X-100 in PBS (RT, 15 min), washed thrice with PBS and finally blocked with 2.5 % milk in PBS (RT, 30 min). Afterwards, the cells were washed with PBS and incubated with primary antibodies overnight at 4 °C or for two hours at 37 °C. After the incubation with the primary antibody, the cells were washed three times with PBS, followed by the incubation (RT, 2 h, in the dark) with the secondary antibody that is conjugated to a fluorescent dye. If the staining of the nucleus was desired, the cells were stained in parallel to the secondary antibodies with To-Pro3. After the staining with the secondary antibody, the samples were washed twice with PBS and once with deionized water. The ibidi µm dishes were directly stored at 4 °C, whereas the coverslips were mounted to the object holder with Vectashield HardSet Antifade Mounting Medium *(Vector Laboratories)*, before they were stored at 4 °C. Finally, the samples were analyzed with the Axiovert 35 confocal laser scanning microscope (Zeiss).

3.2.6 Denaturing polyacrylamide gel electrophoresis (SDS-PAGE)

To separate proteins by their molecular weight, a SDS-PAGE (sodium dodecyl sulfate polyacrylamide gel elecotrophoresis) in a Bis-Tris polyacrylamide gel was performed.

The concentration of the separation gel was adapted to the molecular weight of the desired protein. The polyacrylamide concentration of a standard separation gel was 10 % (gel composition see section 3.1.5). After the liquid separation gel mix was casted in between two glass plates, it was carefully overlaid with deionized water to allow the polymerization of the separation gel without drying out. After polymerization, the deionized water was removed, a 6 % stacking gel was casted on top of the separation gel and a comb with 15 up to 25 pockets was inserted.

The glass plates were installed in an electrophoresis chamber (Peqlab gel), which was filled with the running buffer (1 x MOPS). Afterwards, in SDS sample buffer lysed samples were heated for 10 min at 95 °C and loaded into the pockets of the stacking gel. For the determination of the size of the respective protein bands, the Precision Plus Protein Standard (Biorad) was loaded. After the

electrophoresis chamber was connected to a water cooling system, the gels were run for about three hours at 180 V. Subsequently, the Bis-Tris polyacrylamide gel was washed with extra-dry buffer and the proteins were visualized via immunostaining by Western blotting.

3.2.7 Western Blotting

The separated proteins were transferred by Western blotting from a polyacrylamide gel onto a methanol activated PVDF-membrane (Millipore) by a semi-dry blotting system (Peqlab).
The arrangement in the semi-dry blotting system was as followed. On top of the lower with extra-dry buffer moistened anode plate were three layers of Whatman paper, which were soaked in extra-dry buffer, followed by the methanol activated and in extra-dry buffer washed PVDF-membrane, the polyacrylamide gel (washed in extra-dry buffer), another three layers of soaked Whatman paper and the cathode plate. A standard gel was blotted for 45 min at 400 A. After the electroblotting, the PVDF-membrane was blocked with 2.5 % milk in TBS-T for at least 30 min at RT in order to minimize unspecific binding of antibodies during immunodetection.

3.2.8 Immunodetection

After Western blotting and blocking, the PVDF-membrane was washed three times for 10 min in PBS-T at RT. The respective primary antibody was diluted in TBS-T according to the supplier recommendation and the PVDF-membrane was incubated with the primary antibody solution on a shaker or alternatively on a rolling incubator overnight at 4 °C. On the next day, the membrane was washed thrice for 10 min in TBS-T at RT, followed by an incubation (RT, 2 h) with the appropriate secondary antibody, which was conjugated to a horseradish peroxidase. After the incubation with the secondary antibody solution, the PVDF-membrane was washed thrice with TBS-T. Finally, the Clarity Western ECL Blotting Substrates (Biorad) was applied to the membrane and the chemiluminescent was monitored with the Fusion FX7 system (Viber Lourmat).

3.2.9 Generation of recombinant rabies virus by reverse genetics (virus rescue)

Revers genetics enables the *de novo* generation of recombinant RABV from cDNA. The first rescue of RABV was described by Schnell et al. 1994 (Schnell et al., 1994). In the meantime, several improvements have been done (Buchholz et al., 1999; Ghanem et al., 2012). In the following, the RABV rescue system is described briefly.
A plasmid encoding for the viral cDNA and three “helper” plasmids containing a T7-promoter and an encephalomyocarditis virus (EMCV) internal ribosome entry site (IRES) element were transfected into BSR-T7 cells, which constitutively express the bacteriophage T7 RNA polymerase

(Buchholz et al., 1999). The T7 RNA polymerase transcribes the cDNA into an antigenome-like RNA. Further, it transcribes the helper plasmids into IRES containing helper genes encoding for the helper proteins N, P and L. The EMCV IRES of the helper gene transcripts is recognized by ribosomes, leading to the translation of the viral proteins N, P and L. The introduction of highly efficient self-processing ribozymes on the 5´-end and 3´-end of the viral cDNA generates an antigenome-like genome with an exact 5´-end and 3´-end, which is crucial for a successful rescue, since additional nucleotides especially on the 3´-end hinder the replication (Collins et al., 1991; De and Banerjee, 1993; Ghanem et al., 2012; Pattnaik et al., 1992). After the encapsidation of the antigenome by the nucleoprotein, the N-RNA complex serves as template for the L-P driven replication of the antigenome to the negative-sense RNA genome. Finally, the plasmid-expressed L-P complex transcribes all five viral proteins and thereby initiates the first infectious cycle (Ghanem et al., 2012).

3.2.9.1 Rescue of recombinant full-length SAD

For the generation of a recombinant full-length SAD by reverse genetics, 10 µg of the full-length cDNA, 5 µg pTIT-N, 2.5 µg pTIT-P and 2.5 µg pTIT-L were cotransfected in BSR-T7 cells by of $Ca_3(PO_4)_2$ transfection (day 2).

On day 5, the supernatant was purified by centrifugation (1800 rpm, 5 min, 4 °C) and added onto fresh BSR-T7 cells in a 6-Well (supernatant passage 1). Fresh GMEM 4+ was added onto the transfected BSR-T7 cells. On day 8, the supernatant passage 1 was fixed with 80 % acetone followed by staining for RABV N, to control if the rescue was positive. After a second supernatant passage was performed, the transfected BSR-T7 cells were detached by the addition of 1 mL Trypsin/EDTA. 750 µL of the cell suspension were transferred into a T25 cell culture flask containing 7.25 mL GMEM 4+. The remaining 250 µL were seeded into a fresh 6-Well (cell passage 1). On day 11, supernatant passage 2 and cell passage 1 were fixed with 80 % acetone and stained for RABV N to examine whether infectious virus was already in the supernatant passage 2, or if the virus spread in the transfected BSR-T7 cells. If the RABV N staining of supernatant passage 2 was positive, the 8 mL of the T25 cell culture flask were cleared of cell debris, aliquoted and stored at – 80 °C (rescue harvest 1; day 11) and GMEM 4+ was added to the T25 cell culture flask. Three days later, the supernatant was harvested, purified, and stored as described above (rescue harvest 2). After the viral titers of rescue harvest 1 and 2 were determined by titration, they were used for the stock production of the recombinant RABV.

The supernatant passages as well as cell passages were not performed, when the recombinant RABV expressed a fluorescent protein, since the fluorescent protein enabled directly the monitoring of success of the virus rescue.

3.2.9.2 Rescue of recombinant SAD ΔM eGFP

The RABV matrix protein is a multifunctional protein, which plays an important role in the balance of virus transcription and replication, RABV assembly and budding. Thus to generated an M gene-deficient SAD ΔM eGFP by reverse genetics, the deletion mutant has to be trans-complemented with M.

According to the standard protocol 10 µg of the viral cDNA encoding SAD ΔM eGFP and the three "helper" plasmids pTIT-N, pTIT-P and pTIT-L were cotransfected in BSR-T7 cells (see 3.2.9.1). On day 2 and 3 (24 h and 48 h post transfection), 2 µg pTIT-M were transfected into the BSR-T7 cells using FuGENE HD transfection. On day 7, the success of the rescue was monitored the eGFP expression by fluorescence microscopy. If the rescue was positive, the transfected BSR-T7 cells were detached by trypsinization, transferred into a T25 cell culture flask, and mixed with about 5 x 10^5 MG_{on}136 cells. After the cells settled down, the expression of the matrix protein and the glycoprotein, which are under the control of a tetracycline inducible promoter, were induced by the addition of 1 µg/mL doxycycline. On day 9, the medium was replaced by fresh GMEM 4+ that contained, in addition to 1 µg/mL doxycycline, 4 mg/mL Hygromycin B in order to eliminate the BSR-T7 cells. To remove the dead BSR-T7 cells, the medium was replaced on day 10 by a fresh Hygromycin B and doxycycline containing GMEM 4+. The spread of SAD ΔM eGFP in MG_{on}136 cells was monitored by fluorescence microscopy. As soon as the cell layer was completely infected, the supernatant was cleared of cell debris by centrifugation, aliquoted and stored at – 80 °C. After the titer was determined by titration on BSR-T7 cells, the rescue was used for the stock production of SAD ΔM eGFP on MG_{on}136 cells.

3.2.9.3 Rescue of recombinant SAD ΔG eGFP (SAD G)

The RABV glycoprotein is essential for cell attachment, receptor-mediated endocytosis and the pH-dependent release of the RNP-complex into the cytoplasm. In order to rescue an infectious recombinant G gene-deficient SAD (SAD ΔG eGFP), the virus has to be trans-complemented with the glycoprotein.

BSR-T7 cells were transfected according to the standard rescue protocol (see 3.2.9.1). 24 h and 48 h post transfection, the FuGENE HD transfection kit was used to transfect 2.5 µg pTIT-G into the transfected BSR-T7 cells. On day 7, the success of the rescue was checked by monitoring the eGFP

expression by fluorescence microscopy. If the rescue was successful, the transfected BSR-T7 cells were detached by Trypsinization, transferred into a T25 cell culture flask and mixed with 5 x 10^5 MG_{on}139 cells which express in contrast to MG_{on}136 cells more G than M. After the cells were settled down, the MG_{on}139 cells were induced with 1 µg/mL doxycycline. To kill the BSR-T7 cells, the medium was replace by doxycycline and 4 mg/mL Hygromycin B containing medium. On the next day the dead BSR-T7 cells were replaced by fresh doxycycline and Hygromycin B containing GMEM 4+. As soon as all cells were infected, the supernatant was purified of cell debris, aliquoted and stored at - 80 °C. The rescue was titrated on BSR-T7 cells and used to inoculate MG_{on}139 cells for the generation of the recombinant G gene-deficient SAD.

3.2.10 Virus stock production

In the following, the stock productions of full-length SAD, M gene-deficient SAD ΔM eGFP and G gene-deficient SAD ΔG eGFP (SAD G) are explained.

For the stock production of full-length SAD, 7.5 x 10^5 up to 1 x 10^6 BSR-T7 cells were seeded in a T25 cell culture flask. Two hours post seeding, after the cells settled down, BSR-T7 cells were infected with the virus rescue at a MOI of 0.01. Four days after infection, the supernatant (harvest 1) was replaced by fresh GMEM 4+ and the first harvest was purified from cell debris by centrifugation, aliquoted and stored at - 80 °C. On day 8, the supernatant was harvested, purified and aliquoted for a second time. The viral titers were analyzed by titration on BSR-T7 cells. If the recombinant virus was highly attenuated, the infected BSR-T7 cells were expanded into a T75 cell culture flask and the virus was harvested to a later time point. Furthermore, the virus supernatant was concentrated by an ultracentrifugation step (see section 3.2.15).

The M gene-deficient SAD ΔM eGFP and the G gene-deficient SAD ΔG eGFP (SAD G), were produced on doxycycline induced MG_{on}136 cells or MG_{on}139 cells. MG_{on}139 cells were induced already 4-6 h post infection with 1 µg/mL doxycycline, whereas MG_{ON}136 cells were induced 24 h post infection with 1 µg/mL doxycycline. Otherwise, the protocol was identical to the above described stock production of full-length SAD. Also the titrations were performed on BSR-T7 cells.

3.2.11 Titration of virus

In order to analyze the amount of infectious virus particles in the supernatant, the focus forming unit per mL (ffu/mL) was determined by titration.

First, 100 µL of an about 1.5 x 10^5cells/mL BSR-T7 cell suspension were seeded per 96-well. Two hours post seeding, the titration was performed. Therefore, frozen virus supernatants were thawed and a serial dilution consisting of seven 1/10 dilution steps ranging from 10^{-2} up to 10^{-8}

were prepared in GMEM medium. Finally, the BSR-T7 cells were infected in duplicates with 100 µL of each dilution including the non-diluted supernatant.
48 h post infection with full-length virus or 72 h after the infection with G gene-/M gene- deficient virus, the supernatant was discarded, the cells were fixed with chilled 80 % acetone and stained with Centocor, which is a FITC-conjugated antibody against RABV N. Subsequently, the cells were washed three times with PBS and the foci of the full-length virus infected cells or the infected single cells, which resulted from the infection with G gene-deficient SAD, were counted by fluorescence microscopy. Finally, the ffu/mL were calculated.

3.2.12 Fluorescence labeling of RABV positive cells

The following procedure was used for the evaluation of infectious virus titers and for visualization of RABV infected mESC-derived neurons.
First, the supernatant was discarded or in the case of neurons carefully aspirated, washed once carefully with PBS, once with chilled 80 % acetone and finally fixed with 80 % chilled acetone at 4 °C for 20 min. Afterwards, acetone was removed and the fixed cells were air dried for up to 30 min. Subsequently, the cells were incubated for two hours at 37 °C with the FITC Anti-Rabies Monoclonal Globulin (Fujirebio Diagnostics). Lastly, the FITC-conjugated antibody solution was aspirated, the cells were washed twice with PBS and evaluated by fluorescence microscopy.

3.2.13 Multistep growth curves

The growth kinetics of recombinant viruses were determined by a multistep growth curve. Therefore, 1 x 10^6 BSR-T7 cells, N2A cells or HEK293T cells were seeded per T25 cell culture flask. Two hours post seeding, the cells were infected with the recombinant virus at a MOI of 0.01. Four hours post infection, the cells were washed twice with the appropriate medium and finally covered with 8 mL medium. 4.5 h post infection the first sample was taken. Therefore, two 500 µL samples were taken, cleared from cell debris by centrifugation (1600 rpm, 4 °C, 10 min) and stored at - 80 °C. Afterwards 1 mL fresh medium was added to the cells. Further samples were taken 24 h, 48 h and 72 h post infection. At last, the virus titers were determined by titration.

3.2.14 Generation of SAD ΔG (EnvA)

To pseudotype SAD ΔG with the envelope protein of the avian sarcoma and leucosis virus (EnvA), BHK EnvA cells were seeded in a 10 cm dishes (5-10 plates). On the next day (day 2), the cells were infected with SAD ΔG (SAD G) at a MOI of one. Six hours post infection, the cells were washed thrice with GMEM 4+, followed by trypsinization (5 min at 37 °C) and subsequent inactivation of

Trypsin with GMEM 4+. The cell suspension was centrifuged (1600 rpm, 4 °C, 10 min), the cell pellet was resuspended in fresh GMEM 4+ medium and split 1/1.5. On day three, the cells were washed once with GMEM 4+. Another three days later (day 6) the supernatant was harvested and cleared from cell debris by centrifugation (1600 rpm, 4 °C, 10 min). Fresh GMEM 4+ medium was added onto the cells to enable a second harvest another three days later (day 9). To increase the virus titer, the virions were concentrated by an ultracentrifugation step.

3.2.15 Virion purification by ultracentrifugation

Virus purification via a 20 % Sucrose solution

Virions were purified and accumulated by ultracentrifugation. Therefore, 3.5 mL of a chilled 20 % Sucrose solution were overlaid with 12 mL of a cleared virus suspension, in a Beckman Coulter centrifuge tube. The tubes were transferred into chilled buckets. The ultracentrifugation was performed at 24000 rpm (104838 g), 2 h and 4 °C. Afterwards, the medium and the 20 % Sucrose were carefully aspirated and 100 µL of the desired medium or PBS was added. The pelleted virus was soaked for two hours up to overnight at 4 °C, before the virus pellet was resuspended by carefully pipetting up and down. The virus suspension was aliquoted and stored at – 80°C. Finally, the virus titer was determined by titration.

Virion purification via Sucrose cushion ultracentrifugation

For EM studies, the virions were purified via a sucrose cushion ultracentrifugation in order to remove debris and pellet the virions as gentle as possible. Therefore, a 1 mL of a 60 % sucrose solution was put under 4 mL of a 20 % sucrose solution, which was in turn overlaid with the cleared virus suspension in a Beckman Coulter centrifuge tube. The ultracentrifugation was performed at 24000 rpm, 2 h and 4 °C. Afterwards, exclusively the virion comprising intermediate layer was aspirated with a hollow needle. The virus suspension was aliquoted, stored at – 80 °C and the ffu/mL was determined by titration.

3.2.16 *Trans*-complementation of SAD ΔG

The *trans*-complementation assays of SAD ΔG were performed in HEK293T cells. To investigate the incorporation of the recombinant glycoproteins into the virus 1.5 x 10^6 HEK293T cells were seeded into a 10 cm dish. On the next day, 10 µg DNA/10 cm dish were transfected according to the PEI transfection protocol. 24 h post transfection, the cells were washed twice with DMEM 3+, followed by the infection with G gene-deficient virus at a MOI of one up to three. At 16 h post infection, the cells were washed once with DMEM 3+ and subsequently trypsinized (5 min, 37 °C).

After 5 min, the Trypsin was inactivated by the addition of DMEM 3+, the cells were pelleted (1600 rpm, 4 °C, 10 min) and split 1/1.5. 48 h post infection, the supernatant was cleared from cell debris and samples of the supernatant were taken and stored at - 80 °C to evaluate the infectious titer by titration. The remaining supernatant was undergone an ultracentrifugation step, in order to accumulate the virions. The pelleted virions were lysed in 100 µL lysis buffer and the incorporation of the glycoprotein into the virion was examined by SDS-PAGE, Western blotting and immunostaining. Further, to investigate the transfection efficiency as well as the expression of the recombinant glycoproteins, 1/10 of the transfected cells were lysed in lysis buffer and analyzed in parallel to the virion lysate by SDS-PAGE, Western blotting and immunostaining.

3.2.17 Sequencing of virus

In the following, the different steps to sequence a recombinant virus are listed.

3.2.17.1 RNA Isolation

500.000 BSR-T7 cells were seeded in a 6-well. Two hours post seeding, the cells were infected with virus at a MOI of 0.1. Two days post infection, the supernatant was aspirated, the cells were lysed in 350 µL RLT buffer with 1 % β-mercaptoethanol and stored at –80 °C. The RNA of the infected cells was extracted according to the RNeasy Mini Kit instruction manual.

3.2.17.2 Reverse transcription

The RNA was transcribed into cDNA using the Transcriptor Reverse Transcriptase kit (Roche). Therefore, 1 µg RNA was diluted in 6.6 µL RNAse free water and annealed with an adequate primer (0.3 M) for 10 min at 65 °C in a Thermocycler. After the annealing step, the samples were cooled down to 4 °C. Subsequently, 2 µL of the 5 x buffer, 0.25 µL RNAsin, 0.4 µL dNTPs (25 mM) and 0.25 µL RT were added and incubated for 30 min at 55 °C (cDNA polymerization), followed by heat inactivation of the reverse Transcriptase (5 min, 85 °C). Finally, the reaction mix was cooled down to 4 °C and the cDNA sample was stored at -20 °C.
At last, the cDNA was amplified by PCR with adequate primers, the PCR product was purified and analyzed by Sanger Sequencing, which was performed by GATC Biotech.

4 Results

4.1 Generation of an *in vitro* model to investigate RABV in neurons in a mouse free system

RABV is a highly neurotropic virus, which spreads from the site of infection along neurons of the PNS to the CNS. Nevertheless, most *in vitro* studies of RABV were performed in non-neuronal cells, neuroblastoma cell lines or neuroblastoma cells differentiated into neurons, while biochemical investigations of RABV in its natural target cells were missing. Therefore, an *in vitro* model for the investigation of RABV in neurons of the CNS is needed.

In this thesis, first, the cultivation of mESCs in a feeder-free culture system was introduced. Second, a highly reliable differentiation protocol of mESCs into glutamatergic pyramidal neurons was established. Pyramidal neurons exhibit a pyramidal or teardrop shaped soma, a single axon emerging from the base of the soma, multiple short basal dendrites and one large apical dendrite which connects the cell body with a tuft of dendrites (Spruston, 2008). They are found in the cerebral cortex, hippocampus, and amygdala (Spruston, 2008). Since RABV infects pyramidal neurons of cortex and hippocampus, the mESC-derived glutamatergic pyramidal neurons represent a perfect model to investigate RABV *in vitro* (Jackson and Fu, 2013).

4.1.1 Differentiation of mESCs into glutamatergic pyramidal neurons

The following feeder-free mESC culture system and neuronal differentiation protocol of mESCs to glutamatergic pyramidal neurons is based on published data (Bibel et al., 2004; Garcia et al., 2012a; Silva et al., 2008) and the consulting of Fabio Spada (LMU, Department of Chemistry and Pharmacology).

The protocol was performed with mouse strain 129/SvJ mESCs and its transgenic ROSA-tom-R-I-TVA mESCs, which were provided by Benjamin Arenkiel (Baylor College of Medicine, Houston, Texas, US). During the whole process, the mESCs were cultured at 37 °C and 5 % CO_2.

The workflow for the differentiation of mESCs into glutamatergic pyramidal neurons is depicted in Figure 6.

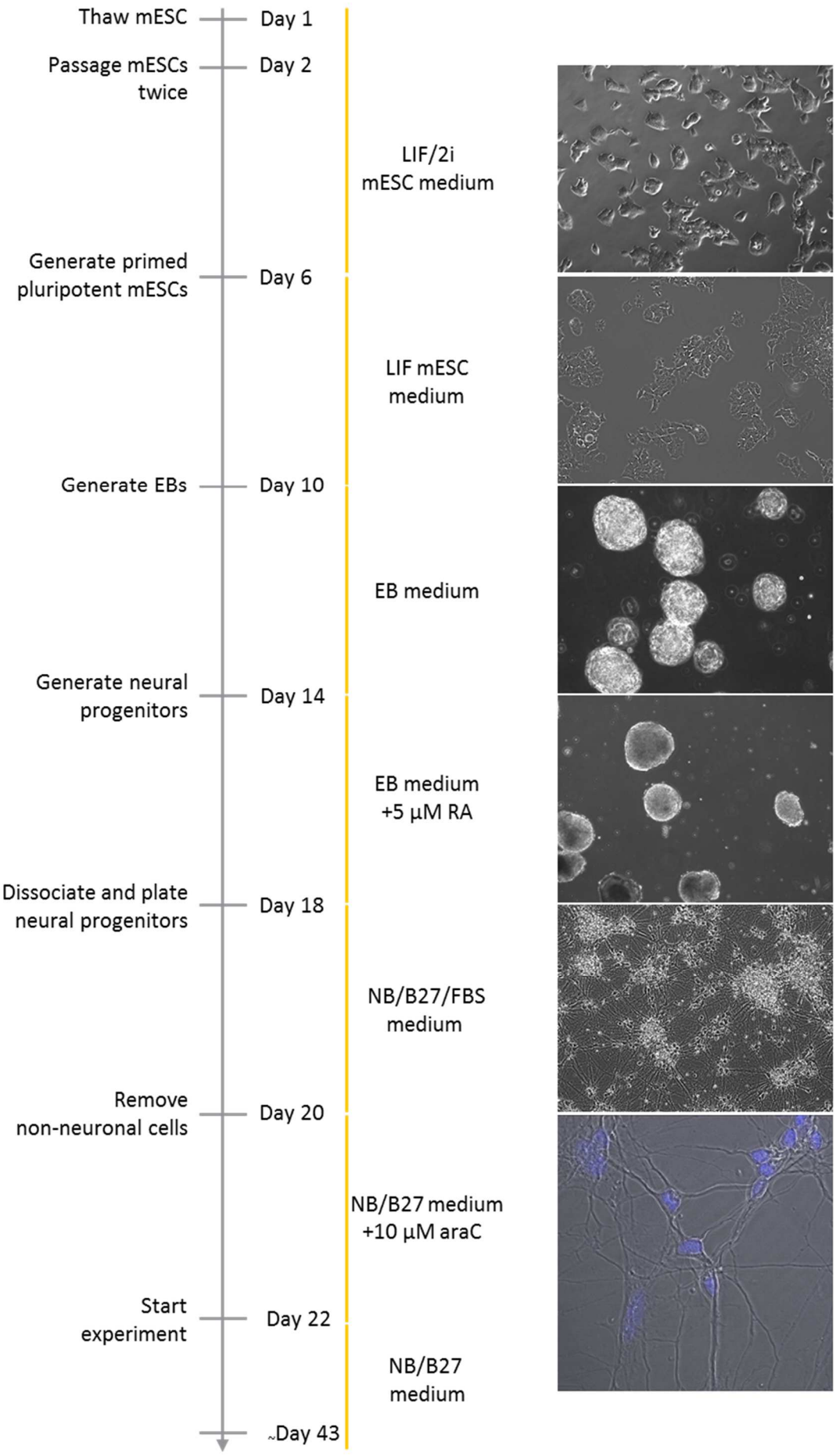
Thaw mESC
Day 1
Passage mESCs twice
Day 2
LIF/2i mESC medium
Generate primed pluripotent mESCs
Day 6
LIF mESC medium
Generate EBs
Day 10
EB medium
Generate neural progenitors
Day 14
EB medium +5 µM RA
Dissociate and plate neural progenitors
Day 18
NB/B27/FBS medium
Remove non-neuronal cells
Day 20
NB/B27 medium +10 µM araC
Start experiment
Day 22
NB/B27 medium
~Day 43

Figure 6: Differentiation of mESCs into glutamatergic pyramidal neurons.
The workflow of the differentiation process is depicted schematically, including the particular medium and representative photographies of each differentiation state. The last photography shows fixed mESC-derived neurons, stained with To-Pro3 and monitored by confocal laser scanning microscopy.

4.1.1.1 Feeder free mESC culture system

Freshly thawed mESCs were cultured for two passages (Figure 6 day 1-6) in LIF/2i mESC medium before the differentiation was started (section 3.2.2.2). Briefly, LIF leads to the receptor-mediated stimulation of JAK and the activation of the transcription factor STAT3 and thereby supports the self-renewal of mESCs (reviewed in (Nichols and Smith, 2012; Ying and Smith, 2017)). In addition to LIF, two inhibitors (2i) were added to the medium. One of the inhibitors is CHIR99021, which inhibits GSK3 of the Wnt signaling pathway, thus stabilizes β-Catenin that interacts in the nucleus with the repressor Tcf3, dissociates the repressor from its DNA binding site and leads therewith to the transcription of pluripotency factors (reviewed in (Nichols and Smith, 2012)). The other inhibitor is PD0325901, which inhibits the ERK pathway by blocking MEK1/2 and thereby blocking the differentiation of the naive pluripotent mESCs (Van der Jeught et al., 2013; Ying and Smith, 2017). Even the 2i are sufficient to keep the mESCs in the naive pluripotent state by blocking the differentiation pathways and conserving the intrinsic metabolic and proliferative program of the mESCs, the combination of LIF and 2i leads to an even better clonal propagation of the naive pluripotent mESCs (reviewed in (Ying and Smith, 2017)). The resulting mESCs formed characteristic round, dome-shaped colonies, which represented the inner cell mass-like pluripotent state (Figure 7A). The LIF/2i mESC medium was replaced approximately 30 h post splitting and the mESCs were split every 48 h (Hanna et al., 2010; Park et al., 2013).
The pluripotency of the cultured mESCs was confirmed by immunostaining for the pluripotency marker Oct4. Filamentous actin was stained with CytoPainter Phalloidin-iFluor 555 in order to discriminate the different single cells in the cell cluster. The nuclei were stained with To-Pro3 (Figure 7A). The mESCs formed clusters exhibited the characteristic small diameter between 10-12 µm, a big nucleus, only little cytoplasm and were Oct4 positive (Totey, 2009; Zeineddine et al., 2014).

4.1.1.2 "Priming" of naive pluripotent mESCs

To make the naive pluripotent mESCs susceptible for the differentiation, they have to be converted into mouse epiblast stem cells (mEpiSCs), also named primed pluripotent stem cells (Nichols and Smith, 2009). The transformation of naive pluripotent mESCs into primed pluripotent stem cells was induced by the withdrawal of the 2i and the cultivation of the cells for two passages

in LIF mESC medium (Figure 6 day 6-10). To examine whether the mESCs transformed into primed pluripotent stem cells, the cell morphology, and the Oct4 expression were investigated by microscopy (Figure 7A). The primed pluripotent stem cells grew in a characteristic flattened monolayer, the diameter of the cells increased, the nucleus to cytoplasm ratio was still large (as it is in mESCs) and the cells were still Oct4 positive. These observations indicated that the naive pluripotent mESCs were transformed successfully into mEpiSCs (Nichols and Smith, 2009).

4.1.1.3 Formation of embryoid bodies

The next step of the differentiation is the transformation of the mEpiSCs to embryoid bodies (EBs). Therefore, three million mEpiSCs cells were seeded into a specific non-adhesive 10-cm petri dish (Greiner cat. no. 633102). The non-adhesive petri dish enabled mEpiSCs to float and thus allowed the formation of EBs, which had still the potential to differentiate into one of the three germ layers (Rungarunlert et al., 2009). The EBs were cultured in 15 mL EB medium per 10 cm petri dish, since previous experiments had shown that smaller volume caused attachment and unspecific differentiation of EBs. On day 12, the floating two days old EBs (EBI) were selectively transferred with a 25 mL pipette into a 50 mL reaction tube. The EBs were passively settled down for 5 min at RT, the supernatant was aspirated, EBs were carefully resuspended in prewarmed EB medium with a 10 mL pipette by pipetting up and down twice and finally split 1/2 up to 1/4 with prewarmed EB medium into a fresh non-adhesive 10-cm petri dish.
On day 14, the differentiation process was only proceeded with plates in which less than 10 % of the four days old EBs (EBII) attached to the dish. Since attached cells were considered unspecifically predifferentiated, a high number of them would have resulted in neuronal cultures with a high content of non-neuronal cells. Exclusively the floating EBs were split 1/1 up to 1/4, as described above.

4.1.1.4 Transformation of EBs to neurospheres

The transformation of the four days old EBs into neurospheres was induced on day 14 by the supplementation of the EB medium with 5 µM retinoic acid (RA). RA is a morphogenic and teratogenic compound, which induces differentiation *in vitro*. All-trans RA activates a retinoic acid receptor (RAR), which is a ligand-dependent transcription factor. After activation, RAR binds to a retinoic acid response element and leads to the transcription of target genes (Rohwedel et al., 1999). Most likely, all-trans RA induces the transcription of Wnt antagonist Dickkopf-1, which blocks the Wnt signaling pathway and induces neural differentiation (Xu et al., 2012).

RA treated cells were handled as far as possible under the exclusion of light, to avoid the metabolization of cis-retinoic acid, which binds in addition to RARs also to retinoic acid X receptors (RXRs), probably leading to the transcription of unwanted target genes (Rohwedel et al., 1999).
On day 16, the all-trans RA-treated neurospheres (NSI) were, dependent on their cell density, split 1/1 up to 1/3 into a fresh non-adhesive 10-cm petri dish, followed by a second round of treatment with 5 µM RA for another 48 h (NSII).
To monitor the transition of EBs to neurospheres, an immunostaining for the pluripotency marker Oct4 and the neural progenitor marker Nestin was performed (Figure 7B). The size of the spherical cluster doubled at least from EBI to NSII. The Oct4 staining was in the periphery of EBI cluster as well as in NSII cluster, more prominent than in the center, but there was no big difference in the fluorescence intensity of Oct4 in EBI or NSII, indicating that the pluripotency marker was expressed in both differentiation states equally. However, the staining with the neural progenitor marker Nestin increased tremendously from EBI to NSII. These observations indicated that the RA driven transformation of embryoid bodies to neurospheres was successful.

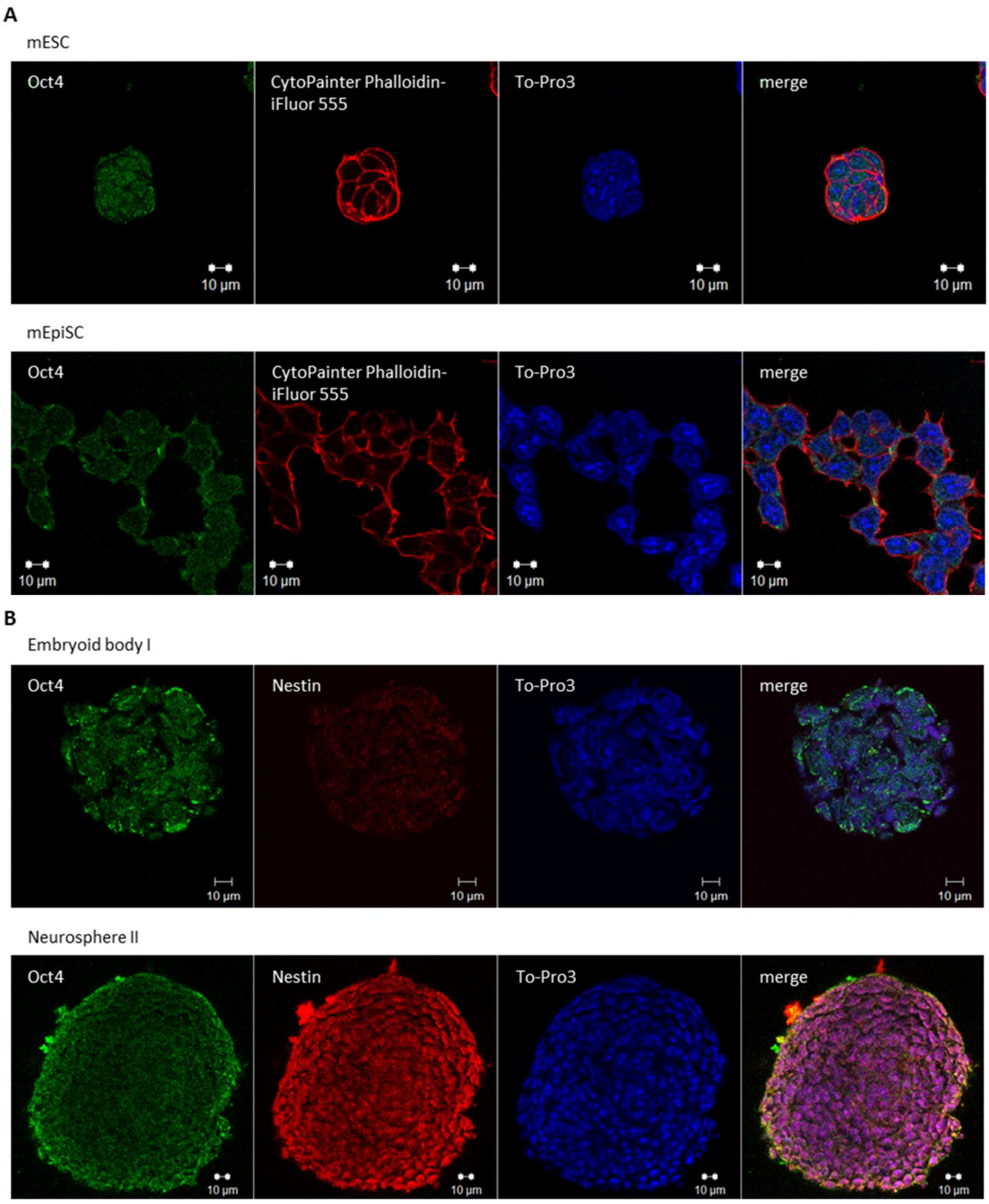

Figure 7: Characterization of naive pluripotent mESCs, mEpiSCs, EBs and neurospheres.

The cells were stained with the indicated markers and examined by confocal laser scanning microscopy. **A**, mESCs and mEpiSCs were stained with the pluripotency marker Oct4, the actin marker CytoPainter Phalloidin-iFluor 555, and the nucleus marker To-Pro3. **B**, Two days old EBs (EBI) and four days old neurospheres (NSII) were stained with Oct4, the neural progenitor marker Nestin and To-Pro3.

4.1.1.5 Differentiation of neurospheres to glutamatergic pyramidal neurons

The success and efficiency of the differentiation depends on the quality of the neurospheres. Small and dark neurospheres were considered nonspecifically predifferentiated and unusable. Hence, only plates with less than 10 % attached neurospheres, containing large neurospheres with a bright or only slightly dark center were used for the differentiation.

One day before differentiation, the desired amount of plastic dishes were coated with 0.1 mg/mL PDL and glass-bottom dishes were coated with 1 mg/mL PDL overnight at 37 °C. On the next morning (day 18), the aqueous PDL solution was aspirated and the plates were carefully washed with water twice. After the second wash step, PBS was added and the plates were stored at 37 °C. On day 18, the neurospheres were passively settled down, the old medium was aspirated and the four days old all-trans RA treated neurospheres were dissociated chemically by incubating the cell pellet with 1 mL Stem Pro Accutase for 5 min at 37 °C, followed by an additional mechanical dissociation step. Therefore, the Stem Pro Accutase treated cells were pipetted up and down 15-20 times with a 1000 µL pipette while it was ensured that the pipette tip was very close to the bottom of the reaction tube and no bubbles were produced. The milky 1 mL cell suspension was diluted in 9 mL prewarmed EB medium, followed by centrifugation (RT, 160 g and 5 min). The pelleted cells were resuspended in prewarmed Neurobasal/B27/FBS medium and the remaining cell clusters were removed by filtration of the cell suspension through a 40-µm Nylon cell strainer. Since only single neurosphere cells result in an efficient differentiation, the dissociation of the neurospheres represents a crucial step during the differentiation.

A suspension with the desired cell concentration was prepared (in most cases 6 x 10^5 cells/mL as the ideal volume in a 12-Well is 1 mL), followed by the aspiration of PBS from the PDL coated dishes, and seeding of 1.5 x 10^5 cells per cm^2 into the dishes. Two hours post seeding the medium was carefully exchanged.

While FBS is essential for the differentiation of neurons during the first two days (at least in our system), it causes the differentiation of non-neuronal cells. For the elimination of non-neuronal cells, the Neurobasal/B27/FBS medium was replaced by Neurobasal/B27/10 µM ara-C medium. The withdrawal of FBS in combination with the application of ara-C, which is a pyrimidine nucleoside analog, kills exclusively dividing cells. The Neurobasal/B27/10 µM ara-C medium was replaced after 48 h by Neurobasal/B27 medium. Finally, an almost pure ready-to-use culture of glutamatergic pyramidal neurons was generated. In order to conserve the neuronal network, only 50 % of the medium were renewed every second day. By this treatment, the neuronal network survived up to three weeks.

4.1.1.6 Characterization of mESC derived neurons

To characterize the mESC-derived neurons, immunostainings for a neuronal marker, an axonal marker, a dendritic marker, and a marker for the postsynaptic density were performed (Figure 8A). The staining for the neuronal marker β-III Tubulin revealed that the cells were differentiated into neurons. The costaining for the dendritic marker MAP2 and the axonal marker NF-H demonstrated the existence of a neuronal network that is composed of axons and dendrites (neurites). Moreover, as the staining was not overlapping, it could be concluded that the protein sorting of axonal and somatodendritic proteins was strict. The costaining of MAP2, To-Pro3 and PSD-95 revealed a teardrop-shaped soma with one apical dendritic tree and several basal dendritic trees. This morphology, in combination with the PSD-95 staining strongly suggests that this are the desired glutamatergic pyramidal neurons ((Sheng and Kim, 2011; Spruston, 2008; Tiffany et al., 2000; Vyas and Montgomery, 2016).

Next, it was examined whether the mESC-derived neurons form functional synapses. Since RABV propagates exclusively via chemical synapses, the virus was used to confirm that the neurons were connected this way (reviewed in (Ugolini, 2011)). Hence, neurons were infected with SAD mCherry at a MOI of 0.0001. At 24 h post infection, only single infected neurons were detected. Already 48 h post infection, multiple synaptically connected neurons were infected, indicating that SAD mCherry infected neighboring cells via transsynaptic spread (Figure 8B).

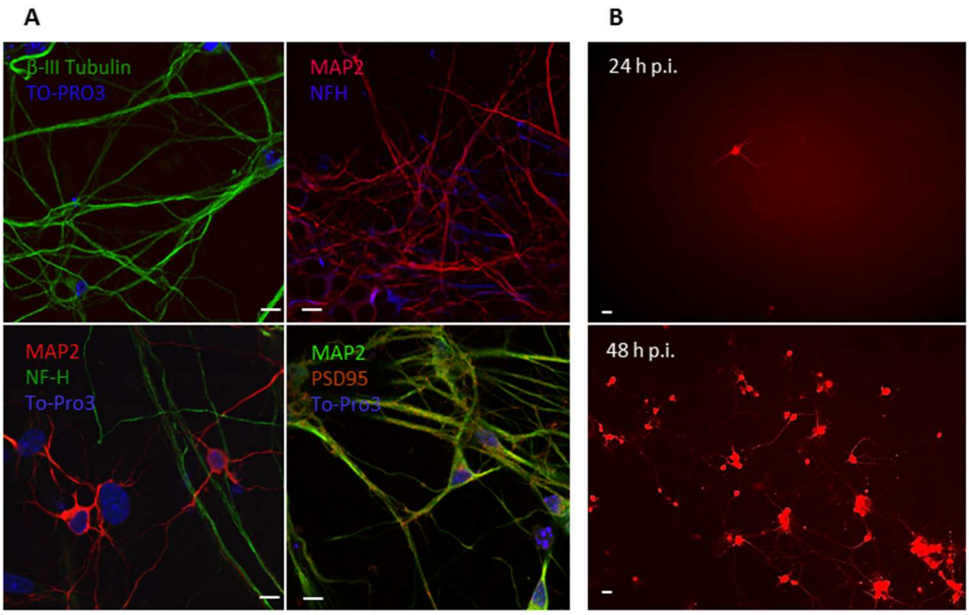

Figure 8: Characterization of mESC-derived glutamatergic pyramidal neurons.
A, Fixed mESC-derived neurons were stained the neuronal marker β-III Tubulin, the dendritic marker MAP2, the axonal marker NF-H, the postsynaptic density marker PSD95 and To-Pro3 and subsequently investigated by confocal laser scanning microscopy. The white scale bar represents 10 µm. **B**, mESC-derived neurons were infected with SAD mCherry at a MOI of 0.0001. RABV spread was examined to the indicated time points by monitoring the expression of virus encoded mCherry. The white scale bar represents 100 µm.

4.1.2 Generation of an *in vitro* model to study the monosynaptic spread of RABV

RABV is a neurotropic virus, which is used for retrograde poly-transsynaptic tracing (Astic et al., 1993; Kelly and Strick, 2000). By using a glycoprotein gene-deficient RABV (RABV ΔG) that is pseudotyped with the envelope protein of the avian sarcoma and leucosis virus (EnvA), a defined TVA-expressing starter cell can be infected. The *in situ* trans-complementation of RABV ΔG with the RABV glycoprotein enables the spread of RABV ΔG to monosynaptically connected neurons, resulting in the retrograde monosynaptic tracing model, which is a milestone in revealing neuronal circuits *in vivo* and in explanted tissue (Wickersham et al., 2007a; Wickersham et al., 2007b) (reviewed in (Callaway and Luo, 2015)).

However, there is no mouse free *in vitro* model described to study monosynaptic spread of RABV in a pure cell culture system.

Using gene targeting, Garcia and colleagues generated the transgenic 129/SvJ ROSA-tom-R-I-TVA mESCs (Garcia et al., 2012a). As the name indicates, the DNA construct is targeted to the ROSA26 locus. The DNA construct consists of an EF1α promoter, followed by a tdTomato reporter that is fused to a self-cleaving P2A peptide, followed by a G gene. The G sequence is followed by an IRES, a Neomycin resistance gene, a second IRES and finally a TVA gene. The organization of that DNA construct results in a simultaneously expression of all four genes (Figure 9A) (Garcia et al., 2012a).

Like the parental 129/SvJ mESCs, the transgenic ROSA-tom-R-I-TVA mESCs were cultured, primed, transformed to EBs and induced by RA to form neurospheres. After the neurospheres were dissociated chemically and mechanically, 99.9 % of the parental 129/SvJ were mixed with 0.1 % of dissociated transgenic ROSA-tom-R-I-TVA neurospheres. That resulted in a neuronal network in which one neuron of 1000 neurons was permissive for the infection with an EnvA pseudotyped G-gene deficient virus.

A model of the retrograde monosynaptic tracing is depicted in Figure 9B.

To investigate if the mixed population of neurons fulfilled the requirements for a reliable mono-transsynaptic spread model, it was examined whether (I) SAD ΔG eGFP (EnvA) exclusively infected tom-R-I-TVA neurons, (II) the starter cells provided sufficient glycoproteins for the *trans*-complementation of SAD ΔG eGFP and (III) the transgenic ROSA-tom-R-I-TVA neurons formed chemical synapses with the parental 129/SvJ neurons.

Thus, a neuronal mix population was infected with SAD ΔG eGFP (EnvA) at a MOI of one. At 24 h post infection, SAD ΔG eGFP (EnvA) infected exclusively the TVA expressing starter cells, since all eGFP positive cells were also tdTomato positive, leading to yellow starter cells. At 48 h post infection, next to 22 yellow starter cells, 64 exclusively green neurons, which represent the monosynaptically connected second order neurons, were detected in the representative photography. As expected, in a population of only parental neurons, which were infected with SAD ΔG eGFP (EnvA) at a MOI of one, no green cell could be detected, even 48 h post infection (Figure 9C).

Taken together, these data indicate that SAD ΔG eGFP (EnvA) exclusively infected TVA expressing transgenic neurons. It was further shown that tom-R-I-TVA neurons expressed sufficient G proteins for the *trans*-complementation of SAD ΔG eGFP and that chemical synapses were formed between the transgenic tom-R-I-TVA and the parental 129/SvJ cells. Hence, a solid mouse free *in vitro* system was established for the investigation of the monosynaptic spread of RABV.

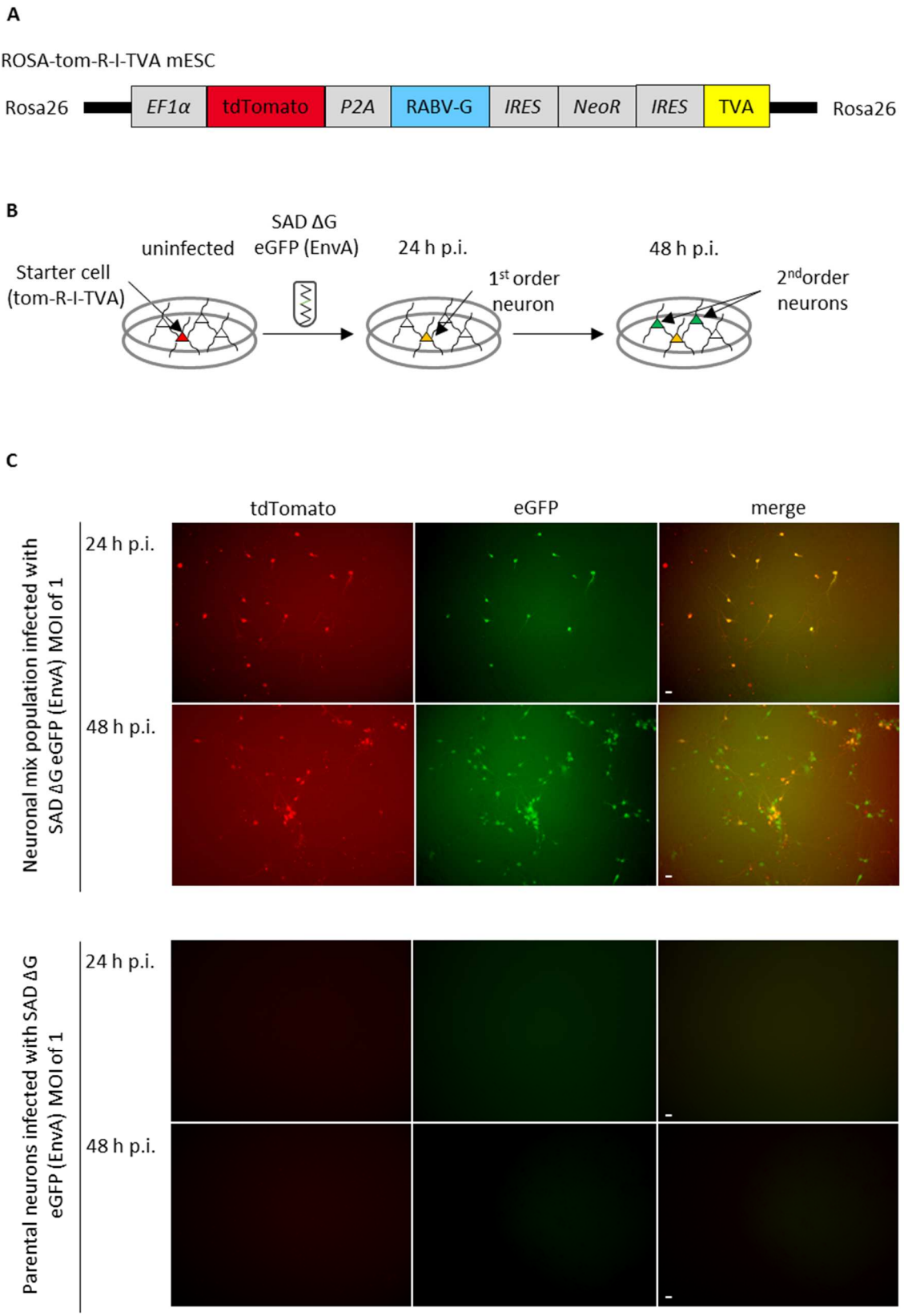

Figure 9: monosynaptic tracing in mESC-derived neurons.

A, Schematic representation of the Rosa26 locus of the transgenic ROSA-tom-R-I-TVA mESCs. **B,** Sketch of the monosynaptic tracing model in a neuronal mix population (detailed described in section 2.1.7). **C,** A neuronal mix population consisting of 99.9 % 129/SvJ and 0.1 % tom-R-I-TVA neurons and a neuronal culture

of only parental neurons were infected with of SAD ΔG eGFP (EnvA) at a MOI of one. The eGFP fluorescence and the tdTomato fluorescence were monitored at the indicated time points. In the upper two rows, photographies of the infected neuronal mix population and in the lower two rows, photographies of the infected parental 129/SvJ neurons are depicted. The white scale bar represents 250 µm.

4.2 Transsynaptic spread of RABV

RABV is a neurotropic virus, which spreads in the nervous system exclusively via chemical synaptic connections. In this thesis, mESC-derived glutamatergic pyramidal neurons were used as an appropriate mouse free *in vitro* model, to study the neuronal transfer of RABV.

4.2.1 Role of RABV M in transsynaptic spread

In 1999, Mebatsion and colleagues have shown in BSR cells that the RABV matrix protein is crucial for the assembly and budding RABV, since an M gene-deficient RABV was unable to bud of the cell membrane, leading to a 500,000-fold reduction in cell-free infectious virus titers (Mebatsion et al., 1999). However, the role of the matrix protein in neuronal transfer of RABV is still unknown.
To enable a direct detection of SAD ΔM infected cells by fluorescence an M gene-deficient, and eGFP encoding recombinant SAD was generated (Figure 10A).

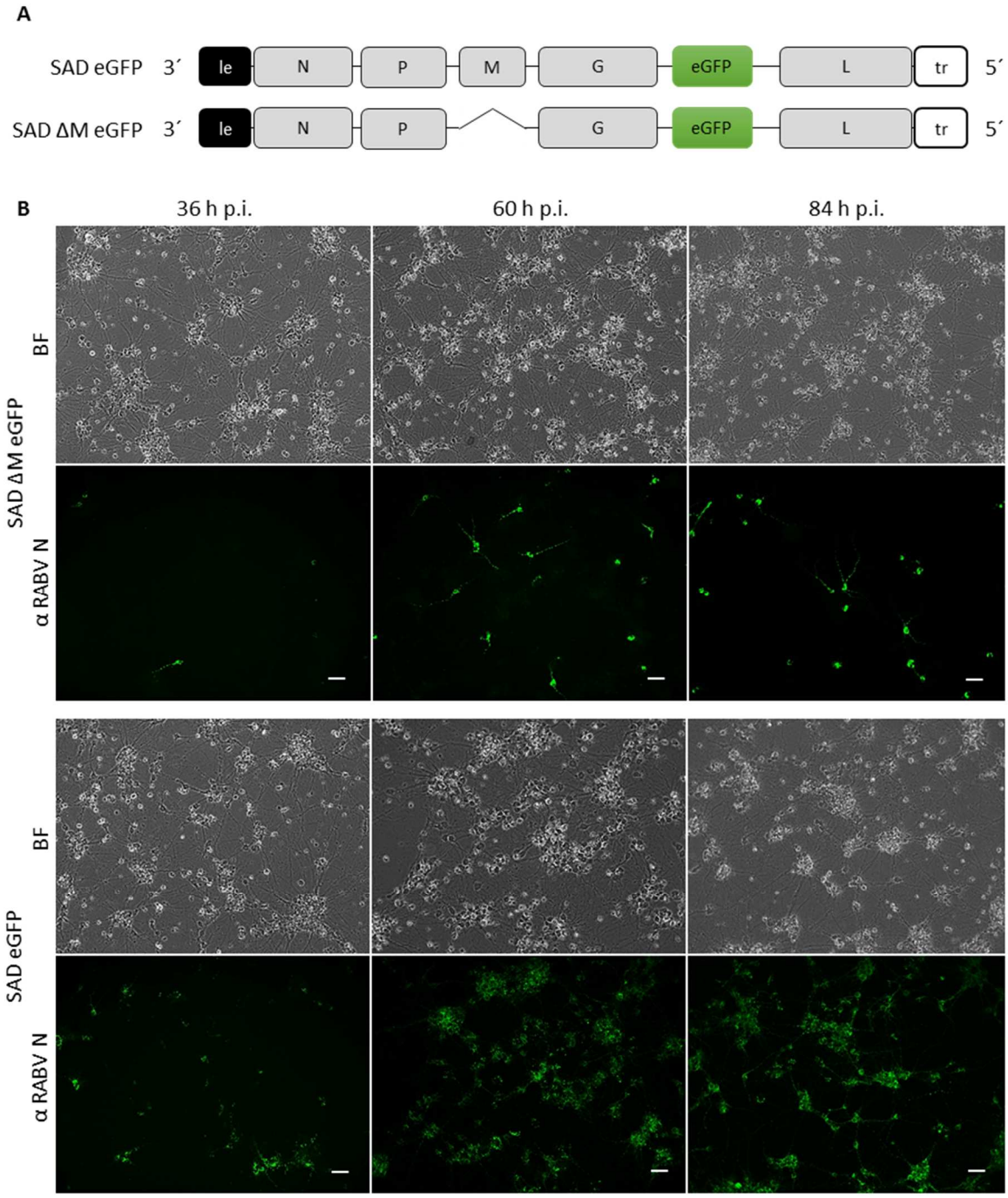

Figure 10: The neuronal transfer of RABV is dependent on the matrix protein.

A, Schematic representation of the genome of SAD eGFP and the M-gene deficient SAD ΔM eGFP. **B,** mESC-derived neurons were infected with SAD eGFP and SAD ΔM eGFP at a MOI of 0.001. The infected neurons were fixed and stained for RABV N protein at the indicated time points. BF represents the bright field images. The white scale bar represents 100 µm.

After the successful generation of SAD ΔM eGFP by reverse genetics, it was investigated whether the matrix protein is crucial for the transsynaptic spread of SAD. Therefore, mESC-derived neurons were infected with SAD eGFP or SAD ΔM eGFP at a MOI of 0.001. The infected neurons were fixed with chilled 80 % acetone 36 h, 60 h or 84 h post infection. Finally, the neurons were stained for

RABV N. In contrast to SAD eGFP, SAD ΔM eGFP exhibited a severe defect concerning the neuronal transfer, since the M gene-deficient virus hardly infected synaptically connected neurons, even 84 h post infection. This indicates that the matrix protein plays also in neurons a crucial role for RABV budding and thus for the neuronal transfer of RABV (Figure 10B).

4.2.2 Role of the ESCRT machinery in the neuronal transfer of RABV

The ESCRT machinery has numerous cellular functions like the biogenesis of MVBs or the protein sorting from the endosome to the lysosome and cytokinesis. Furthermore, several enveloped virus utilize the ESCRT machinery for virus budding. The interaction between a component of the ESCRT machinery and a viral protein is mediated by a late domain (Votteler and Sundquist, 2013). The RABV matrix protein contains two late domains, which are overlapping. Wirblich and colleagues demonstrated that the ^{38}YVPL^{41} motif had no effect on RABV spread, whereas the disruption of the ^{35}PPEY^{38} motif led to an approximately 100-fold reduction of viral titers in a single step growth curve in NA cells and BSR cells (Wirblich et al., 2008).

With the aim of analyzing the role of the ^{35}PPEY^{38} motif in the transsynaptic spread of RABV, I used the two recombinant matrix proteins M34AAA and M35AA. In M34AAA three prolines, including the proline in front of the late domain (P34) were replaced by alanines and in M35AA only the two prolines of the late domain were substituted by alanines.

First, it was examined which late domain mutant has the biggest negative impact in terms of the budding of RABV in HEK293T cells. Thus a *trans*-complementation assay of M gene-deficient SAD was performed. Since M regulates also the transition from transcription to replication, an overexpression of the matrix protein before the infection would inhibit the viral transcription and stimulate viral replication, before enough viral proteins and consequently enough RNPs are produced (Finke et al., 2003). Thus, HEK293T cells were infected first with SAD ΔM eGFP at a MOI of one. Three days post infection, the M gene-deficient virus was *trans*-complemented by transfecting M-wt, M35AA or M34AAA. Two days post transfection, the virus containing supernatants were harvested for an endpoint titration, and the cells were harvested in order to control the protein expression levels of the M variants by SDS-PAGE, Western blotting and immunostaining against M.

As illustrated in Figure 11A, M35AA and M34AAA were slightly better expressed than M-wt. The trans-complementation of SAD ΔM eGFP with M35AA resulted only in a modest reduction in virus release, whereas M34AAA caused a 10-fold reduction of infectious virus titers compared to M-wt. In comparison to the negative control, whose titer was only 100-fold reduced, the 10-fold reduction of M34AAA represents a solid effect. Interestingly, P34A appears to play an important role in RABV budding, even it is not part of the late domain motif.

To gain a deeper insight into the effect of the late domain mutant M34AAA on the release of RABV in non-neuronal cells and to study particularly the effect of M34AAA on the neuronal transfer of RABV, reverse genetics was used to generate the recombinant virus SAD M34AAA eGFP. As a control for the rescue, SAD eGFP was rescued in parallel. Interestingly, the rescue of SAD M34AAA eGFP resulted in an increased cell-cell fusion activity of the infected cells (Figure 11B), a phenotype which was previously described for SAD ΔM infected BSR cells (Mebatsion et al., 1999). Since the rescue of SAD M34AAA eGFP resulted in a very low titer, the stock production was performed on $MG_{on}136$ cells, which express M under the control of a Tetracycline regulated inducible promoter. The growth kinetics of SAD M34AAA eGFP were characterized by multistep growth curves in BSR-T7 cells, HEK293T cells and N2A cells in order to rule out a cell line dependent effect. In each cell line, SAD M34AAA eGFP exhibited a strong attenuation in the viral growth kinetics compared to SAD eGFP (Figure 11C). These data indicate, in agreement with the published data, that the spread of SAD was dependent on the late domain and the ESCRT pathway, albeit no total blockade of the virus release was detected. Remarkably, SAD M34AAA eGFP exhibited a 10-fold up to 100-fold stronger budding defect compared to the published phenotype of SPBN M35S (Wirblich et al., 2008), which is also a SAD strain, indicating that P34 plays an important role in virus release, although it is not part of the canonical PPEY late domain motif.

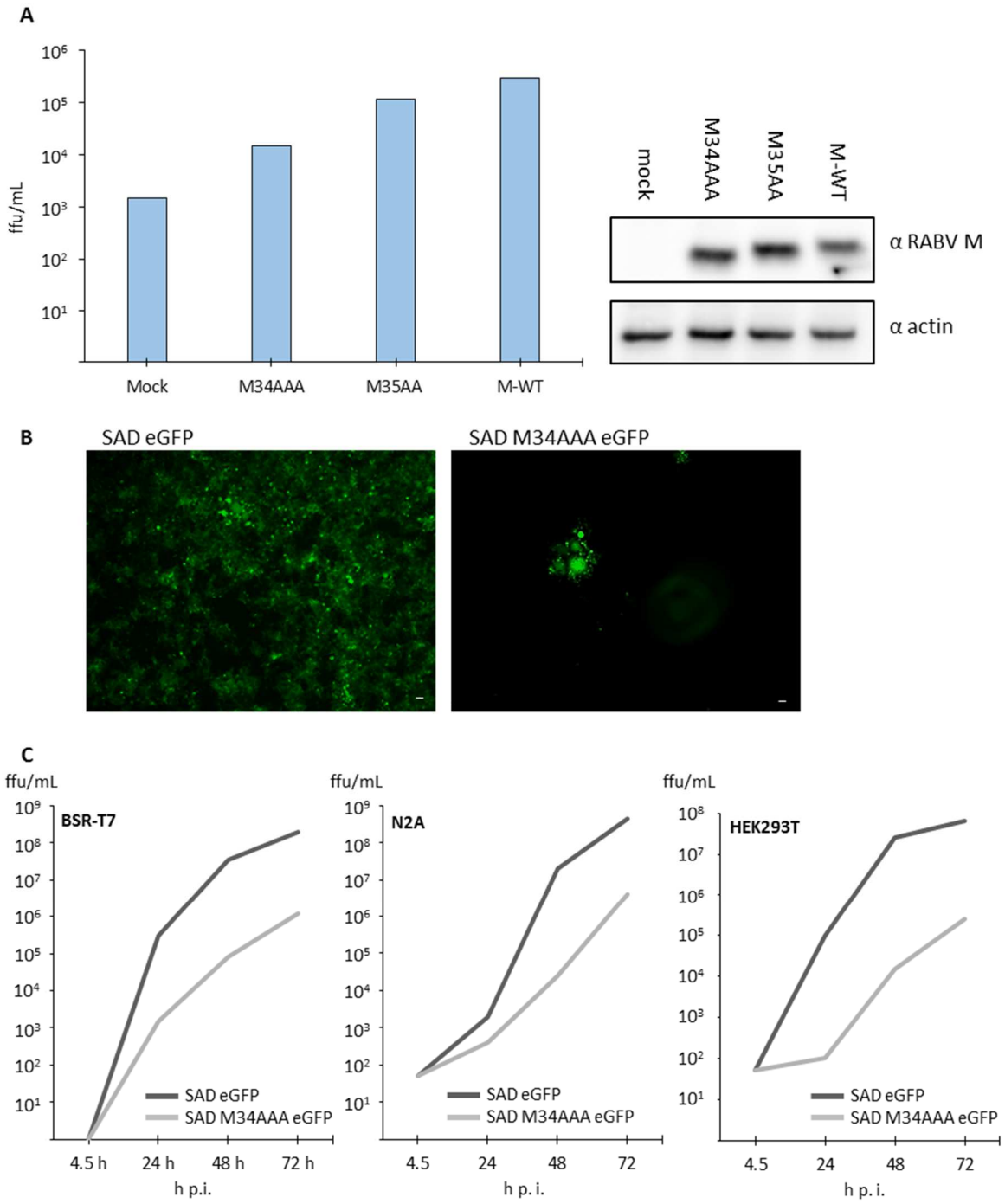

Figure 11: The budding of the late domain mutant M34AAA is more strikingly impaired than of M35AA.

A, Trans-complementation assay of SAD ΔM eGFP in HEK293T cells. HEK293T cells were infected with SAD ΔM eGFP at a MOI of one. Three days post infection the cells were transfected with the annotated M constructs. Another two days post transfection the supernatants were harvested and titrated on BSR-T7 cells. The protein expression levels of the M constructs were evaluated by SDS-PAGE, Western blotting and immunostaining for the indicated antibodies. **B**, Representative photographies of foci in BSR-T7 cells, which were taken five days post transfection of the rescue. The white scale bar represents 100 µm. **C**, Multistep growth curves of SAD M34AAA eGFP in comparison to SAD eGFP in HEK293T cells, BSR-T7 cells and N2A cells. The samples were taken to the indicated time points and titrated on BSR-T7 cells.

After confirmation of the budding defect of SAD M34AAA eGFP in non-polarized cell lines, it was investigated whether the disruption of the late domain also has an effect on the spread of SAD in mESC-derived neurons. Therefore, mESC-derived neurons were infected with SAD M34AAA eGFP and SAD eGFP at a very low MOI. At the indicated time points, one plate of neurons was fixed with chilled 80 % acetone and stained with Centocor for RABV N. Subsequently, the total number of RABV N positive neurons in a 12-well was evaluated. Note that the 44 h value of SAD eGFP infected neurons was determined by screening the entire well with 128 photos, since the virus already infected too many neurons. Because of that, single infected cells could be hardly directly identified. Thus, it might be that the total number of SAD eGFP infected neurons at 44 h p.i. is even higher. Already at 38 h p.i., SAD M34AAA eGFP infected 1.4-fold less neurons than SAD eGFP. At 44 h post infection, SAD eGFP infected at least two-fold more neurons compared to SAD M34AAA eGFP. The reduced neuronal transfer of SAD M34AAA eGFP suggests that the ESCRT system is involved in the neuronal spread of RABV. However, like in BSR-T7 cells, HEK293T cells and N2A cells, no total blockade of the RABV transmission could be detected.

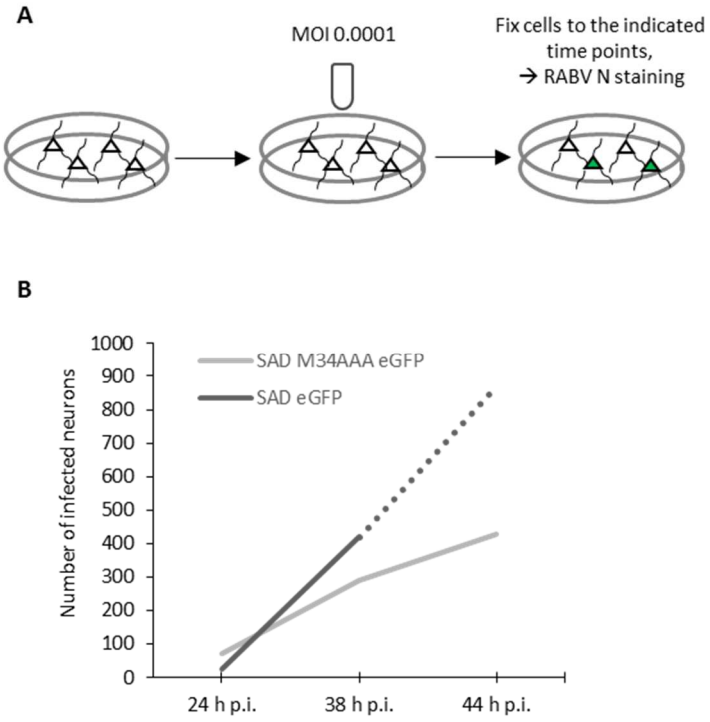

Figure 12: The ESCRT machinery is involved in the neuronal transfer of RABV.

A, Schematic illustration of the experimental setup to determine the neuronal transfer efficiency of recombinant RABV. mESC-derived neurons were infected with a very low MOI. The cells were fixed to the indicated time points, stained for RABV N and the number of infected cells was evaluated by fluorescence microscopy. **B**, Evaluation of the number of RABV N positive neurons to the indicated time points in an entire 12-well. The pointed line of SAD eGFP infected neurons indicates that the actual number of infected neurons for the 44 h p.i. value might be even higher, as this value represents the number of infected neurons in 128 photographies (objective 20x). For a detailed explanation see above.

The current knowledge of the impact of the late domain on RABV budding is based on SAD L16 and SPBN, which differs only in two restriction sites from SAD L16 (Schnell et al., 2000). SAD L16 is a recombinant clone of SAD B19, an attenuated vaccine strain that was adapted on BHK cells. It is unknown, whether the late domain in more neurotropic and virulent viruses, e.g. CVS-N2c, is as important as in the attenuated SAD virus. To address to the question, reverse genetics was used to replace SAD M by N2c M and N2c M34AAA, respectively, resulting in the chimeric SAD N2c M virus or SAD N2c M34AAA virus. Whereas rescue experiments for SAD N2c M resulted in titers of 10^7 ffu/mL already seven days post transfection, the titers of SAD N2c M34AAA were only in the range of 10^1 ffu/mL, indicating a severe budding defect of SAD N2c M34AAA. While the stocks of SAD N2c M were produced according to the standard protocol in BST-T7 cells, the SAD N2c M34AAA stocks were produced on $MG_{ON}136$ cells, in order to trans-complement the chimeric virus with SAD M.

The growth kinetics of SAD N2c M and SAD N2c M34AAA were examined by multistep growth curves in N2A cells and BSR-T7 cells. In both cell lines, SAD N2c M34AAA was attenuated compared to SAD N2c M. Interestingly, the level of attenuation between SAD N2c M and SAD N2c M34AAA was in a slightly smaller range than of SAD eGFP and SAD M34AAA eGFP (Figure 11A and Figure 13A).

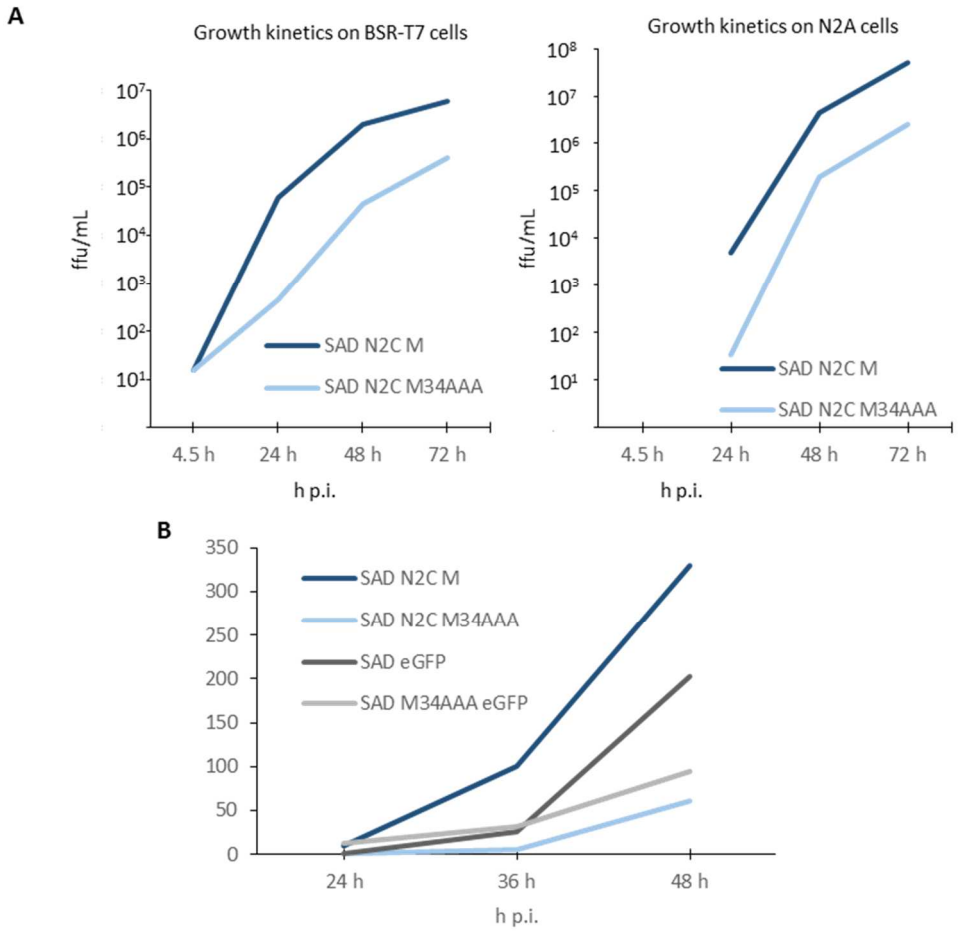

Figure 13: ESCRT-dependent budding of the chimeric SAD N2CM.

A, Multistep growth kinetics of the chimeric SAD N2c M34AAA in comparison to and SAD N2c M in BSR-T7 cells and N2A cells. The focus forming units per mL were determined on BSR-T7 cells. **B**, Evaluation of the transsynaptic spread of SAD, the chimeric SAD N2c M and their respective late domain mutants in mESC-derived neurons.

In order to investigate the effect of the disrupted late domain in the chimeric SAD N2c M on the neuronal transfer, mESC-derived neurons were infected with SAD eGFP, SAD eGFP M34AAA, SAD N2c M and SAD N2c M34AAA at a MOI of 0.00001. SAD N2c M spread much more effective than SAD eGFP (Figure 13B). Interestingly, the disruption of the late domain in N2c M protein caused a bigger attenuation of the virus in mESC-derived neurons than the disruption of the late domain in SAD M protein.

4.2.3 Role of the SNARE machinery in the transsynaptic spread of RABV

The data shown so far provide some evidence for an involvement of the M-late domain and the ESCRT system in the neuronal transfer of RABV. Nevertheless, the disruption of late domain does not completely block the neuronal spread of RABV.

SNARE proteins are essential for the attachment and fusion of vesicles in general. Further, specific SNARE proteins are essential for the fusion of synaptic vesicles with the presynaptic membrane and the resulting anterograde signal transmission. SNARE proteins are also located at the postsynaptic membrane, where they realize important tasks e.g. regulation of postsynaptic plasticity (reviewed in (Kennedy and Ehlers, 2011)). Since RABV spreads from a postsynaptic neuron to a presynaptic neuron by a transsynaptic spread, the SNARE machineries at the postsynaptic membrane might be involved in the budding and spread of RABV.

In the following, a potential involvement of SNARE proteins in the transsynaptic spread of RABV in mESC-derived neurons was investigated.

4.2.3.1 Effect of dominant-negative Syntaxin-1, -3 and -4 on the transsynaptic spread of RABV

The syntaxin family consists of 15 members but only syntaxin-1, that comprises two isoforms (A and B) (Bennett et al., 1992; Bennett et al., 1993), syntaxin-2, syntaxin-3, and syntaxin-4 are located at the plasma membrane (Hussain et al., 2016; Teng et al., 2001). By the deletion of the transmembrane domain, a dominant-negative syntaxin is produced, which still binds to its cognate SNARE complex, but is unable to drive the membrane fusion (Kennedy et al., 2010; Olson et al., 1997).

In 2010, Kennedy and colleagues published that the dendritic exocytosis of the glutamate receptor AMPA is dependent on syntaxin-4 during LTP (Kennedy et al., 2010). Three years later Jurado and colleagues published that not syntaxin-4, but syntaxin-3 is an essential Q-SNARE for the postsynaptic fusion machinery during LTP (Jurado et al., 2013). In 2016, Hussain and colleagues showed that syntaxin-1 is not only localized at the active zone but also at the opposite site of the synapse, at the PSD (Hussain et al., 2016). Taken together, syntaxin-4, syntaxin-3 and syntaxin-1 might be good targets to addressee to the question if the SNARE machinery plays a critical role in the neuronal transfer of RABV.

The investigation of the effect of the dominant-negative syntaxins in the transsynaptic spread of RABV faced two problems. First, mESC-derived neurons are hardly transfectable and second it had to be ensured that every RABV infected neuron expressed the dominant-negative syntaxin. To meet those requirements, recombinant viruses were generated by reverse genetics. These

recombinant viruses had an extra transcription unit that encodes for a dominant-negative human syntaxin with an N-terminal fluorescent tag (expression plasmid was kindly provided by Ehlers) (Figure 14). Additionally to viruses expressing individual dominant-negative variants of Stx1A, Stx3 and Stx4, a recombinant virus encoding for dominant-negative eGFPStx4 and dominant-negative Stx3 was generated.

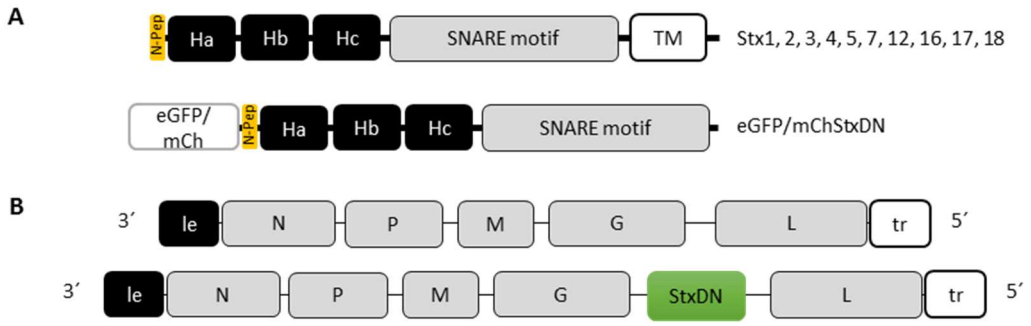

Figure 14: Schematic representation of N-terminal tagged, dominant-negative syntaxin and schematic representations of the genome organization of SAD with an extra transcription unit.
A, Schematic representation of the syntaxins is adopted from (Hong and Lev, 2014). Functional syntaxins consists of an N-terminal peptide (N-Pep) that interacts with SM proteins, a Habc region that can fold back onto its own SNARE motif (Rathore et al., 2010) and therewith leads to the closed conformation, a SNARE motif, and a transmembrane domain. The deletion of the transmembrane domain results in a dominant-negative syntaxin (StxDN). The StxDN constructs were fused N-terminally with a fluorescent tag (eGFP or mCherry) **B**, Schematic representation of a viral genome with an extra transcription unit encoding for StxDN.

Before SAD mChStx1ADN, SAD mChStx3DN, SAD eGFPStx4DN, SAD eGFPStx4DN/Stx3DN were analyzed in neurons, the recombinant viruses were characterized in cell lines.

To confirm the expression of the dominant-negative syntaxins by the recombinant virus, BSR-T7 cells were infected with the respective recombinant full-length virus at a MOI of 0.01. Three days post infection, the infected cells were lysed in SDS sample buffer and examined by SDS-PAGE, Western blotting and immunostaining. The infected cells expressed the respective dominant-negative, N-terminally tagged syntaxin of the correct size (Figure 15A). Note that SAD eGFPStx4DN/Stx3DN infected BSR-T7 cells expressed much more eGFPStx4DN than Stx3DN.

Subsequently, the growth kinetics of the recombinant dominant-negative syntaxin expressing viruses were investigated by a multistep growth curve in the neuroblastoma cell line N2A (Figure 15B). At 4.5 h post infection, titers were nearly identical, indicating that the cells were infected with the same amount of virus. At 24 h post infection, the biggest difference could be monitored. While SAD eGFP grew to a normal titer of 3 x 10^4 ffu/mL, the titer of SAD mChStx1ADN was 10-fold lower and SAD mChStx3DN, SAD eGFPStx4DN and SAD eGFPStx4DN/Stx3DN grew even 100-fold slower than SAD eGFP. However, the growth defect of SAD mChStx1ADN, SAD mChStx3DN and SAD eGFPStx4DN was compensated after 48 h and 72 h post infection, as they grew to nearly

the same titers as SAD eGFP. Only the recombinant virus coexpressing eGFPStx4DN and Stx3DN was 40-fold attenuated compared to SAD eGFP at 48 h post infection. At 72 h p.i., also SAD eGFPStx4DN/Stx3DN caught up and showed nearly the same titers as SAD eGFP. These data indicated that the expression of dominant-negative syntaxins has no big effect with respect to viral spread, at least in N2A cells.

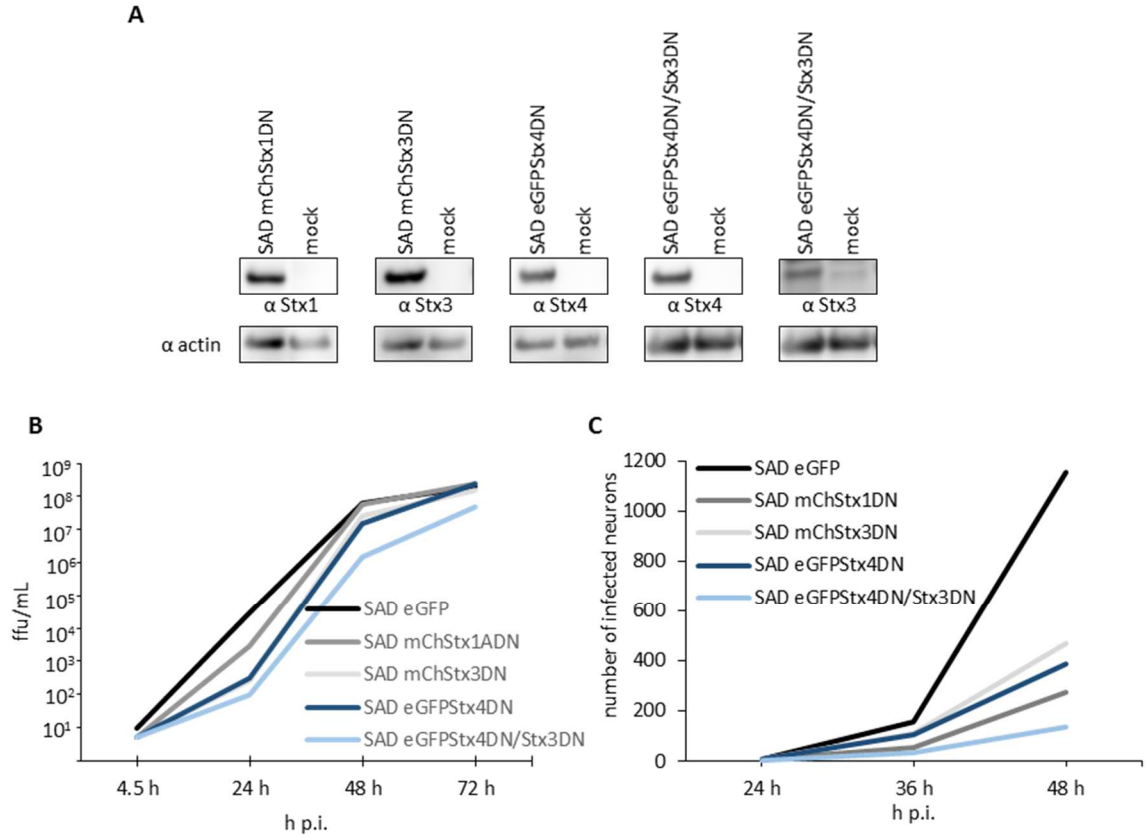

Figure 15*: Characterization of recombinant, dominant-negative syntaxin expressing RABV.*

A, BSR-T7 cells were infected with SAD mChStx1ADN, SAD mChStx3DN, SAD eGFPStx4DN, SAD eGFPStx4DN/Stx3DN at a MOI of 0.01. The cells were harvested at 72 h post infection and the cell lysates were subjected to SDS-PAGE, Western blotting and immunostaining for the indicated antibodies. **B**, Multistep growth curves for indicated recombinant viruses in N2A cells. The samples were taken to the indicated time points and titrated on BSR-T7 cells. **C**, mESC-derived neurons were infected with the indicated recombinant viruses at a very low MOI. The infected neurons were fixed to the indicated time points, stained for RABV N and the number of N positive neurons was evaluated.

The next step was to investigate, whether the dominant-negative syntaxins could prohibit or slow down the neuronal transfer of RABV in neurons. For this purpose, three plates of mESC-derived neurons, one plate for each time point, were prepared. The neurons were infected with SAD eGFP, SAD mChStx1ADN, SAD mChStx3DN, SAD eGFPStx4DN or SAD eGFPStx4DN/Stx3DN at a very low MOI, corresponding theoretically to six virus particles per neurons in a 12-Well. At 24 h, 36 h and 48 h post infection neurons were fixed and stained with Centocor for RABV N. While the number

of infected cells was counted in an entire 12-well at 24 h p.i., the 12-wells were screened with 43 photos (10 x objective) at 36 h p.i. and 48 h p.i. since SAD eGFP infected already too many neurons, which made the identification of single infected neurons by direct counting impossible.
The primary infected cells could be detected at 24 h p.i.. All five recombinant viruses led to the infection of four up to seven neurons and thereby confirmed that the neurons were infected with an equal MOI. After 36 h p.i. and 48 h p.i. the dominant-negative syntaxin expressing viruses infected less neurons compared to SAD eGFP (Figure 15C). Of the recombinant viruses encoding for a single dominant-negative syntaxin, SAD mChStx1ADN exhibited the strongest attenuation since it infected 4.2-fold less neurons than SAD eGFP at 48 hp.i.. SAD mChStx3DN and SAD eGFPStx4DN exhibited a moderate attenuation, as they infected 3-fold respectively 2.5-fold less neurons than SAD eGFP. Interestingly, at 48 h p.i. the recombinant SAD coexpressing eGFPStx4DN and Stx3DN infected even 8.5-fold less neurons than SAD eGFP and exhibited therewith the most striking decline regarding the neuronal transfer of SAD. These data indicate that the syntaxins play an important role in the neuronal spread of SAD.

4.2.3.2 Effect of neurotoxins on transsynaptic spread of SAD

Clostridium botulinum neurotoxins (BoNT/A-H) and tetanus neurotoxins (TeNT) are zinc metalloproteases, which hydrolyze specific peptide bonds of SNARE proteins and therewith inhibit the fusion of synaptic vesicles at the presynaptic membrane. However, CNTs are also active at the postsynaptic membrane. Therefore, CNTs may provide a good insight into the role of the SNARE machinery in the virus release and transsynaptic spread at the postsynaptic membrane.
The CNTs are heterodimers, which are composed of a heavy chain (HC) that is responsible for receptor binding and translocation of the light chain (LC) form the synaptic vesicle into the cytosol (Blum et al., 2014), and a light chain that harbors the metalloprotease activity.
To investigate the role of synaptobrevin-1/2 (VAMP1/2) and cellubrevin (VAMP3) in the transsynaptic spread of RABV in mESC-derived neurons, a recombinant G gene-deficient virus encoding for the LC of TeNT with an N-terminal eGFP-tag (GFP-TeNT-LC) was generated by reverse genetics (Figure 16A).
Before SAD ΔG eGFP-TeNT-LC was used in mESC-derived neurons, the proteolytic activity of eGFP-TeNT-LC was confirmed in N2A cells. N2A cells were infected with SAD ΔG eGFP-TeNT-LC at a high MOI. Two days post infection, the infected N2A cells were harvested and subjected a SDS-PAGE, Western blotting and immunostaining against Vamp3, eGFP and actin. As illustrated in Figure 16B, eGFP-TeNT was expressed and led to an effective cleavage of Vamp3 since no uncleaved Vamp3 could be detected.

In order to investigate the dependency of the transsynaptic spread of RABV on Vamp1, -2 and -3, the monosynaptic tracing *in vitro* model, which was established in this thesis, was used. The neuronal mixed population consisting of 99.9 % 129/SvJ cells and 0.1 % Tom-RITVA cells was infected with SAD ΔG eGFP-TeNT-LC (EnvA) or SAD ΔG eGFP (EnvA) at a MOI of 0.5. Four days post infection, the number of yellow neurons (starter cells) and the number of green neurons (2nd order neurons) was evaluated. On average, SAD ΔG eGFP spread from a yellow starter cell to 6.8 green monosynaptically connected cells, while SAD ΔG eGFP-TeNT-LC infected 6.4 monosynaptically connected neurons (Figure 16C). The results indicate that the cleavage of Vamp1, -2 and -3 has no obvious effect on the neuronal spread of SAD, at least in this model.

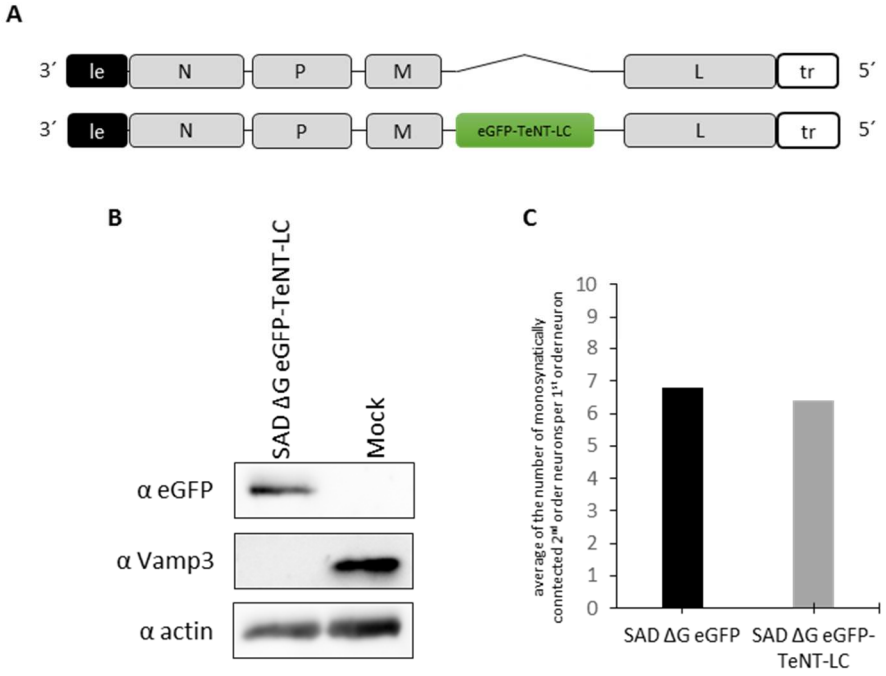

Figure 16: The monosynaptic spread of SAD ΔG eGFP-TeNT-LC is as efficient as of SAD ΔG eGFP.
A, Schematic representation of the genomic organization of SAD ΔG eGFP-TeNT-LC. **B**, N2A cells were infected with SAD ΔG eGFP-TeNT-LC at a MOI of three. The infected N2A cells were harvested at 72 h p.i., and the cell lysates were subjected to SDS-PAGE, Western blotting and immunostaining for the indicated antibodies. **C**, A mESC-derived neuronal mix population was infected with SAD ΔG eGFP (EnvA) and SAD ΔG eGFP-TeNT-LC (EnvA) at a MOI of 0.5. The diagram shows the average number of mono-synaptically infected neurons per yellow starter cell four days post infection.

A major drawback of the usage of SAD itself as a vector for the eGFP-TeNT-LC expression might be, that TeNT-LC is expressed contemporaneous with the viral proteins. Thus, it is possible that at the time point of the viral spread, not all Vamp1, -2 and -3 proteins were cleaved. Therefore, although SAD ΔG eGFP-TeNT-LC was still able to spread in neurons, a participation of Vamps in the neuronal spread of SAD could not be excluded.

Because of the just described disadvantages of the expression of the neurotoxin by the virus itself and in regard to the possibility that other components of the SNARE complex e.g. SNAP25 are

more important for the transsynaptic spread of RABV, lentiviral vectors (LV) encoding for the light chain of TeNT, BoNT/A or BoNT/C were produced in collaboration with Alexandra Lepier (Faculty of medicine, LMU). To enable an efficient translation of BoNT/A-LC and BoNT/C-LC in mammalian cells, codon optimization was performed. The constructs were synthesized by Genscript. The codon optimized BoNTs-LC and TeNT-LC were additionally fused with eGFP on their N-terminus to enable the detection of transduced neurons.

The required volume of each LV for an efficient cleavage of its target proteins was determined by transduction of mESC-derived neurons with different concentrations of LV. At 60 h post transduction, eGFP expression was evaluated by fluorescence microscopy, and the cleavage of its target protein was monitored by SDS-PAGE, Western blotting and immunostaining (data not shown).

To investigate the dependency of the neuronal spread of different RABV strains on SNARE proteins, mESC-derived neurons were transduced with purified LV-eGFP, LV-eGFP-BoNT/A-LC, LV-eGFP-BoNT/C-LC or LV-eGFP-TeNT-LC. In addition to one plate of mESC-derived neurons for each time point, an extra plate of mESC-derived neurons was prepared to control the enzymatic activity of the neurotoxins by SDS-PAGE, Western blotting and immunostaining. 60 hours post transduction, one plate of transduced neurons was harvested to analyze if eGFP-BoNT/A-LC cleaved all Snap25 and eGFP-TeNT-LC cleaved all Vamp1, -2 and -3. The remaining plates with the transduced neurons were infected with (I) the attenuated, on BHK cells adapted recombinant SAD eGFP strain, (II) the neurotropic, on mouse neuroblastoma cells adapted N2c strain, or (III) the street stain THA at a very low MOI. At 24 h post infection and at 36 h post infection one plate of neurons was fixed and stained with Centocor for RABV N. Subsequently, the transsynaptic spread of SAD eGFP and THA were analyzed by counting all RABV N positive cells per well. Since N2c is perfectly adapted to neuronal cells, it exhibited an extremely efficient transsynaptic transfer, what made it impossible to count the infected neurons directly. Thus, each well of a 12-well plate was screened with 121 photographies (objective 20x). The number of infected neurons was used to evaluate the neuronal transfer of the respective RABV strain in dependence on BoNT/A-LC or TeNT-LC.

As expected, only the neurons transduced with LV-eGFP-BoNT/C-LC, which cleaves Snap25 and Stx1, were dead 60 h post transduction (Figure 17A). The examination of the enzymatic activity of TeNT-LC and BoNT/A-LC by SDS-PAGE, Western blotting and immunostaining revealed, that 60 h post transduction Vamp1, -2 and -3 were cleaved highly efficiently, since no Vamp could be detected, and Snap25 shifted completely from 25 kDa to 22 kDa, indicating that all Snap25 proteins were cleaved, too (Figure 17B).

At 24 h post infection neither for SAD eGFP nor THA or N2c a difference in numbers of RABV infected neurons was detected, indicating that the entry of the different RABV strains is not affected by the neurotoxins (Figure 17C). At 36 h post infection, in LV-eGFP-TeNT-LC transduced neurons THA infected 1.8-fold less neurons, N2c infected 2.3-fold less neurons and SAD eGFP infected 3.8-fold less mESC-derived neurons compared to the neuronal spread in LV-eGFP transduced mESC-derived neurons. The proteolysis of Snap25 in LV-eGFP-BoNT/A-LC transduced neurons resulted in 1.3-fold less N2c infected cells, 2.0-fold less THA infected neurons and 2.3-fold less SAD eGFP infected cells than in LV-eGFP transduced neurons.

Interestingly, the attenuated SAD strain appeared to be most sensitive to the disruption of Vamps and Snap25, while BoNT/A-LC and TeNT-LC exhibited only minor effects on the neuronal spread of the neurotropic N2c and the wildtype isolate THA.

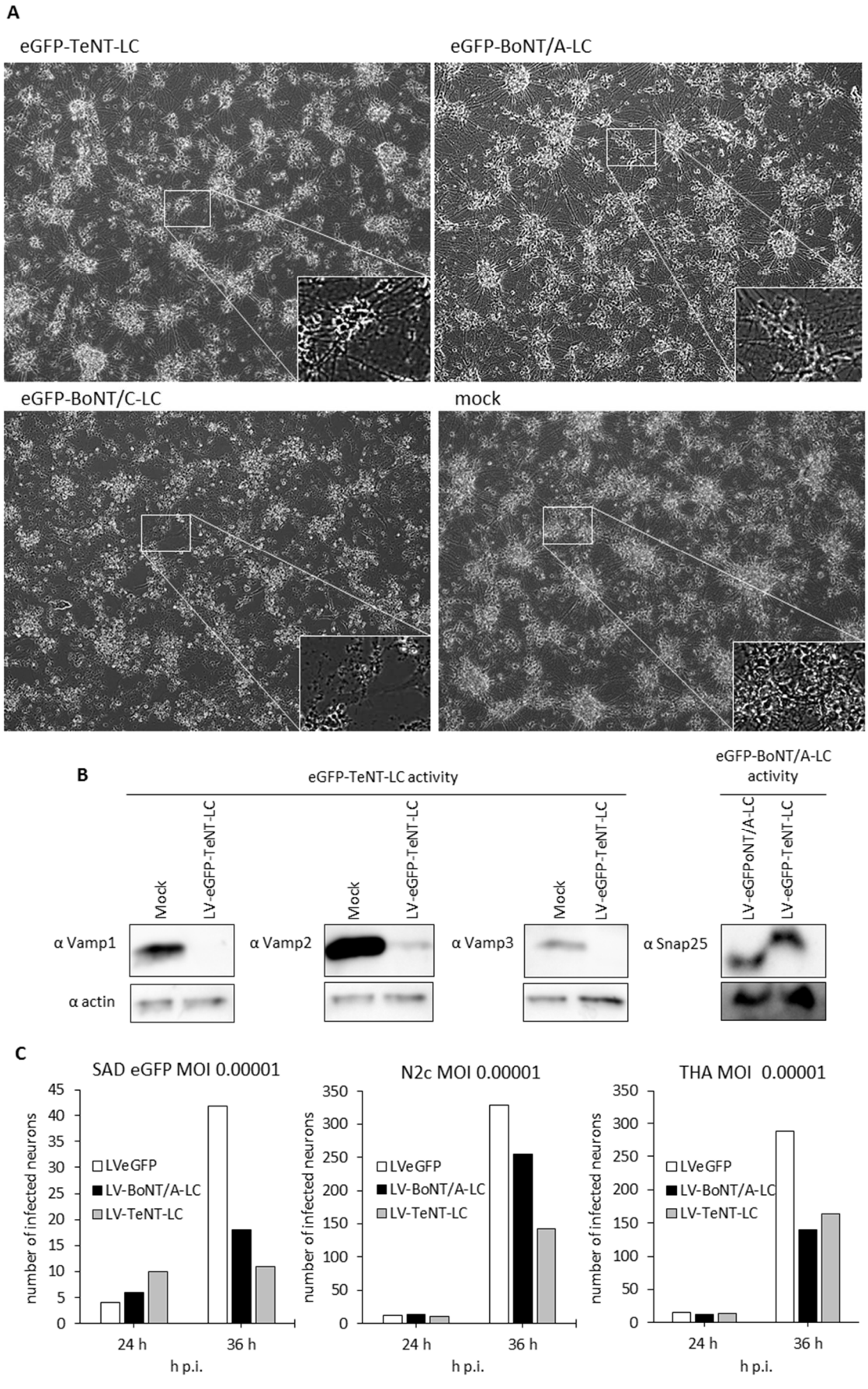
A
eGFP-TeNT-LC
eGFP-BoNT/A-LC
eGFP-BoNT/C-LC
mock
B
eGFP-TeNT-LC activity
eGFP-BoNT/A-LC activity
Mock
LV-eGFP-TeNT-LC
LV-eGFPoNT/A-LC
α Vamp1
α Vamp2
α Vamp3
α Snap25
α actin
C
SAD eGFP MOI 0.00001
N2c MOI 0.00001
THA MOI 0.00001
number of infected neurons
LVeGFP
LV-BoNT/A-LC
LV-TeNT-LC
24 h
36 h
h p.i.

Figure 17: The neuronal spread of SAD eGFP, N2c and THA is sensitive to the expression of TeNT-LC and BoNT/A-LC.

mESC-derived neurons, which were transduced with LV-eGFP, LV-eGFP-TeNT-LC or LV-eGFP-BoNT/A-LC, were infected 60 h post transduction with SAD eGFP, N2c and THA at a very low MOI. **A,** mESC-derived neurons are depicted 60 h post transduction. The white rectangle represents the area of the magnification. **B**, At 60 h post transduction neurons were harvested and the activity of the respective neurotoxin light chain was monitored by SDS-PAGE, Western blotting, and immunostaining for the indicated antibodies. **C**, Evaluation of the effect of eGFP-TeNT-LC and eGFP-BoNT/A-LC on the neuronal transfer of RABV to the indicated time points.

4.2.4 EM studies to visualize the transsynaptic spread of RABV

The previous experiments provided some evidence that the ESCRT machinery as well as SNARE complexes might be involved in the release of RABV at the postsynaptic membrane. Electron microscopy might be a powerful tool to reveal the subcellular localization of RABV transcription and replication, the transport of RABV to the postsynaptic membrane (e.g. association of the RNP on synaptic vesicles or transport of a complete virus within a vesicle), the localization of virus assembly (e.g. at the plasma membrane, at synaptic vesicles) and the place of virus budding (e.g. PSD) in an infected neuron.

To address the aforementioned questions by electron microscopy, we started a collaboration with Andreas Klingl (Faculty of Biology, LMU). To enable the operational steps of the sample preparation for EM, the mESC-derived neurons were differentiated on ibidi glass bottom dishes, which were coated with 1 mg/mL PDL. The neurons were infected with SAD eGFP at a MOI of one. Two days post infection, the infected neurons were fixed by the addition of PFA and glutaraldehyde directly to the Neuron medium. The final concentration was 4 % PFA and of 2 % glutaraldehyde. The samples were stored at 4 °C. The following fixation with 1 % OsO_4, the 2 % uranyl acetate staining, the drain of the samples with acetone, the embedding of the samples in resin, the sample preparation with a microtome as well as the monitoring of the samples by a TEM (Zeiss EM 912) was performed by our collaboration partner.

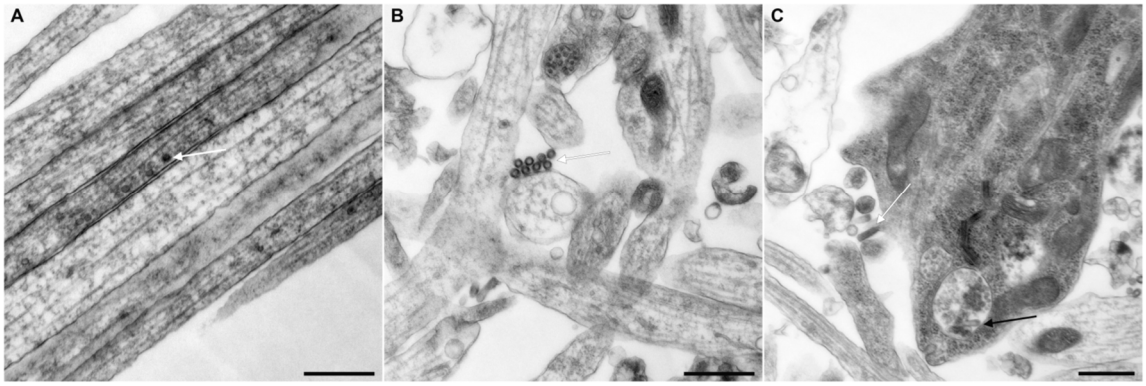

Figure 18 TEM of SAD eGFP infected mESC derived neurons (in collaboration with Andreas Klingl)
The white and black arrows point to virus particles. The black scale bar represents 500 nm.

In Figure 18A, the white arrow points to a virus particle, which is probably within a vesicle that is most likely associated via a motor protein complex to a microtubule within an axon. In Figure 18B, RABV particles were released in bundles or the extracellular virions tend to form clusters after their release. In Figure 18C the black arrow points to a RABV particle, which is most likely within a MVB, and the white arrow points to a single virus particle that is still associated with the plasma membrane.

4.3 Manipulation of the RABV glycoprotein

The RABV glycoprotein (G) is a type I transmembrane protein, thus consisting of an N-terminal glycosylated ectodomain (aa 1 -439), a hydrophobic 22 aa long transmembrane anchor domain and a 44 aa long cytoplasmic domain. RABV G forms homotrimers, resulting in trimeric spikes on the virion surface. It is responsible for receptor-mediated endocytosis, low pH-dependent fusion of the viral membrane with the endosomal membrane, retrograde axonal transport of virus particles and the transsynaptic spread of RABV (reviewed in (Wunner and Conzelmann, 2013)).

Although it is well accepted that RABV G is responsible for the exclusive retrograde transsynaptic spread in the CNS, the molecular mechanisms involved are still unknown (Ghanem and Conzelmann, 2016).

The aim of this part of the thesis was the identification of a site within the glycoprotein that is permissive for the insertion of external trafficking signals for rerouting the subcellular localization of the glycoprotein, or retargeting RABV to alternative receptors, without interfering with the essential functions of the glycoprotein. Thus, well-described sites within the ectodomain as well as the cytoplasmic domain were manipulated and analyzed concerning their functionality and impact in RABV G rerouting.

4.3.1 Manipulation of the SAD G ectodomain

The ectodomain of SAD G was analyzed by deletion mutants and by replacement of the deleted sequence with substance P (SP). Substance P is an eleven aa long neuropeptide that binds to tachykinin receptors like NK1R (Martinez and Philipp, 2016). Due to its small size and its natural presence in neurons, SP is a good candidate to investigate whether the insertion of a short peptide into the ectodomain of G still results in an infectious virus particle (Martinez and Philipp, 2016). Furthermore, SP might provide an additional binding site to the NK1 receptor, which could lead to an altered cell entry or transport of RABV.

Since at the beginning of this project, no structure and even no structure prediction of RABV G was available, I looked for sites which were described to be on the surface of the glycoprotein. Therefore, the nAChR binding site and the antigenic site III were selected for deletion or replacement with SP. In Figure 19, schematical representations of the different recombinant glycoproteins are depicted.

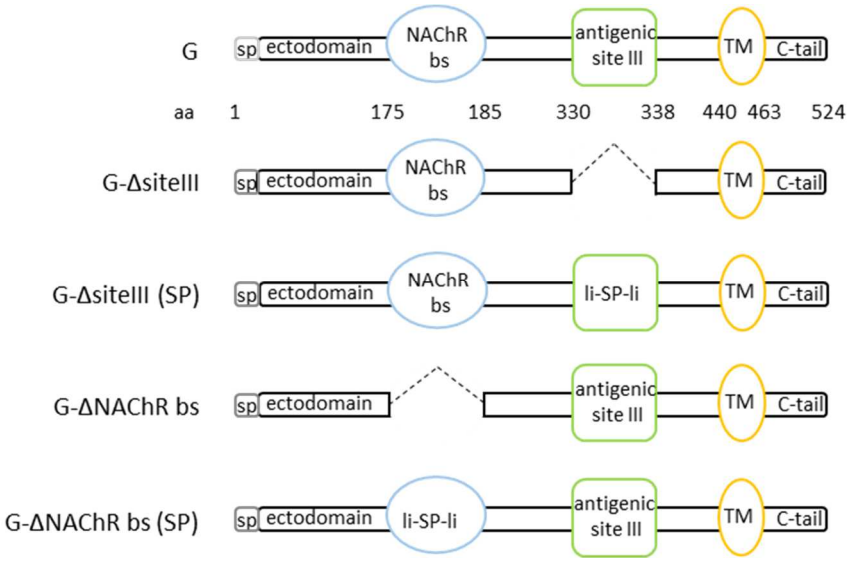

Figure 19: Schematic representation of the different SAD glycoproteins with a manipulated ectodomain.
The grey box with the label sp represents the signal peptide, nAChR bs within the blue oval stands for the nAChR binding site, the green square represents the antigenic site III and the orange oval with the label TM represents the transmembrane domain. Deletions are indicated by a dotted link and replacements of the respective sites are indicated by the exchange of the original label with li-SP-li, which stands for Substance P with an N-terminal and a C-terminal GSGS-linker sequence.

Constructs encoding G-ΔnAChR bs, G-ΔnAChR bs(SP), G-ΔsiteIII and G-ΔsiteIII (SP) were cloned in an expression vector and examined with respect to their protein expression, their incorporation into virions and the infectiousness of their virions. To this end, a *trans*-complementation assay with SAD ΔG was performed. To determine whether the recombinant proteins are expressed and incorporated into the virion, the transfected HEK293T cells were lysed and the supernatant of the transfected cells was pelleted by an ultracentrifugation step and subsequently the virion pellet was lysed. The lysed cells as well as the lysed supernatant virions were analyzed by SDS-PAGE, Western blotting and immunostaining. The infectivity of the trans-complemented virions was examined by endpoint titration of virus containing cell supernatants.

As monitored by SDS-PAGE, Western blotting and immunostaining of the cell lysates, all recombinant glycoproteins were expressed and probably glycosylated, since they exhibited the expected molecular weight. However, the examination of virion lysates revealed that only the unmodified G was incorporated at detectable levels into the G gene-deficient SAD ΔG. Accordingly, the endpoint titration demonstrated that only the G trans-complemented viruses were infectious (Figure 21).

4.3.2 Manipulation of the cytoplasmic tail

In 2015, Farias and colleagues demonstrated that the fusion of three copies of kinesin-light-chain-binding sequence (KBS) of the cargo adaptor protein SKIP to the C-terminus of the Nipah Virus F glycoprotein (NiV-F) directs NiV-F, which is usually sorted into somatodendritic vesicles, to the axon tips. They showed that NiV-F binds via KBS to the axonally-directed kinesin (e.g. KIF5), resulting in the transport of the NiV-F-KBS containing somatodendritic vesicle through the "pre-axonal exclusion zone" (PAEZ) to the distal axons (Farias et al., 2015). In order to redirect the RABV glycoprotein from the postsynaptic membrane to the axon tips, three copies of KBS were fused directly downstream of the transmembrane domain, or alternatively at the C-terminus of G (Figure 20).

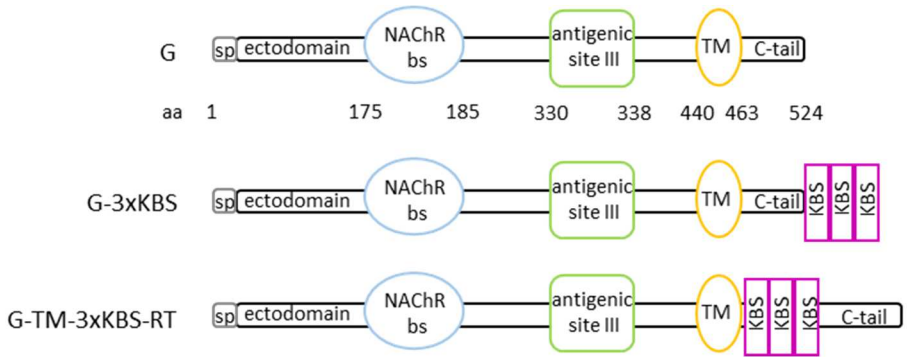

Figure 20: Schematic representation of the different G glycoproteins with manipulated cytoplasmic domain. The grey box with the label sp represents the signal peptide, nAChR bs within the blue oval stands for the nAChR binding site, the square represents the antigenic site III and the orange oval with the label TM represents the transmembrane domain. One pink rectangle with the label KBS represents one copy of the kinesin-light chain-binding site.

To investigate whether the recombinant G-KBS variants were expressed, incorporated into virions and led to infectious virions, a trans-complementation assay, followed by SDS-PAGE, Western blotting and immunostaining of the cell lysates as well as the pelleted virion lysates and an endpoint titration of the supernatant of the transfected cells was performed. Unfortunately, G-3xKBS could not be detected by immunostaining, most likely because the G antibody used binds to the terminal 13 aa of the C-tail, which were probably not accessible for the antibody due to the KBS-tag. However, G-TM-3xKBS-RT was detected in the lysate of the transfected HEK293T cells and the molecular weight of G-TM-3xKBS-RT indicated that the recombinant protein was also glycosylated. Notably, the examination of the trans-complemented, pelleted virion lysates by Western blotting and immunostaining indicated that G-TM-3xKBS-RT was also incorporated into the SAD ΔG virions (Figure 21A).

Next, it was analyzed by endpoint titration on BSR-T7 cells, whether the trans-complemented SAD ΔG (G-TM-3xKBS-RT) virions were infectious as well. While the positive control with the unmodified G resulted in an infectious titer of $1x10^7$ ffu/mL, the *trans*-complementation with G-TM-3xKBS-RT led to a titer of 3×10^5 ffu/mL, indicating that the recombinant G-TM-3xKBS-RT was able to support all steps during the infection of BSR-T7 cells (Figure 21B). The lower titer of G-TM-3xKBS-RT compared to the unmodified G could be explained partially by the slightly reduced expression level of G-TM-3xKBS-RT. Notably, also the *trans*-complementation with G-3xKBS resulted in an infectious titer of $8.5x10^2$ ffu/mL. Since our antibody could not detect G-3xKBS and the trans-complementation resulted in a much lower titer than with G-TM-3xKBS-RT, following experiments focused on the recombinant G-TM-3xKBS-RT.

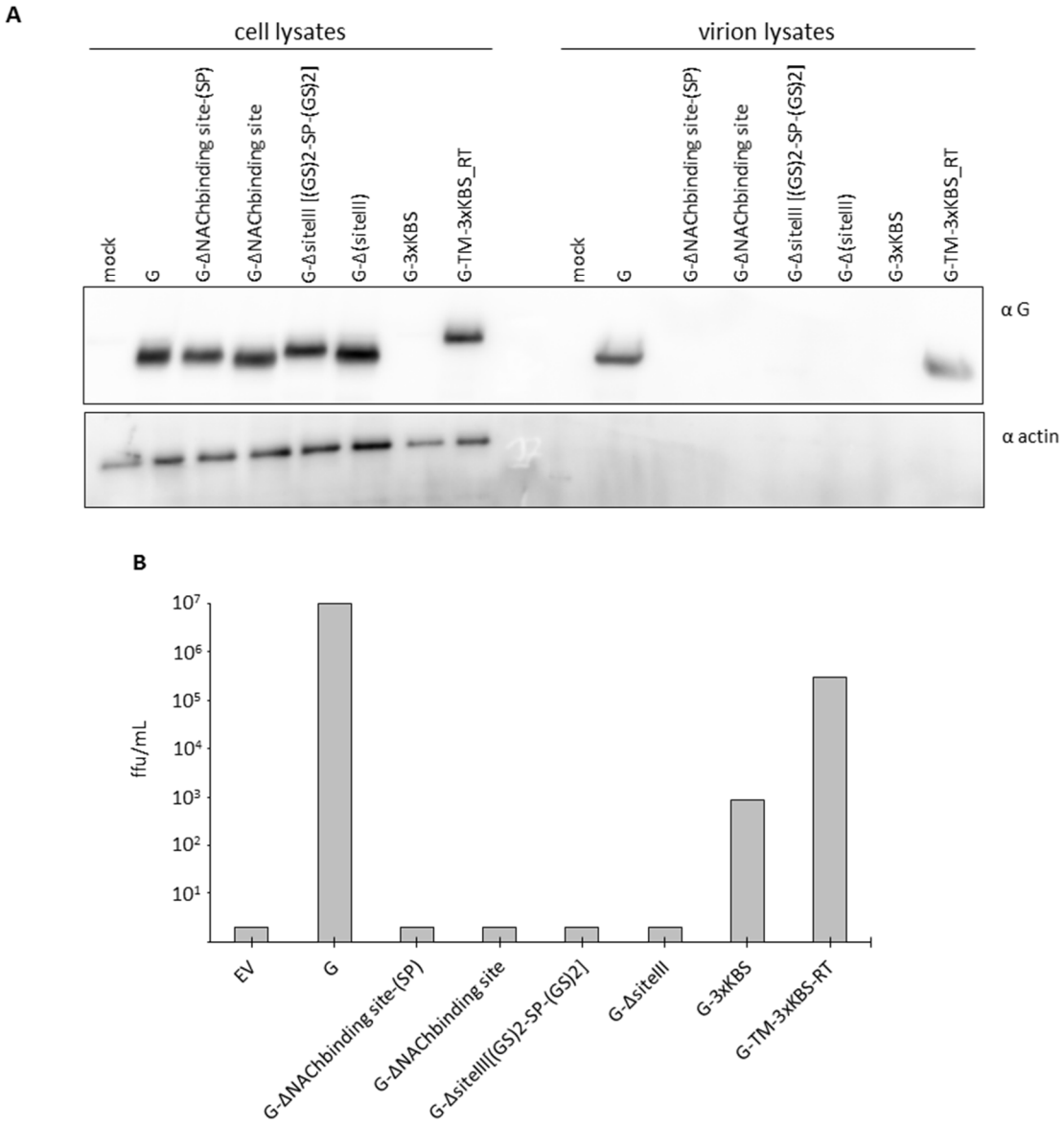

Figure 21: Trans-complementation of SAD ΔG eGFP with G-TM-3xKBS-RT results in infectious virus particles. SAD ΔG eGFP was trans-complemented in HEK293T cells with the annotated recombinant glycoproteins. The transfected HEK293T cells and the supernatant were harvested 48 h post infection. **A**, SDS-PAGE,

Western blotting and immunostaining of the transfected cell lysates and the purified virions with the indicated antibodies. **B**, Evaluation of the number of infectious virus particles in supernatant of the transfected HEK293T cells by titration on BSR-T7 cells.

Next, a recombinant SAD eGFP virus was generated by reverse genetics, in which the glycoprotein was replaced by G-TM-3xKBS-RT. In the following, it is referred to as SAD G-TM-3xKBS-RT eGFP.
First, the growth kinetics of SAD G-TM-3xKBS-RTeGFP was evaluated by performing a multistep growth curve in BSR-T7 cells. At 24 h post infection, SAD G-TM-3xKBS-RTeGFP resulted in a 10-fold lower titer compared to SAD eGFP. The slower growth kinetics of SAD G-TM-3xKBS-RTeGFP became even more prominent during the next 48 h, which resulted at 72 h p.i. in a 100-fold reduction in infectious virus titers (Figure 22A).
To get a first clue whether G-TM-3xKBS-RT influenced the virion composition, BSR-T7 cells were infected with SAD eGFP or SAD G-TM-3xKBS-RTeGFP at a MOI of 0.1. After two days, the infected cells were lysed and the supernatants were pelleted by an ultracentrifugation step and the pelleted virions were subsequently lysed. The virus protein content of the infected cells and the composition of virions was examined by SDS-PAGE, Western blotting and immunostaining against N, M, P and G (Figure 22B). Finally, the protein expression levels of N, P, G and M were quantified using ImageJ and normalized to the respective N protein level (Table 1). According to the staining against actin, equal amounts of SAD eGFP and SAD G-TM-3xKBS-RTeGFP infected cells were loaded. It seems like the viral protein levels of SAD G-TM-3xKBS-RTeGFP infected cells were lower compared to SAD eGFP infected cells. The normalization of the viral protein levels showed that the composition of the viral proteins was also different. While the ratios of the RNP proteins N and P in the lysates of the infected cells were quite similar, the portions of the envelope proteins M and G in SAD G-TM-3xKBS-RTeGFP were two-fold and four-fold diminished, respectively. The examination of the virion composition demonstrated that the ratios of the RNP proteins N and P were nearly the same again, whereas differences were detected for M/N and G/N ratios. Interestingly, it seems like SAD G-TM-3xKBS-RTeGFP virions contained slightly more M and G than SAD eGFP.

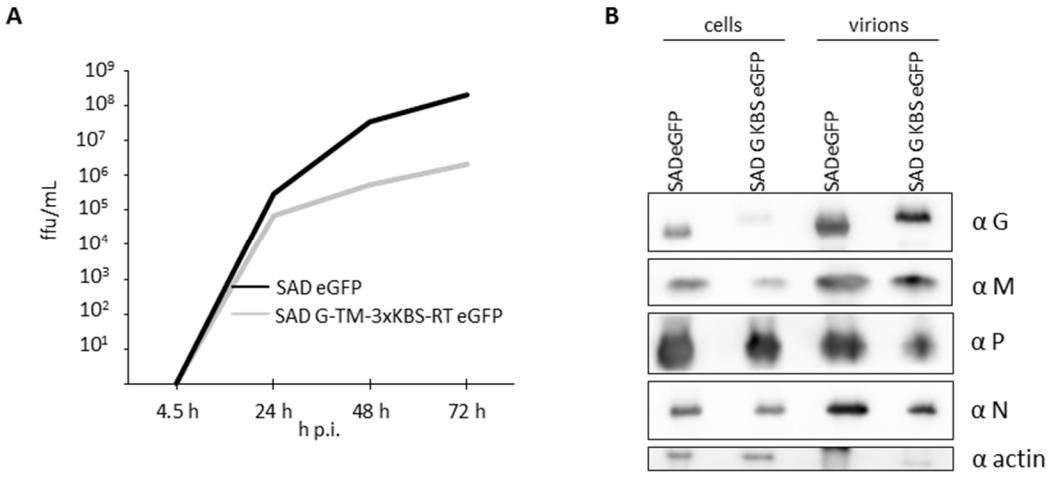

Figure 22: Characterization of SAD G-TM-3xKBS-RT eGFP.

A, Multistep growth curve of SAD eGFP and SAD G-TM-3xKBS-RTeGFP on BSR-T7 cells. Samples were taken to the indicated time points and titrated on BSR-T7 cells. **B**, BSR-T7 cells were infected with SAD eGFP and SAD G-TM-3xKBS-RTeGFP at a MOI of 0.1. Two days post infection, the infected cells and the purified virions were lysed and analyzed by SDS-PAGE, Western blotting and immunostaining against the indicated antibodies.

	cell lysate		virion lysate	
ratio	**SAD eGFP**	**SAD G-TM-KBS-RT eGFP**	**SAD eGFP**	**SAD G-TM-KBS-RT eGFP**
M/N	1.2	0.6	1.2	2.0
G/N	0.8	0.2	1.2	2.0
P/N	4.4	5.3	1.9	1.8

Table 1: Quantification of the viral proteins in SAD eGFP and SAD G-TM-3xKBS-RT eGFP infected BSR-T7 cells and their respective.

Protein bands of the immunostaining, depicted in Figure 22B, were quantified with the software ImageJ and normalized against N.

4.3.3 Characterization of SAD G-TM-3xKBS-RTeGFP in mESC-derived neurons

First, it was investigated whether SAD G-TM-3xKBS-RTeGFP was also able to infect neurons and whether the G-TM-3xKBS-RT protein could support the transsynaptic spread of RABV in mESC-derived neurons. Thus, neurons were infected with SAD eGFP or SAD G-TM-3xKBS-RTeGFP at a very low MOI. The spread was investigated in living neurons by monitoring the eGFP expression of the recombinant viruses two days, three days and four days post infection (Figure 23). SAD G-

TM-3xKBS-RTeGFP spread was slightly slower compared to that of SAD eGFP, which already infected nearly each cell at 72 h p.i..

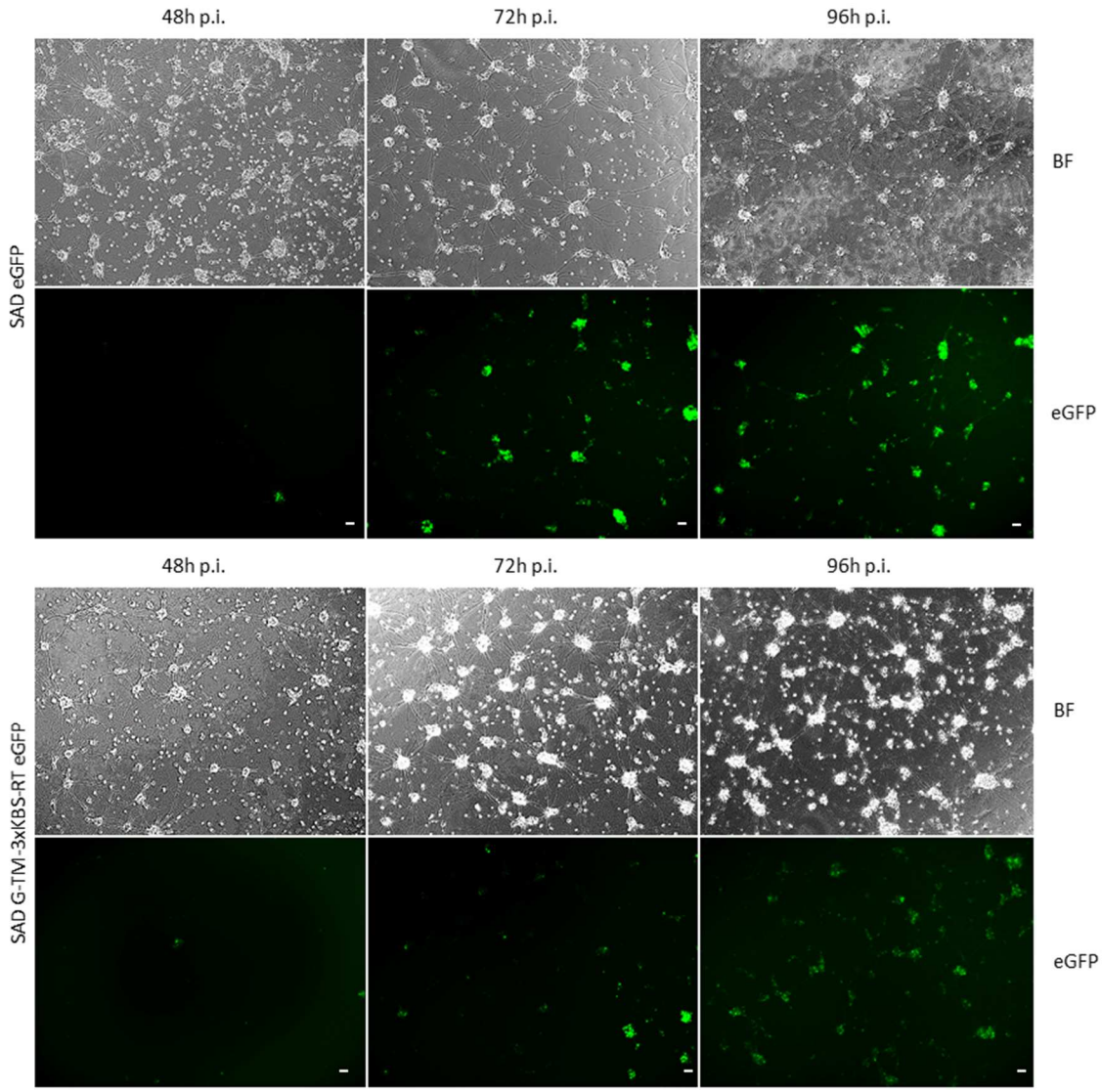

Figure 23: Transsynaptic spread of SAD G-TM-3xKBS-RTeGFP.
mESC-derived neurons were infected with SAD eGFP and SAD G-TM-3xKBS-RTeGFP at a very low MOI. The spread was evaluated by monitoring the eGFP fluorescence to the indicated time points. BF indicates bright field illumination. The white scale bar represents 250 µm.

Next, the influence of the KBS-tag on the intracellular distribution of G in infected mESC-derived neurons was investigated. To this end, neurons differentiated on glass coverslips were infected with SAD eGFP or SAD G(KBS)eGFP at a MOI of 0.1. Three days post infection, the neurons were fixed and stained for G. In order to distinguish between axons and dendrites, co-immunostainings for G and the axonal marker neurofilament H (NF-H), or the dendritic marker microtubule associated protein 2 (MAP2) were performed (Figure 24).

Interestingly, the staining of G in SAD eGFP infected mESC-derived neurons revealed a granular distribution, which could resemble the distribution of PSDs. In contrast, the staining of G-TM-

3xKBS-RT in SAD G-TM-3xKBS-RT eGFP-infected neurons indicated a more homogenous G distribution. However, the co-staining with the axonal marker NF-H or the dendritic marker MAP2 demonstrated that at least in mESC-derived neurons no clear-cut difference between the intracellular distribution of G and G-TM-3xKBS-RT could be detected, as even G was also unexpectedly located in axons.

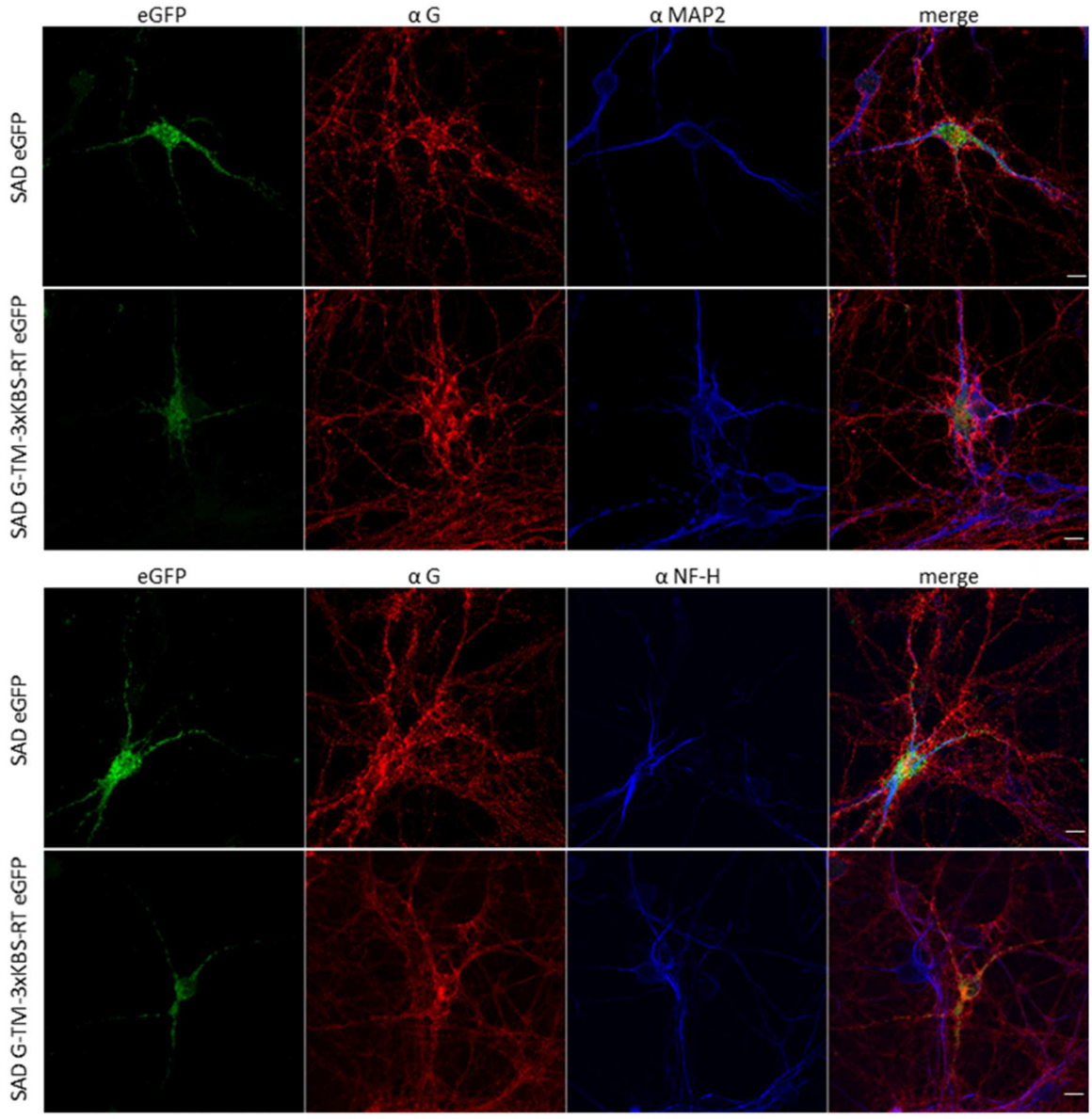

Figure 24: Distribution of G in SAD eGFP and SAD G-TM-3xKBS-RT eGFP infected mESC-derived neurons.
mESC-derived neurons, differentiated on PDL coated coverslips, were infected with SAD eGFP or SAD G-TM-3xKBS-RTeGFP at a MOI of 0.01. At 72 h p.i. neurons were fixed and stained with the indicated antibodies and monitored by confocal laser scanning microscopy. MAP2 is a dendritic antibody and NF-H is an axonal antibody. The white scale bar represents 10 µm.

4.4 Generation of a less cytotoxic RABV for long-term studies of RABV infected neurons *in vitro* and *in vivo*

The following project and experiments were performed in collaboration with Alexander Ghanem. Although RABV has only a mild cytopathic effect (CPE), culture cells and neurons infected with the SAD virus eventually die of the infection. The molecular mechanism behind the cell death of SAD virus infected culture cells and neurons is unknown. The availability of a non-toxic RABV would be of great interest for long-term studies of RABV infected neurons *in vitro* and *in vivo*. Thus, an *in vitro* evolution experiment was performed in order to possibly generate a virus with an attenuated or at best a non-toxic SAD eGFP.

4.4.1 Generation of persistently infected HEK293T cells

The experimental approach for the *in vitro* evolution of SAD eGFP is schematically depicted in Figure 25A. First, HEK293T cells were infected with SAD eGFP with a MOI of three to ensure that every cell is infected. Three days post infection the cells were split 1/4 (passage 2) which led to the death of most infected HEK293T cells within two days post splitting. However, a few infected cells survived. The dead cells were removed carefully by repeated medium exchange. 15 days post infection, the living cells were trypsinized and replated in a fresh plate (passage 3). Interestingly, although the fluorescence of the individual HEK293T cells varied it nevertheless seemed like all cells were still eGFP positive, indicating that they were still infected with eGFP-expressing virus. The medium was replaced by fresh medium twice per week. The cells recovered slowly over time and remained persistently infected, since the HEK293T were still eGFP positive. On day 35, the cells were split for the first time 1/6 (passage 4) (Figure 25B). From passage 4 on the cells started to divide faster and could be split one week later (day 42) for a second time 1/6 (passage 5). Beginning with passage 5 on (day 42), the eGFP expressing cells could be split twice per week 1/6 and the fluorescence intensity of the infected cells became more homogenous. The infected cells resembled more and more uninfected HEK293T cells, in terms of morphology and cell growth. From passage 13 on, the infected cells were split twice per week 1/8 up to 1/10. By comparison, uninfected HEK293T cells were split twice per week 1/10 up to 1/12. From passage 5 on, every second supernatant passage was harvested, purified from cell debris, and stored at - 80 °C for further analyses. Also cells from every second passage were harvested, resuspended in DMEM 3+ that contained 10 % DMSO and stored at - 80 °C. The frozen cells could be thawed and expanded just like HEK293T cells. The cells were still eGFP positive, indicating that they were still infected (data not shown).

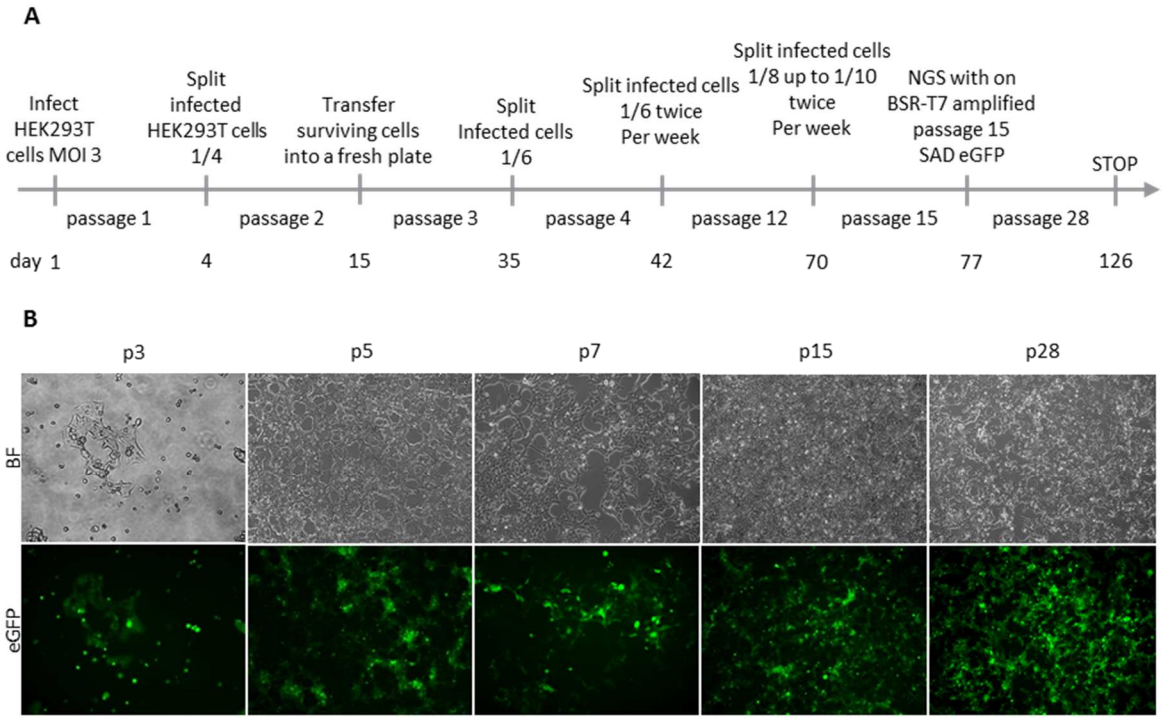

Figure 25: In vitro evolution of SAD eGFP in HEK293T cells.

A, Schematic representation of the SAD eGFP *in vitro* evolution experiment. **B**, Bright field images and fluorescence images of the different stages of the infected HEK293T cells during the *in vitro* evolution experiment. The photography of passage three was kindly provided by Alexander Ghanem.

4.4.2 Characterization of non-cytotoxic SAD eGFP

After it was confirmed that the supernatant of passage 15 was still infectious (data not shown), it was used for a stock production on BSR-T7 cells in order to amplify the virus (SAD eGFP p15). The growth kinetics of the SAD eGFP p15 stock was examined by a multistep growth curve in BSR-T7 cells. As can be seen Figure 26A, SAD eGFP p15 grew as fast as the parental SAD eGFP (SAD eGFP wt), indicating that SAD eGFP p15 was not attenuated.

In order to investigate the cytotoxicity of SAD eGFP p15 virus for HEK293T cells, cells were infected with the SAD eGFP p15 stock or the parental SAD eGFP at MOI of three. One day post infection, all infected cells were eGFP positive and exhibited the same morphology as mock infected cells. However, the eGFP fluorescence of SAD eGFP p15 infected cells was slightly reduced compared to the eGFP fluorescence of parental SAD eGFP infected cells. Note that the photographies were taken with the same light exposure time, therefore the eGFP fluorescence should correlate with the eGFP expression. Interestingly, already 48 h p.i. the parental SAD eGFP infected cells were dying while HEK293T cells, which were infected with SAD eGFP p15, were as viable as mock cells. Furthermore, the eGFP fluorescence in SAD eGFP p15 infected HEK293T cells was as intense as in parental SAD eGFP infected cells at that time point. Already three days post infection, almost all

SAD eGFP infected cells were dead, whereas SAD eGFP p15 infected cells were still eGFP positive and exhibited the same morphology as the mock cells (Figure 26B). These data suggest that the lack of cell death in the selection experiment was due to changes in the virus genome and not due to the selection of more resistant HEK293T cells.

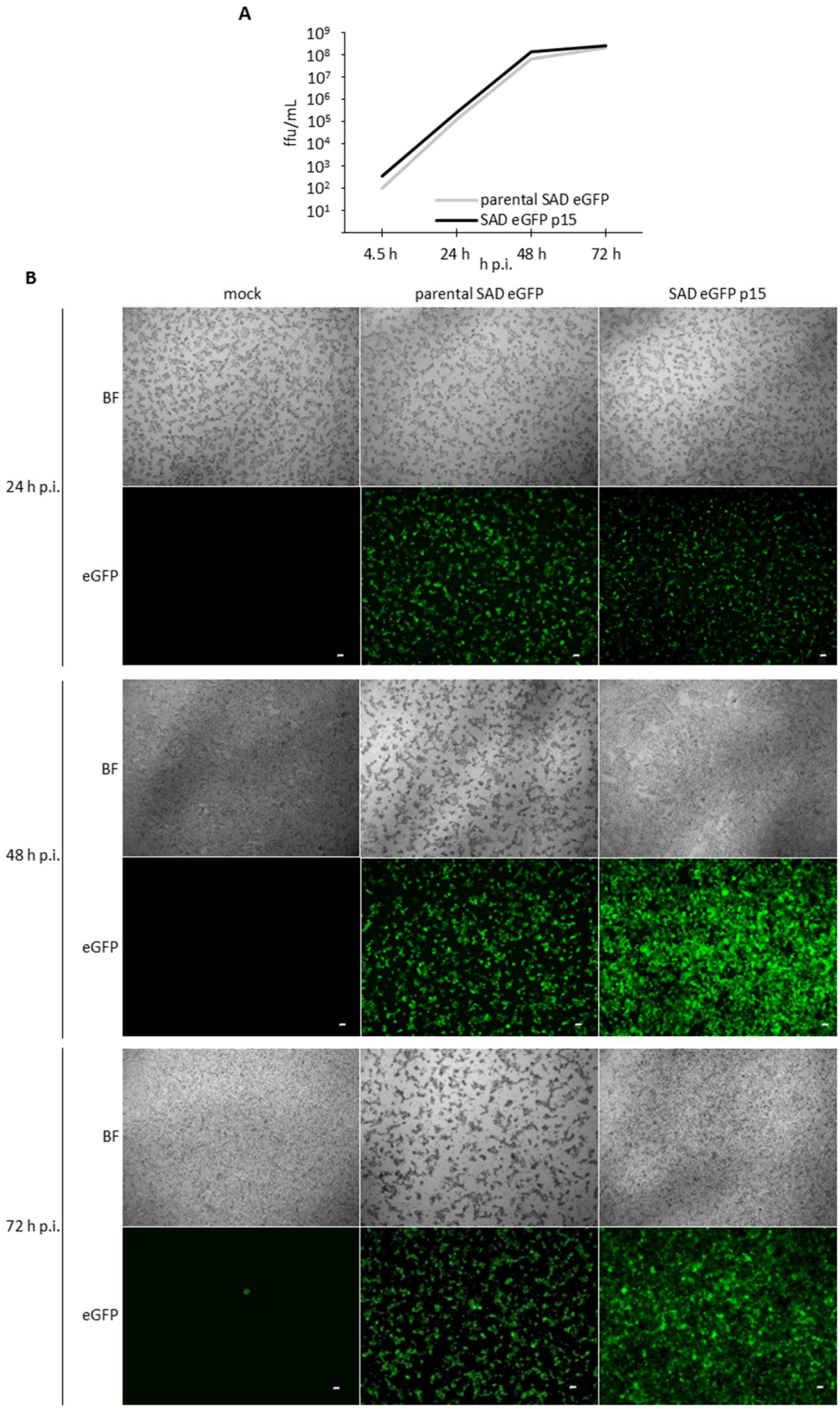
A
ffu/mL
10^9
10^8
10^7
10^6
10^5
10^4
10^3
10^2
10^1
parental SAD eGFP
SAD eGFP p15
4.5 h
24 h
48 h
72 h
h p.i.
B
mock
parental SAD eGFP
SAD eGFP p15
24 h p.i.
48 h p.i.
72 h p.i.
BF
eGFP

Figure 26: SAD eGFP p15 exhibits the same growth kinetics but an attenuated cytotoxicity compared to parental SAD eGFP

A, Multistep growth curve of SAD eGFP p15 and SAD eGFP on BSR-T7 cells. Supernatant samples were harvested at the indicated time points. The titers (ffu/mL) of the samples were determined by titration on BSR-T7 cells. **B**, HEK293T cells were infected with parental SAD eGFP or SAD eGFP p15 at a MOI of three. The eGFP fluorescence intensity as well as the cytotoxicity of the viruses were monitored at the indicated time points. The white scale bar represents 250 µm.

4.4.3 Deep sequencing of non-cytotoxic SAD eGFP

For the identification of the mutations, which could cause the reduced cytotoxicity of SAD eGFP p15, the viral genomes were analyzed by deep sequencing. Therefore, 6 x 10^6 BSR-T7 cells were seeded into a T175 flask. Two hours post seeding, the BSR-T7 cells were infected with SAD eGFP p15 or the parental SAD eGFP at MOI of 0.1. After two days, when all cells were infected, the supernatants were harvested, cleared of cell debris and purified by an ultracentrifugation step. Then, each virus pellets was lysed in 350 µL RLT buffer, containing 1 % β-Mercaptethanol. Subsequently, it was proceeded according to the RNA-isolation protocol (RNeasy Mini Kit). Finally 6.8 ng/µL RNA with a 260/280 ratio of 2.03 of the parental SAD eGFP virus and 6.9 ng/µL RNA with a 260/280 ratio of 2.19 of SAD eGFP p15 virus were isolated. The samples were stored at - 80 °C.
The next generation sequencing of viral genomic RNA was performed by Stefan Krebs (LAFUGA Gene Center, LMU) and the evaluation of the data was performed together with Konstantin Sparrer.
As depicted in Figure 27A, only six prevalent mutations were identified. With A52G and A54T two mutations were located in the leader region. They were present in 85 % and 67 % of the reads, respectively. The mutation T1761G located in the phosphoprotein gene occurred in 32 % of the reads and resulted in an aa exchange from Met to Arg, causing a loss of the P4 isoform start codon. In the RNA-dependent RNA polymerase L gene two mutations were located. The first mutation T6431C occurred in 61 % of the respective reads and resulted in a point mutation of the hydrophobic Ile to the hydrophilic Thr aa residue. The second mutation in L (G9149A) was present in 78 % of the reads and led to the introduction of an in frame stop codon. The mutation in the trailer region A12845G was the most prevalent among the six mutations and occurred in 94 % of the reads. In order to investigate which mutation caused the non-cytotoxic phenotype, reverse genetics was used to generate viruses with specific mutations, namely SAD eGFP carrying P(M83R), L(I30T), L(stop), mut52/54, mut12845 and mut52/54/12845 (Figure 27B). SAD mut52/54 eGFP, SAD mut52/54/12845 eGFP and SAD mut12845 eGFP were cloned and produced by Alexander Ghanem. All viruses were generated in BSR-T7 cells.

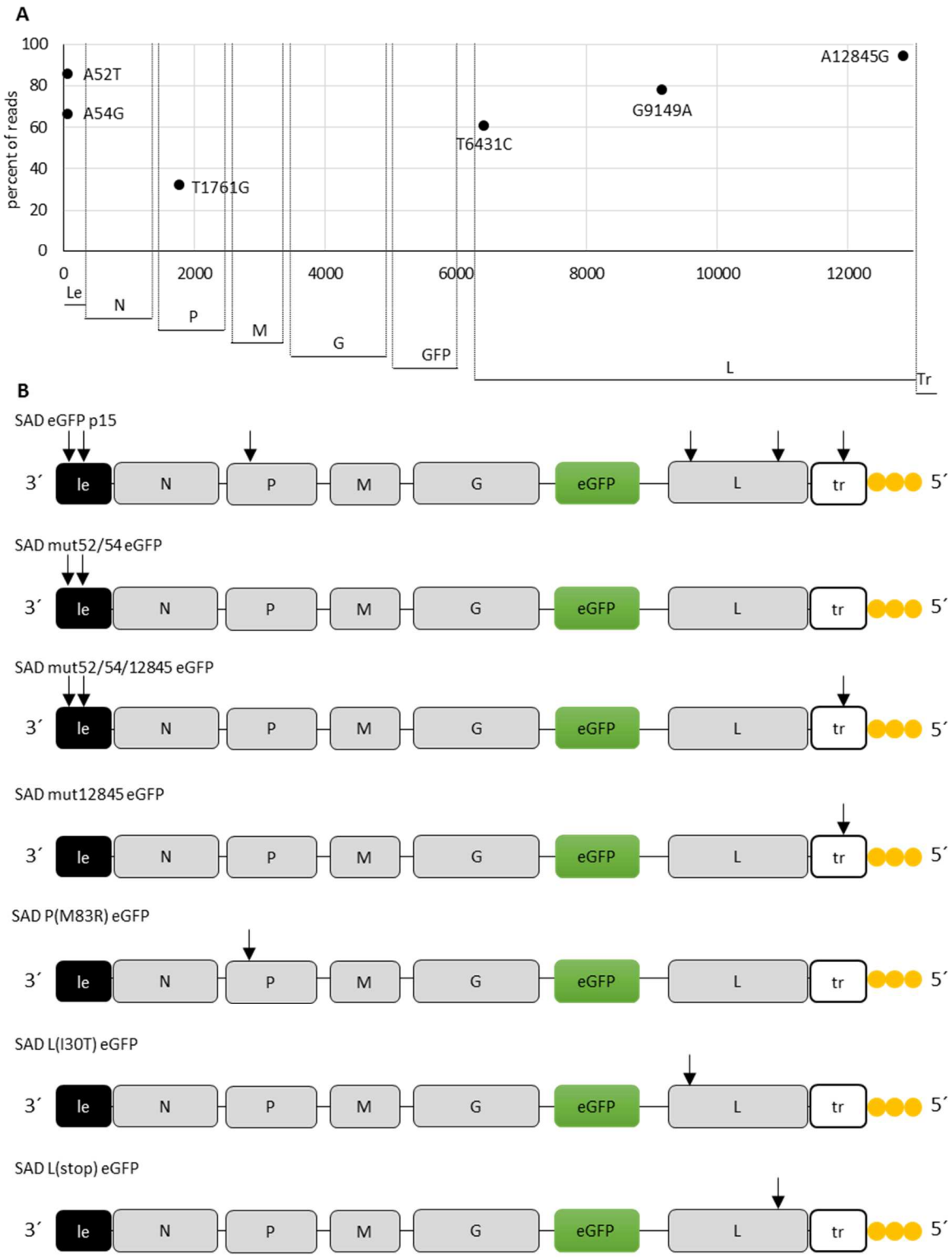

Figure 27: Schematic representation of the NGS results of the in vitro evolution experiment and the genomes of the recombinant viruses encoding for a single mutated region.

A, Viral genome of SAD eGFP, the sites of the mutations, and the percentage share of reads, in which the mutations were detected are depicted. **B**, Schematic representation of the genomes of the recombinant viruses that were generated in order to investigate, which mutated region caused the non-cytotoxic phenotype of SAD eGFP p15. Each black arrow marks one point mutation.

4.4.4 Characterization of potential non-cytotoxic viruses

First, the growth kinetics of the six recombinant viruses and SAD eGFP were determined in HEK293T cells by multistep growth curves, followed by a titration on BSR-T7 cells. Since previous experiments demonstrated that SAD mut52/54 eGFP and SAD mut52/54/12845 eGFP grow slower compared to SAD eGFP, the titrations of these two viruses were fixed and stained after 72 h, not after 48 h as usual. 4.5 h post infection, the titers were within one log range, indicating that the amount of input virus were nearly the same. Interestingly, SAD P(M83R) eGFP, SAD L(I30) eGFP, SAD L(stop) eGFP and SAD mut12845 eGFP exhibited nearly the same titers as SAD eGFP at all time points. In contrast, SAD mut52/54 eGFP and SAD mut52/54/12845 eGFP grew tremendously slower during the first 24 h (133-fold and 12000-fold) (Figure 28A). However, 72 h post infection SAD mut52/54 eGFP reached nearly the same titer as SAD eGFP and the titer of SAD mut52/54/12845 eGFP was finally only 13-fold reduced.

Next, the cytotoxicity of SAD P(M83R) eGFP, SAD L(I30T) eGFP, SAD mut52/54 eGFP, SAD mut12845 eGFP and SAD mut52/54/12845 eGFP was investigated. The cytotoxicity of SAD L(stop) eGFP was not analyzed, since previous experiments had shown that the virus did not express detectable eGFP levels, although it exhibited normal growth kinetics.

To investigate the cytotoxicity of the different viruses, 1.25 x 10^5 HEK293T cells were seeded per 12-well. Two hours post seeding, the cells were infected with one of the respective recombinant viruses with a MOI of three. After two days, the cell viability was assessed by microscopy. Subsequently, the infected cells were split 1/4 and the cell viability was monitored again another 24 h later (72 h p.i.).

Two days post infection, SAD mut52/54 eGFP, SAD P(M83R), SAD L(I30T) eGFP and SAD mut52/54/12845 eGFP infected HEK293T cells exhibited the same morphology and grew as fast as the non-infected mock cells (Figure 28B). Only SAD mut12845 eGFP and SAD eGFP infected cells grew slower, but the cell morphology was still indistinguishable from mock cells. Interestingly, while the eGFP fluorescence in SAD mut12845 eGFP, SAD P(M83R) eGFP, SAD L(I30T) eGFP and SAD eGFP infected cells was equal, SAD mut52/54 eGFP and SAD mut52/54/12845 eGFP showed a weaker eGFP fluorescence. Note, the eGFP fluorescence should correlate with the expression, since each photo was taken with the same light exposure time.

Three days post infection and 24 h post splitting SAD eGFP, SAD mut12845 eGFP, SAD L(I30T) eGFP, and SAD P(M83R) eGFP infected cells were dying, but SAD mut52/54 eGFP and SAD mut52/54/12845 infected HEK293T cells were growing like the uninfected mock cells. Interestingly, the eGFP fluorescence of these two viruses were still reduced compared to SAD eGFP infected HEK293T cells.

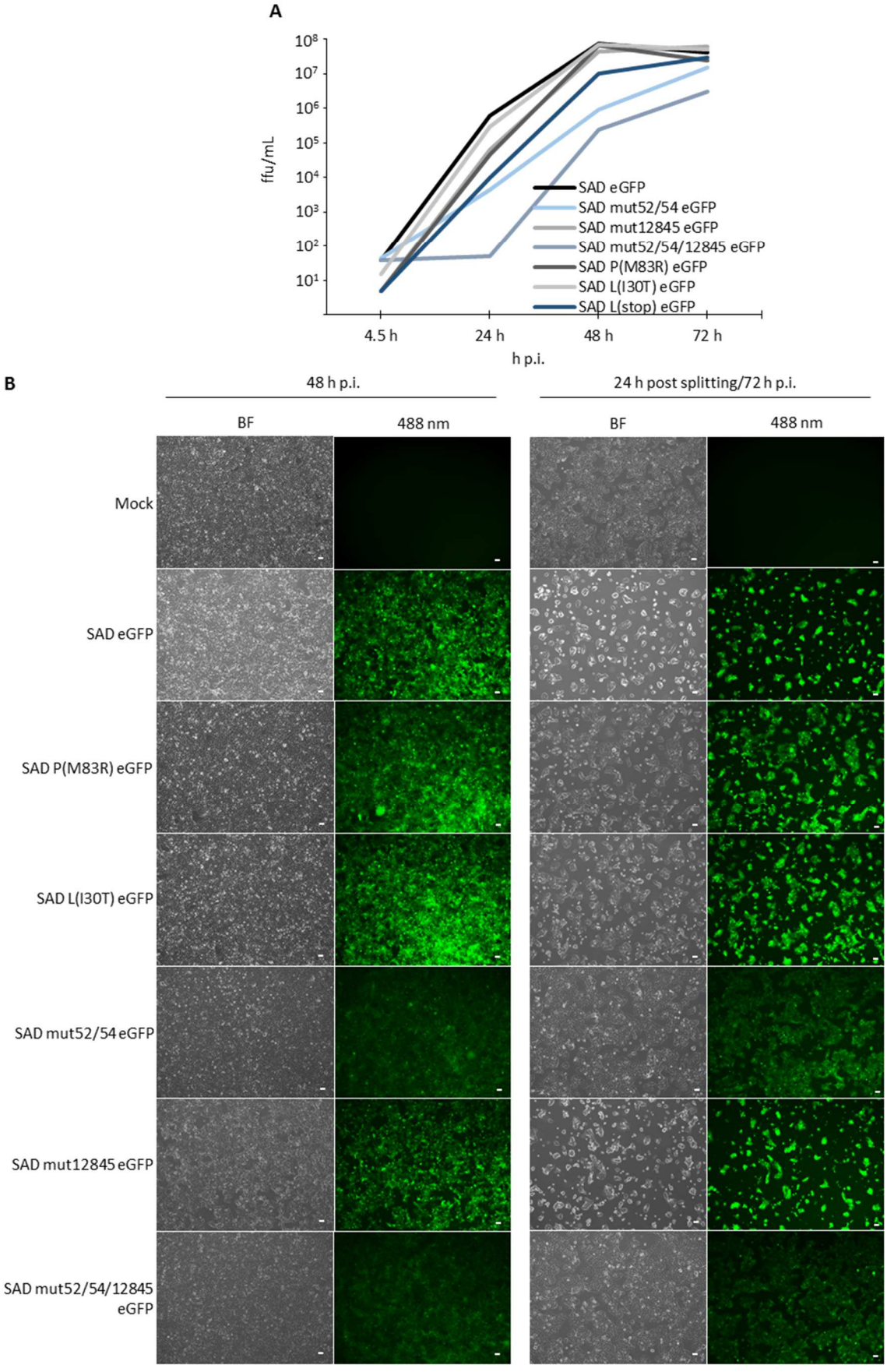
A
ffu/mL
h p.i.
4.5 h
24 h
48 h
72 h
SAD eGFP
SAD mut52/54 eGFP
SAD mut12845 eGFP
SAD mut52/54/12845 eGFP
SAD P(M83R) eGFP
SAD L(I30T) eGFP
SAD L(stop) eGFP
B
48 h p.i.
24 h post splitting/72 h p.i.
BF
488 nm
Mock
SAD eGFP
SAD P(M83R) eGFP
SAD L(I30T) eGFP
SAD mut52/54 eGFP
SAD mut12845 eGFP
SAD mut52/54/12845 eGFP

Figure 28: Evaluation of the growth kinetics and the cytotoxicity of the recombinant SAD P(M83R) eGFP, SAD L(I30T) eGFP, SAD mut52/54 eGFP, SAD mut12845 eGFP and SAD mut52/54/12845 eGFP.
A, Multistep growth curve in HEK293T cells. Supernatant samples were taken to the indicated time points and the ffu/mL were determined by titration on BSR-T7 cells. **B**, HEK293T cells were infected with the recombinant viruses at a MOI of three. After two days, the infected cells were split ¼. The cell morphology and the eGFP fluorescence were monitored 48 h p.i. and 24 h post splitting (72 h p.i.). The white scale bar represents 250 µm.

4.4.5 Reduced cytotoxicity of SAD mut52/54 eGFP and SAD mut52/54/12845 in mESC-derived neurons

It has been shown that SAD mut52/54 eGFP and SAD mut52/54/12845 have a reduced cytotoxicity in HEK293T cells. Next, it was investigated whether these recombinant viruses show a reduced cytotoxicity also in mESC-derived neurons. Therefore, mESC-derived neurons were infected with SAD P(M83R) eGFP, SAD L(I30T) eGFP, SAD mut52/54 eGFP, SAD mut12845 eGFP and SAD mut52/54/12845 eGFP at a MOI of two. The cell viability was monitored by observing the shape of the axons and dendrites by light microscopy. To reduce artificial cytotoxic effects, which might occur during the examination of the infected neurons with the microscope, e.g. exposure to oxygen or temperature fluctuation, separate plates of neurons were infected per time point. Additionally the virus stocks were purified by an ultracentrifugation step and the virus pellets were resuspended in Neurobasal medium. Hereby, it was ensured that the neurons wouldn´t be harmed by non-neuronal medium or any undesired cellular factors present in the virus supernatants. During the experiment 50 % of medium was replaced by prewarmed neuron medium every second day, in order to preserve the neuronal network.

To determine the cell viability, the neurite degeneration and the cell body distribution were documented. The morphology of the axons and dendrites was classified in the following four categories. In category (+++) the neuron culture exhibited an intact network and the cell bodies were not clustered. This category represents young and healthy neurons. The categorie (++-) represents older neurons that start looking non-healthy. The neuronal neurites are fine, but the cell bodies form clusters. As soon as the neurite degeneration started, the neurons were classified as dying cells in category (+--). When the neurites were degenerated, meaning that axons and dendrites were fragmented, the neurons were classified as dead cells (---). In the following a representative photography for each category is depicted (Figure 29).

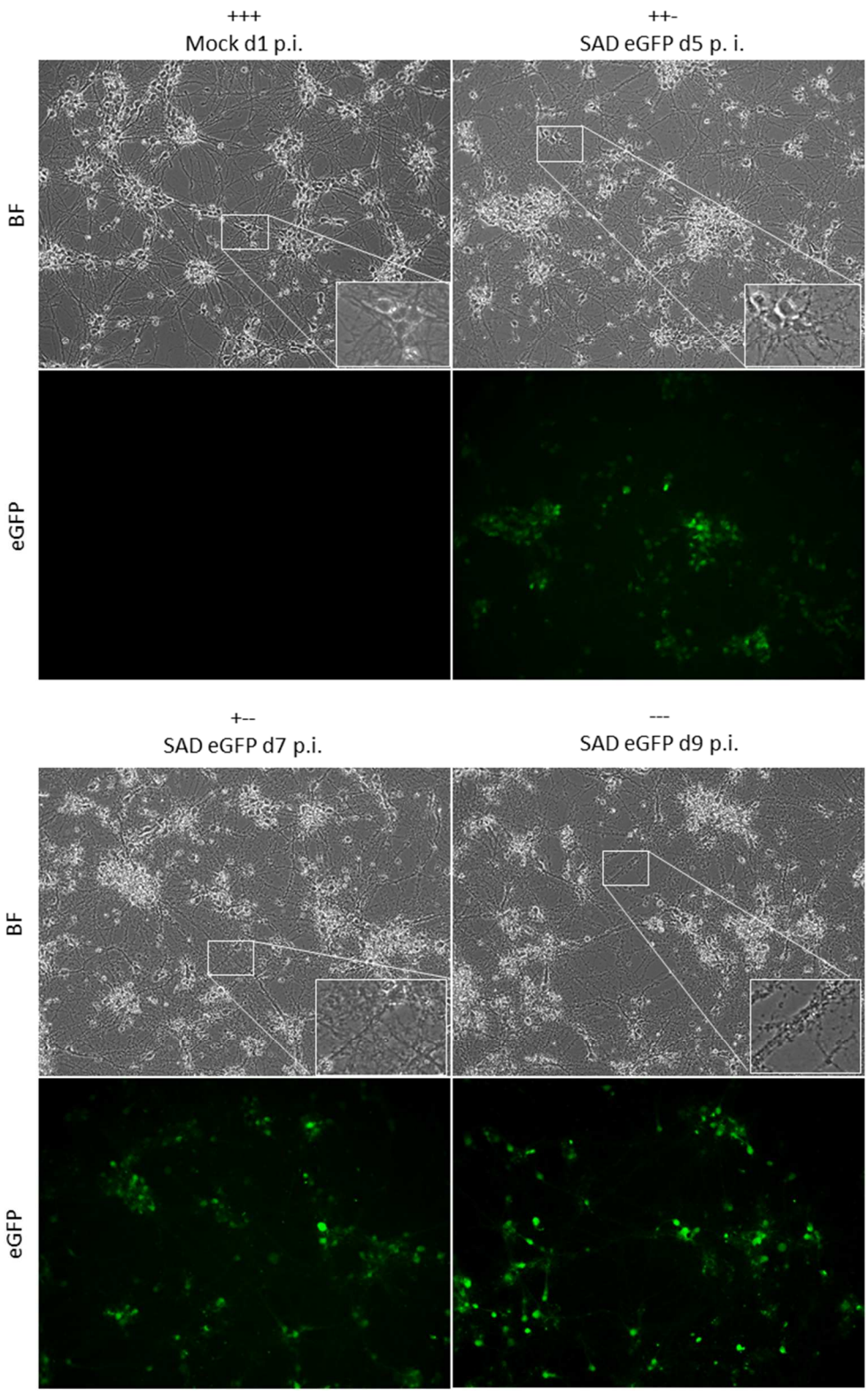

Figure 29: Classification of the neuron fitness.

Representative photos of the four stages of the neuronal cell viability. Young and healthy neurons are classified as (+++). Older or non-healthy neurons are categorized as (++-). Dying cells are represented by (+--) and dead cells are classified as (---). For a detailed description see above.

Dependent on the quality of neuron preparations, the experiments run between ten to 14 days. Initial experiments with all five recombinant viruses demonstrated that SAD P(M83R) eGFP, SAD L(I30T) eGFP, SAD mut12845 eGFP did exhibit a comparable cytotoxicity as SAD eGFP. Hence, the experiment depicted in table 2 was only performed with SAD eGFP SAD mut52/54 eGFP and SAD mut52/54/12845 eGFP.

Day	Mock	SAD eGFP	SAD mut52/54 eGFP	SAD mut52/54/12845 eGFP
8	+++	++-	+++	+++
10	++-	---	+++	+++
12	++-	---	+++	++-
14	+--	---	+--	++-

Table 2: Evalution of a representative experiment, for the investigation of the cytotoxicity of different recombinant viruses in mESC-derived neurons

For the evaluation of the toxicity of the three virus, the morphology of the axons and dendrites was monitored to the indicated time points and classified in healthy neurons (+++), non-healthy neurons (++-), dying neurons (+--) and dead neurons (---).

SAD mut52/54 eGFP and SAD mut52/54/12845-infected neurons lived as long as non-infected cells. Remarkably, it seems that SAD mut52/54/12845 eGFP is even less toxic to the neurons than SAD mut52/54 eGFP, possibly reflecting the slower growth kinetics monitored in HEK293T cells (Figure 28A).

A publication that includes the findings of the *in vitro* evolution experiment, together with findings arising from that project, but which were not part of this thesis, is in preparation.

5 Discussion

RABV is a highly neurotropic virus that apparently enters neurons almost exclusively at the presynaptic membrane by a G-dependent receptor-mediated endocytosis. Once in the neuron, the entire virus particles travels within vesicles retrogradly, in a G-dependent manner, along microtubules to the cell body. Subsequently, a pH-dependent conformational change of G (during the endosomal maturation) induces the fusion of the viral membrane with the endosomal membrane and leads to the release of the RNP complex into the cytoplasm. After viral transcription and replication, taking place in Negri bodies, the RNPs, the matrix proteins, and the glycoproteins or entire virus particles are transported by unknown mechanisms in the anterograde direction to the dendrites. RABV buds from the postsynaptic membrane and infects exclusively presynaptically connected neurons (reviewed in (Davis et al., 2015)).

The G-dependent transsynaptic spread to exclusively presynaptically connected neurons is unique for viruses and predestine RABV as a widely used tool to map neuronal connections, which is a pillar of modern neuroscience. Especially mono-transsynaptic tracing, using pseudotyped G-gene deficient RABV for the infection of defined starter cells and subsequently in situ trans-complementation with RABV glycoprotein, resulting in a single transsynaptic transfer of RABV ΔG has become a popular tool for monosynaptic circuit tracing (reviewed in (Callaway and Luo, 2015; Ghanem and Conzelmann, 2016)).

However, while practically applied, the molecular mechanisms behind the anterograde transport of RABV in dendrites and the exclusive retrograde transsynaptic spread of RABV in the CNS are still not revealed. The discovery of the cellular machineries and mechanisms, which direct the retrograde transsynaptic spread, would be of great interest in order to optimize RABV neuronal tracers, and more importantly, to gain a better insight in the RABV biology and pathogenesis and to devise therapeutic strategies for RABV infection.

The first and overarching aim of this thesis was the establishment of a feeder-free mESC culture system and the establishment of a reliable differentiation protocol of mESCs into mESC-derived glutamatergic pyramidal neurons, to generate an *in vitro* model that allows the examination of the RABV biology in its natural target cells, avoiding extensive animal experiments. While the mESC/neuron system was used in this thesis to study different recombinant RABV, it also provides access to genetically modified neurons by applying CRISPR/Cas9 editing to mESCs, and to derive gene knock-out neurons, as recently demonstrated in our group (unpublished).

Here, the mESC-derived neurons were used for the investigation of the neuronal transfer of RABV. Using reverse genetics to generate recombinant RABVs the influence of the RABV matrix protein, and its interactions with the cellular ESCRT-system on the neuronal transfer of RABV was investigated. Further, recombinant RABVs were generated in order to examine the impact of the SNARE machinery on the transsynaptic spread of RABV.

In addition, engineered G proteins were investigated. Specifically, a site within G that is suitable for the insertion of a trafficking signal should be identified, in order to reroute G and to explore the possibility to generate anterograde travelling viruses in neurons. The possibility to use RABV as an anterograde transsynaptic tracer would greatly extend the applications of RABV for transsynaptic tracing. To this end, specific sites of the ectodomain and the cytoplasmic domain of G were mutated or deleted and the functionality of the resulting G proteins in terms of incorporation into the virion and infectivity were investigated. A recombinant virus was generated by reverse genetics, and the neuronal phenotype of the recombinant virus was investigated in mESC-derived neurons.

Finally, less cytotoxic RABV should be generated which may be useful for long-term studies of RABV infected neurons *in vitro* and *in vivo*. To this end an *in vitro* evolution experiment of SAD eGFP in HEK293T was performed. The genomes of the resulting non-cytotoxic virus mix population were analyzed by NGS, recombinant viruses encoding for some of the identified mutations were generated by reverse genetics and their toxicity was investigated in mESC-derived neurons.

5.1 Establishment of a feeder-free mESC culture and a differentiation protocol of mESCs into mESC-derived glutamatergic pyramidal neurons

The subject matter of this thesis was the successful establishment of a feeder-free mESC culture system and the establishment of a reliable differentiation protocol of mESCs into glutamatergic pyramidal neurons in order to create an *in vitro* model that enables the investigation of the RABV biology in its natural target cells under exclusion of animal experiments.

This was achieved by combining published work, collecting unpublished experience and trial and error approaches. Finally, a reliable protocol for the differentiation of mESCs into glutamatergic pyramidal neurons could be established.

The various states of differentiation were analyzed, using specific markers and observing the morphological changes of the cells. The mESC colonies exhibited the typical round and dome-shaped structure, an increased nucleus to cytoplasm ratio and expressed the pluripotency marker Oct4. The fact that mESCs of passage 28 could be still differentiated efficiently into neurons emphasizes the high-quality mESC culture system that was established in this thesis. The transformation of naive pluripotent mESCs into primed pluripotent mESCs led to Oct4 positive cells that exhibit the characteristic flattened monolayer colonies, indicating that the naive pluripotent mESCs could be successfully transformed into mEpiSC (Figure 7A). The following transformation of mEpiSCs into EBs and neurospheres led to a tremendous increase of the Nestin expression, demonstrating that the cells started to differentiate into neural progenitor cells (Figure 7B). The differentiated neurons exhibited a teardrop-shaped cell body, a single apical dendritic tree, and several basal dendritic trees, leading to the assumption that the mESC-derived neurons were the desired pyramidal neurons (Figure 8A) (Spruston, 2008). Additionally, the non-overlapping staining for an axonal and a dendritic marker indicates a strict sorting of axonal and somatodendritic proteins (Figure 8A). Further, the neurons expressed a marker, which exclusively localizes at glutamatergic synapses (Figure 8A), indicating the mESCs were differentiated into glutamatergic pyramidal neurons (Hunt et al., 1996; Prange et al., 2004). Finally, due to RABV spread within the mESC-derived glutamatergic pyramidal neuron culture (Figure 8B), it can be expected that the mESC-derived neurons were connected via chemical synapsis, as RABV spreads exclusively via chemical synapses(Ugolini, 2011).

In summary, the established feeder-free mESC culture system and the established differentiation protocol enabled a highly reliable production of almost pure, mESC-derived glutamatergic pyramidal neurons, which represent a great model to study the RABV biology in its natural target cells.

5.2 Transsynaptic spread of RABV

5.2.1 M-dependent spread of RABV in neurons

The entire knowledge in respect to the role of the matrix protein in the virus egress is based on studies in immortalized non-neuronal cells or neuroblastoma cells. Hence, the influence of M on the neuronal transfer of RABV in mESC-derived neurons that represents to this date the best *in vitro* model for neurons of the CNS, was investigated.

To this end, mESC-derived neurons were initially infected with an M gene-deficient virus (Figure 10B). In contrast to the observations in non-neuronal non-polarized cell culture cells, SAD ΔM did not exhibit an enhanced CPE. This might be consistent with the neuroprotective effect of the glycoprotein that is described for different RABV strains (Conzelmann, 2011; Prehaud et al., 2010). Another explanation might be that the neurons were not directly in contact with each other. Thus, the possible enrichment of glycoproteins on the cell surface, which was described for SAD ΔM in BSR cells (Mebatsion et al., 1999), did not result in an increased cell-cell fusion activity. Besides, it is conceivable that the mESC-derived neurons are more resistant to the induced cell death pathway that kills SAD ΔM infected BSR cells.

Moreover, the M-deletion mutant exhibited a tremendously impaired neuronal transfer, which most likely was due to a severe budding defect. These findings point out the essential role of the matrix protein in virus budding in neurons and consequently in the neuronal transfer of RABV.

5.2.2 The ESCRT machinery contributes to the neuronal spread of RABV

The RABV matrix protein encodes for the overlapping late domain motif sequence ^{35}PPEYVPL^{41}, but only PPEY is essential for the RABV budding, as was shown in NA cells and BSR cells (Wirblich et al., 2008). However, whether the ESCRT machinery is involved in the neuronal transfer of RABV is unknown.

I started the investigation of the impact of the late domain on the budding of RABV by performing trans-complementation assays of M-gene deficient RABV with two different M mutants, in which the late domain was mutated by alanine substitutions. The trans-complementation of the M-gene deficient virus with M35AA (^{34}PAAEY^{38}) resulted in a minor reduction of infectious virus titers compared to the striking reduction observed with M34AAA (^{34}AAAEY^{38}) (Figure 11A). Probably P34, which was not described as part of the late domain, has an overlooked strong supporting effect in respect to the late domain-dependent, ESCRT-mediated virus release. Indeed, in the epithelial sodium channel (ENaC) the PY-motif PPxY is defined as core motif, which has an N-terminal and a C-terminal extension. The consensus sequence PPPxYxxL is conserved in many

mammalian ENaCs. The three prolines form a poly-proline type II helix and the tyrosine and leucine form a helical turn. Thereby, PPPxYxxL allows a high affinity binding of ENaC to the WW3 of human Nedd4 isoforms (Bobby et al., 2013; Henry et al., 2003). Perhaps, the ^{35}PPEYVPL^{41} motif of M does not represent overlapping late domains but rather an elongated PPxY-motif, as observed in ENaC. This theory is supported by the finding that the recruitment of ALIX by YxxL is not involved in RABV budding (Wirblich et al., 2008), indicating that the late domain motif YVPL in ^{35}PPEYVPL^{41} does not act as an independent late domain, but as an important elongation of the PPEY late domain motif. The extended PPEY-motif may enable a high affinity binding of the RABV matrix protein to Nedd4 and thereby supports a highly efficient recruitment of the ESCRT machinery. Perhaps, additional mutations of tyrosine (Y38) and leucine (L41) would result in an even more severe reduction in the ESCRT-dependent virus release of RABV.

In order to study M34AAA in the viral context, recombinant SAD M34AAA eGFP virus was generated. Interestingly, SAD M34AAA eGFP infected hamster BSR-T7 cells and mouse N2A cells formed multinucleated syncytia, which probably resulted from an increased cell-cell fusion activity (data not shown). Wirblich et al. did not observe an increased cell-cell fusion activity for one of their late domain mutants, although they performed the infection experiments also in BSR-T7 cells and neuroblastoma cells (Wirblich et al., 2008). However, Mebatsion et al. described the formation of syncytia in M gene-deficient SAD infected BSR cells (Mebatsion et al., 1999). These authors explained the cell-cell fusion activity of SAD ΔM as an effect of the accumulation of glycoproteins on the cell surface of the infected cells (Mebatsion et al., 1999). Perhaps, the inefficient recruitment of Nedd4 via the disturbed late domain of SAD M34AAA, resulted in an accumulation of glycoproteins at the plasma membrane, leading due to the G fusion activity to the cell-cell fusion of neighboring cells. Supposedly, the previously published RABV M late domain mutations had a higher rest-activity in terms of Nedd4 binding, resulting in a faster recruitment of the ESCRT machinery and a quicker virus budding. Hence, probably not enough glycoproteins accumulated at the plasma membrane and therewith no cell-cell fusion activity could be observed. The examination of the viral growth kinetics of SAD M34AAA eGFP demonstrated a cell line-independent up to 1000-fold reduction of infectious virus titers in non-polarized cell lines (Figure 11C). In comparison, the M35S single mutant and the M4 multi-mutant exhibited at the most a 100-fold slower growth kinetics (Wirblich et al., 2008). These data support the hypothesis that the extended late domain has a beneficial effect in terms of efficient virus egress.

Since SAD is an attenuated vaccine strain adapted on BHK cells, it is less neurotropic compared to the CVS-N2c strain, which was adapted in mouse brains and on a mouse neuroblastoma cell line (Morimoto et al., 1998; Morimoto et al., 1999; Reardon et al., 2016). To analyze which of the matrix proteins is more severely affected by the disruption of the late domain, a chimeric SAD in

which the SAD M gene was replaced by the CVS-N2c M gene or by the CVS-N2c M34AAA gene was generated. In BSR-T7 cells and N2A cells, the disruption of the late domain in N2c M caused a milder reduction in terms of the viral growth kinetics (Figure 13A) compared to the disruption of the late domain in SAD M (Figure 11C).

The comparison of SAD eGFP and SAD N2c M and the respective late domain mutants in terms of the neuronal transfer in mESC-derived neurons, however, revealed that the chimeric SAD N2c M spread much more efficiently than SAD eGFP (Figure 13B). This indicates that the matrix protein of the highly neurotropic, fixed RABV strain CVS-N2c is better adapted for the budding in neurons, whereas the less neurotropic, attenuated vaccine strain SAD is adjusted to the efficient budding in non-neuronal cells. These date imply that, next to the glycoprotein, the matrix protein might be an important factor for an efficient transsynaptic spread of RABV. Most importantly, the disruption of the late domain in the chimeric SAD N2c M resulted in a more striking blockade of the neuronal transfer compared to the mutation of the late domain in SAD eGFP. After all, also the chimeric SAD N2c M34AAA was still able to spread, albeit poorly, to synaptically connected neurons.

In summary, these data imply that the matrix protein of the neurotropic CVS-N2c supports the neuronal transfer of SAD better than the SAD M protein. Further, it seems like the neuronal spread of the chimeric SAD N2c M is much more adapted and dependent on the ESCRT machinery than SAD eGFP, whereas in non-polarized cell culture lines, the opposite applies. These observations could be interpreted such that RABV may use different budding mechanism in neurons and non-neuronal cells or non-polarized neuroblastoma cells.

It is tempting to speculate that in neurons especially the ESCRT machinery is highly important for RABV to spread to synaptically connected neurons. This might explain why the chimeric SAD with the neuron adapted N2c M spreads more efficiently than the wildtype SAD. Additionally, it might explain why the mutation of the late domain affects the transsynaptic spread of SAD N2c M more severely than that of SAD wildtype. In contrast, the observation that disruption of the N2c M late domain had a minor effect on virus release in BSR-T7 cells and N2A cells compared to the disruption of the SAD M protein late domain might indicate the presence of alternative mechanisms in those cells. Perhaps, the generation of a non-chimeric CVS-N2c M34AAA virus might provide a more consistent insight in terms of the effect of the late domain in the neurotropic CVS-N2c, as chimeric viruses may behave different from the parental virus.

5.2.3 Destruction of SNARE complexes attenuates transsynaptic spread of RABV

5.2.3.1 Dominant-negative syntaxin-1, -3, and -4 hinder the neuronal transfer of SAD

In light of the essential role of SNARE complexes in ubiquitous vesicle fusion events, members of the SNARE family are obvious candidates for RABV egress.

To examine whether one of the plasma membrane located syntaxins is crucial for the spread of RABV in neurons, recombinant SAD encoding for N-terminally fluorescence tagged, dominant-negative syntaxin-1A, -3, -4 and -4/-3 were generated by reverse genetics. Interestingly, in N2A cells only SAD eGFPStx4DN/Stx3DN was moderately attenuated (Figure 15B).

In contrast, in mESC-derived neurons, it seems that the expression of each dominant-negative syntaxin hinder the neuronal transfer of the respective recombinant virus (Figure 15C). Among the recombinant viruses encoding for a single dominant-negative syntaxin, SAD mChStx1ADN showed the strongest defect in neuronal transfer, whereas SAD mChStx3DN and SAD eGFPStx4DN exhibited a rather moderate reduction. Remarkably, the transsynaptic spread of SAD eGFPStx4DN/Stx3DN was at least two-times stronger impaired than the spread of recombinant viruses encoding only for a single dominant-negative syntaxin. Of note, the expression of the dominant-negative syntaxins did not affect the viability of the neurons, indicating that the reduced neuronal transfer is not caused by neurodegeneration, rather by the blockade of the membrane fusion of the cognate SNARE complexes by the respective dominant-negative syntaxin. Appropriate controls to verify the integrity of synapses would include electrophysiological assays, which were not available in the laboratory.

In summary, these data indicate that syntaxin-1A, -3 and -4, which are located at the pre- and postsynaptic membrane (Hussain et al., 2016; Kennedy et al., 2010), might play a role in the neuronal transfer of SAD. Since every dominant-negative syntaxin reduce the neuronal spread of SAD and as the expression of two dominant-negative syntaxins caused an at least two-fold stronger inhibition of the neuronal transfer than the expression of a single dominant-negative syntaxin, it seems possible that SAD is able to alternatively use all three syntaxins and their respective cognate SNARE complexes for the neuronal spread. Therefore, it might be interesting to investigate the effect of the expression of all three dominant-negative syntaxins in parallel, which should result in the blockade of nearly all SNARE complexes (except SNARE complexes which are composed of syntaxin-1B and syntaxin-2), on the neuronal transfer of SAD. Moreover, the effect of the syntaxin-1B isoform on the neuronal transfer of RABV should be investigated. Keeping in mind that the constitutive knockout of syntaxin-1B in mice is lethal (Wu et al., 2015) the use of conditional interference is emphasized. Furthermore, syntaxin-2, which is distributed homogenously at the pre- and postsynaptic compartment, should be included in future studies as

another potential candidate that might support the neuronal transfer of RABV (Kennedy et al., 2010).

5.2.3.2 TeNT and BoNT/A hinder the neuronal transfer of RABV

Using the *in vitro* model for monosynaptic tracing, established in this thesis, and a recombinant G gene-deficient virus encoding for the Vamp-cleaving TeNT-LC, also the involvement of vSNAREs (VAMPs) in the neuronal transfer of RABV was addressed. Surprisingly, the mono-transsynaptic spread of SAD ΔG eGFP-TeNT-LC was as efficient as of SAD ΔG eGFP, indicating that SNARE complexes consisting of the toxin-targeted Vamp1, -2 or -3 do not participate in the neuronal transfer of SAD (Figure 16). However, a potential drawback of using the virus itself as a vector to deliver the TeNT-LC into the neuron is that the neurotoxin is expressed simultaneously with the viral proteins. This might result in a still insufficient cleavage of the Vamps at the time point of viral spread, thus pretending a false negative result in terms of a potential involvement of the three Vamps.

To bypass this problem, neurons were transduced with lentiviruses encoding for eGFP-TeNT-LC to cleave Vamp1, -2 and -3 or encoding for eGFP-BoNT/A-LC to cleave Snap25. Another advantage of this approach was that next to the vaccine strain SAD, also the neurotropic CVS-N2c and the wildtype strain THA could be tested with respect to their sensitivity to these neurotoxins. Interestingly, the transsynaptic spread of the attenuated SAD was most sensitive to the disruption of Vamps and Snap25 (50 % less infected neurons), whereas the neurotropic CVS-N2c and THA were less affected by the cleavage of Snap25 and Vamp1, -2 and -3. In any case, the neuronal transfer of the three virus strains were only slightly reduced in the presence of BoNT/A-LC or TeNT-LC (Figure 17C).

In summary, these data imply that Vamp1, -2 and -3 as well as Snap25 (i.e. fusion of vesicles to the postsynaptic membrane, or release of neurotransmitters from the presynaptic membrane) have only little effect on the neuronal transfer of SAD, THA and CVS-N2c.

The incomplete blockade of the neuronal transfer might be explained by the presence of uncleaved Vamps and Snap25, which were under the detection limit of Western blotting (Figure 17B). As a control for the neurotoxin kinetics, neurons were also transduced in parallel with an eGFP-BoNT/C-LC encoding lentiviruses. BoNT/C-LC cleaves Snap25 as well as syntaxin-1 and causes rapid neurodegeneration *in vivo* and *in vitro* as soon as nearly all syntaxin-1 proteins and Snap25 proteins are cleaved (Peng et al., 2013). Since the mESC-derived neurons were dead at 60 h post transduction with BoNT/C-LC (Figure 17A) it can be assumed that to the time point of

infection with RABV (60 h post transduction), the target proteins of TeNT-LC and BoNT/A-LC were nearly completely cleaved, as also indicated by Western blotting experiments (Figure 17B).

Since Fasshauer et al. demonstrated that SNAREs of the same subclass can substitute each other to a certain extent, the cleaved Vamps or Snap25 might have been complemented by neurotoxin-insensitive R-SNAREs or Qb,c-SNAREs, leading to non-cognate SNARE complexes that support the vesicle fusion and therewith virus budding (Fasshauer et al., 1999; Holt et al., 2006; Yang et al., 1999).

Specifically Snap25 might be replaced by Snap23, Snap29 or Snap47, since all three are resistant to BoNT/A (reviewed in (Verderio et al., 2006).

Snap29 is able to interact with a broad range of syntaxins (Steegmaier et al., 1998). However, Snap29 is not palmitoylated and it is localized at intracellular membranes e.g. Golgi (Steegmaier et al., 1998). Therefore, it is unlikely that Snap29 substitutes Snap25.

Snap47 is distributed in neurons at intracellular membranes and in synaptic vesicle fractions where it exhibits a similar distribution as VAMP2 (Holt et al., 2006). Murine Snap47 preferentially exhibits a somatic and postsynaptic localization (Munster-Wandowski et al., 2017). Additionally, Snap47 is able to substitute Snap25 *in vitro* (Holt et al., 2006). Because of the postsynaptic location and its ability to substitute Snap25 at least *in vitro*, Snap47 might substitute Snap25 and thereby promote the spread of RABV in the absence of uncleaved Snap25. However, since Snap47 is not palmitoylated it is less likely that Snap47 rescues the loss of functional Snap25.

Suh et al. demonstrated that Snap23 is enriched in dendritic spines and colocalizes with constituents of the PSD (Suh et al., 2010). Furthermore, exogenous Snap23 is able to compensate the cleavage of Snap25 by BoNT/E in neurons (Peng et al., 2013). Since Snap23 is like Snap25 palmitoylated (Vogel and Roche, 1999), located at the postsynaptic membrane (Suh et al., 2010), cleaved only inefficiently by BoNT /A (Vaidyanathan et al., 1999) and able to substitute Snap25 (Peng et al., 2013), it might be a good candidate for the substitution of Snap25. However, at least in hippocampal neurons, Snap25 and Snap23 exhibit a different subcellular distribution pattern (Suh et al., 2010).

Possible candidates for the substitution of the tetanusneurotoxin-sensitive Vamp1, -2 and -3 are the tetanusneurotoxin-insensitive Vamp4, -5, -7 and -8.

Since Vamp5 is expressed mainly in muscle cells and it is unable to form a SNARE complex with syntaxin-1 and Snap25 or syntaxin-4 and Snap25 it is unlikely that Vamp5 substitutes the cleaved Vamps and thus enables the neuronal spread of RABV (Hasan et al., 2010).

Vamp8 plays an important role especially in exocrine tissues but not in neurons, making it unlikely that Vamp8 substitutes the cleaved VAMPs in neurons, even it is able to form complexes with syntaxin-1 and Snap25 or syntaxin-4 and Snap25 (Hasan et al., 2010; Wang et al., 2007).

Vamp4 interacts like Vamp2 with syntaxin-1 and Snap25 as well as with syntaxin-4 and Snap25, albeit it exhibits a reduced fusion activity (Hasan et al., 2010). However, it was shown that Vamp4 is present in presynaptic terminals (Raingo et al., 2012), if Vamp4 is also present in the postsynaptic terminals is unknown.

The tetanusneurotoxin-insensitive VAMP (TI-VAMP/VAMP7) is located amongst others in the somatodendritic compartment (Coco et al., 1999). VAMP7 is able to form a functional SNARE complex with syntaxin-1 and Snap25 as well as with syntaxin-4 and Snap25. However, it exhibits a reduced fusion activity compared to VAMP1, -2 or -3. That might explain why RABV spreads slower in the presence of TeNT-LC (Hasan et al., 2010). Due to that, Vamp7 might be a good candidate for the substitution of the Vamp1, -2 and -3.

Taken together, it seems like the SNARE machinery participates in the neuronal spread of RABV. Since all dominant-negative syntaxins caused a reduction in respect to viral spread of SAD, which was greatest after simultaneous expression of dominant-negative syntaxin-4 and syntaxin-3, it seems like the neuronal transfer of RABV is dependent on SNARE complexes, which are composed of one of the three syntaxins. However, a participation of syntaxin-1B or syntaxin-2 is also possible. Further, it seems like SNARE complexes, which consists of Snap25 or Vamp1, -2 or -3 play a role in the spread of RABV. However, a major problem to be solved is that members of a SNARE-subclass can substitute each other. That might explain why there is no total elimination of the RABV spread despite the expression of TeNT-LC or BoNT/A-LC. Considering the subcellular localization and their ability to substitute the respective SNARE-subclass, the most likely candidates for the substitution of Vamp1, -2 and -3 is probably Vamp7 and for the substitution of Snap25 it is probably Snap23.

Interestingly, it seems that there is no noteworthy difference in the influence of the SNARE machinery on the neuronal spread of the attenuated SAD, the neurotropic CVS-N2c and the wildtype THA, although CVS-N2c spreads in mESC-derived neurons much more efficiently than THA or SAD.

5.2.4 Visualization of the spread of RABV in neurons by EM

Since previous results indicated that the ESCRT machinery and the SNARE machinery are involved in the neuronal spread of SAD, EM studies were performed in order to visualize the subcellular localization of SAD during the post-replicative transport of the virus to the postsynaptic membrane and during the budding process. Our preliminary EM data showed probably a bullet shaped SAD particle within an MVB (Figure 18C). This observation would support a working hypothesis in which SAD hijacks MVBs in an ESCRT-dependent manner, followed by a SNARE-driven fusion of the MVB with the plasma membrane.

Notably, in the same cell a single SAD particle was found associated with the plasma membrane (Figure 18C), indicating that SAD might bud by alternative routes. This observation might support a model proposed by Bauer et al. (Bauer et al., 2014) in which the glycoprotein of RABV is embedded in the membrane of a postsynaptic vesicles like an AMPA containing endosome (Jurado et al., 2013). The vesicle with the embedded G proteins, the associated M proteins, and RNP travels to the membrane, and fuses in a SNARE-dependent mechanism with the plasma membrane. Finally, the matrix protein recruits the ESCRT machinery, which drives the budding of SAD into the synaptic cleft.

The preliminary EM studies of SAD infected mESC-derived neurons indicate that SAD can use at least two different routes to bud out of the cell. Interestingly, it seems like SNARE proteins as well as the ESCRT system are involved in the budding of SAD in mESC-derived neurons.

5.2.5 Prospective approaches for studying the neuronal transfer of RABV

The results of this thesis indicate that the extended ^{34}PPPEYVPL^{41} late domain plays an important role in the neuronal transfer of SAD. Further, the results suggest that the neurotropic CVS-N2c strain predominantly exploits the ESCRT complex, since the disruption of the late domain of N2c M affected the neuronal spread of SAD N2c M much more severely than the spread of SAD, which was only moderately affected by the disruption of the late domain. That finding suggests that SAD has a better alternative for budding than the ESCRT machinery. Further, the non-mutated chimeric SAD N2c M spread much more efficiently compared to the parental SAD. It might be interesting to additionally mutate Y38 and L41 (M34AAAEAVPA), since these mutations should further decrease the binding affinity of the extended late domain to Nedd4 (Henry et al., 2003), possibly leading to a stronger blockade of the neuronal spread of SAD and SAD N2c M than M34AAA.

Moreover, it might be interesting to monitor by EM studies, whether the disruption of the extended late domain causes a different subcellular localization of the matrix protein and thereby a different location of virus assembly sites in mESC-derived neurons. Perhaps, the disrupted late domain causes an enrichment of RNPs at the cytoplasmic face of MVBs, since the mutated matrix protein is unable drive the ESCRT-dependent budding into MVBs. Further, an even stronger enrichment of membrane-associated viruses particles at the plasma membrane, as previously described in HeLa cells (Wirblich et al., 2008), could be expected since the interaction of this M late domain-mutant with Nedd4 should be completely impaired, resulting in an inhibition of RABV budding.

Since the most dramatic reduction of the neuronal transfer of RABV was observed for the recombinant virus encoding for dominant-negative Stx4 and Stx3, it might be interesting to investigate the neuronal spread of RABV in the presence of dominant-negative Stx1A, 3 and 4. To

ensure that SNARE complexes are already blocked before virus assembly, the neurons should be transduced with lentivirus encoding for the respective dominant-negative syntaxins. Further, Stx2 and syntaxin-1B should be included in the studies as further potential components of the SNARE-complex used for the neuronal spread of RABV. As SNARE complexes are essential for neuron survival, it remains to be investigated whether neurons would survive the simultaneous expression of three, four or even five different dominant-negative syntaxins, which would reduce the amount fusion capable SNARE complexes at the plasma membrane dramatically. Especially the expression of dominant-negative syntaxin-1B might be toxic to the cells (Wu et al., 2015). Furthermore, the investigation of the neuronal transfer of RABV in neurons, which were transduced with dominant-negative VAMPs, Snaps or combinations of dominant-negative syntaxins, Vamps and Snaps might provide a good insight into the exact composition of a potentially favored SNARE complex used by RABV for the transsynaptic spread. However, especially Vamp2 and Snap25 are the most interesting candidates because of their postsynaptic localization (Antonucci et al., 2016; Hussain and Davanger, 2015).

If none of the above mentioned approaches regarding the participation of SNAREs and ESCRT led to a nearly total blockade of neuronal transfer of RABV, this might support the model that the SNARE proteins and the ESCRT machinery provide two independent routines for virus egress. This model could be addressed by analyzing the transsynaptic spread of RABV, bearing the mutated extended late domain M34AAAEAVPA, in mESC-derived neurons, which were transduced with lentiviruses encoding for different combinations of dominant-negative SNARE proteins.

5.2.6 Working hypothesis for the neuronal transfer of RABV

Indeed there are now three working hypothesis for the RABV budding at the postsynaptic membrane. In the first model a virus particle buds in an ESCRT-dependent mechanism into a exocytotic vesicle (e.g. AMPA-containing endosome) that is sorted to the postsynaptic membrane, the vesicle fuses in a SNARE-driven process with the plasma membrane and the entire virion is released into the synaptic cleft (Bauer et al., 2014). In the second model, RABV buds into a MVB in an ESCRT-dependent way, followed by a SNARE-dependent fusion of the MVB with the presynaptic membrane. One component of the SNARE complex is probably the tetanus neurotoxin-insensitive Vamp7, as it participates in the fusion of the MVB with the plasma membrane (Fader et al., 2009). In the third model, RABV glycoproteins are embedded into the membrane of an exocytotic vesicle that is sorted to the postsynaptic membrane. The cytoplasmic RNP-complex is associated via matrix proteins with the glycoproteins (Bauer et al., 2014). The vesicle travels to the postsynaptic membrane. After a SNARE-drive fusion of the vesicle with the plasma membrane, the G is embedded into the plasma membrane and the cytoplasmic RNP-

complex is still associated via M with G. The matrix protein recruits the ESCRT-machinery and thereby initiates the ESCRT-dependent virus budding into the synaptic cleft.

5.3 Insertion of a trafficking signal downstream of the transmembrane domain is a potential site for rerouting SAD G

The aim of the this part of the thesis was the identification of permissive sites within the SAD glycoprotein for the insertion of external trafficking signals in order to change the subcellular distribution of G, or to retarget RABV to alternative receptors.

The first approach was the insertion of the eleven aa long neuropeptide Substance P into the nAChR binding site or the antigenic site III within the ectodomain of G. However, neither of the recombinant glycoproteins in which these sites were deleted or substituted by SP were incorporated into virus particles. Probably, each of the mutations interfered with the correct folding of the glycoprotein and thereby prevented the correct trafficking, glycosylation and/or incorporation into the viral membrane (Figure 21).

Since the ectodomain appeared too sensitive for modifications, the cytoplasmic domain of G was targeted for the insertion of a trafficking signal. Three copies of KBS were inserted directly downstream of the transmembrane domain (G-3xKBS) or at the C-terminus of the C-tail (G-TM-3xKBS-RT). The latter was incorporated effectively into the virion and led to the formation of infectious virus particles (Figure 21). While the recombinant SAD G-TM-3xKBS-RT eGFP was in BSR-T7 cells clearly attenuated (Figure 22A), it exhibited only a mildly reduced transsynaptic spread compared to SAD eGFP (Figure 23). Since the glycoprotein should not have an effect on viral transcription or replication, the slower growth kinetics in BSR-T7 cells as well as the slightly reduced neuronal transfer in mESC-derived neurons indicate a less efficient virus assembly, budding, attachment, or entry of SAD G-TM-3xKBS-RT eGFP. Analysis of the protein composition of the SAD G-TM-3xKBS-RTeGFP virions showed an enrichment of the envelope proteins M and G, which was not reflected in the cellular expression level of the infected cells (Table 1). Keeping in mind that the virions were pelleted by an ultracentrifugation step it cannot be excluded that the pellet contained extracellular vesicles like exosomes and microvesicles. Perhaps, the KBS copies downstream of the transmembrane domain reduced the interaction of the cytoplasmic tail with the matrix protein and thereby with the RNP complex, resulting in a less efficient virus release, which would explain the slower growth kinetics. Furthermore, it might lead to the release of G and M containing vesicles into the supernatant, which would be an explanation for the enrichment

of G and M in the pelleted supernatant. To gain a more sophisticated insight into the composition of the virions, the supernatant of infected cells should be subjected to a gradient ultracentrifugation to separate virions and extracellular vesicles, followed by SDS-PAGE, Western blotting and immunostaining of the virion fraction and the extracellular vesicle-containing fraction.

Regarding the rerouting of the G-TM-3xKBS-RT in mESC-derived neurons, no notable difference concerning dendritic and axonal distribution could be identified (Figure 24). Notably, even the staining for wildtype G that was expected to be restricted to the somatodendritic compartment, overlapped with the staining for an axonal marker. Since axonal and dendritic marker did not overlap, it might be that the mESC-derived neurons have a less clear-cut sorting at the PAEZ for the glycoprotein than primary hippocampal neuronal cultures, which were used by Farias et al. (Farias et al., 2015). Another explanation for the less efficient sorting at the PAEZ might be that Farias transfected the NiV-F-KBS constructs, while in this thesis the neurons were infected with the recombinant virus.

However, whereas the staining of G revealed a granular distribution, which might resemble the distribution of PSDs, the staining for G-TM-3xKBS-RT was homogenous, indicating that the trafficking signal does change the distribution of G in mESC-derived neurons. Therefore, it might be interesting to monitor the distribution of G-TM-3xKBS-RT in primary hippocampal neuronal cultures, in which the axonal transport of NiF-KBS was demonstrated. Perhaps, these cells exhibit a more strict sorting of the glycoprotein as mESC-derived neurons, which could result in a more distinct axonal sorting of G-TM-3xKBS-RT. Furthermore, it would be interesting to address the question whether G-TM-3xKBS-RT is able to change the subcellular localization of the matrix protein and/or the RNP-complex or another control protein. If not, it should be considered to tag M and the RNP proteins (N, P, and L) with KBS in order to direct them to the presynaptic membrane. In case this can be achieved, it must be investigated, whether the virus is able to bud from the presynaptic membrane and can infect postsynaptically connected neurons. It might be that additional components of the postsynaptic density, which are absent at the presynaptic membrane, are needed for the virus budding. However, the SNARE and the ESCRT machinery are also located at the presynaptic membrane, which could be sufficient to drive the virus budding. Further, it has to be clarified if RABV can enter neurons of the CNS at the postsynaptic membrane by receptor-mediated endocytosis. However, previous work already demonstrated that RABV can travel anterogradely in peripheral sensory neurons and from peripheral neurons to the CNS (Astic et al., 1993; Bauer et al., 2014; Zampieri et al., 2014). Taken together, G-TM-3xKBS-RT might be the first step in a very long journey towards an anterograde transsynaptic tracing model, which would be a powerful tool to investigate neuronal circuits in the CNS.

5.4 *In vitro* evolution experiment of SAD eGFP

In contrast to virulent RABV street viruses, the attenuated SAD L16 exhibits a more pronounced cytopathogenicity. An *in vitro* evolution experiment of SAD eGFP in HEK293T cells was performed in order to identify non-cytotoxic SAD variants and to study a persistently infected cell culture system. For this approach, it was expected that toxic SAD eGFP kills infected cells, while mutated, non-toxic viruses do not kill the cells and therefore could be enriched by cell passaging. However, survival of the cells could be caused by mutations in the cell genome, which make the cells less sensitive to the toxic effect of SAD eGFP, too.

5.4.1 SAD eGFP *in vitro* evolution resulted in a non-cytotoxic virus

The *in vitro* evolution experiment resulted in virus producing HEK293T cells, whose viruses were still infectious for fresh cells. Investigation of the growth kinetics and cytotoxicity of the virus pool SAD eGFP p15 in fresh cells revealed that SAD eGFP p15 stock grew as fast as the parental SAD eGFP, but SAD eGFP p15 exhibited a strikingly reduced cytotoxicity in HEK293T cells (Figure 26). The loss of the cytotoxicity of SAD eGFP p15 indicates that the cells of the *in vitro* evolution experiment survived most likely due to mutations in virus genome, rather than mutations in the cell genome. However, an additional adaption of the HEK293T cells cannot be excluded.

The next generation sequencing of the viral genome demonstrated that only six mutations had an incidence rate of at least 30 %. The six mutations appeared in a diversified frequency, reflecting the existence of a mixed SAD eGFP p15 population. Two mutations are located within the non-coding but transcribed leader region, one mutation is located in the non-coding and non-transcribed trailer region, another one is located within the phosphoprotein gene, and two point mutations were identified within the RNA-dependent RNA polymerase L.

To clarify, whether the non-cytotoxic phenotype of SAD eGFP p15 can be attributed to a single mutated region, recombinant viruses encoding for a single mutated region and a recombinant virus containing the mutated leader and trailer region were generated and characterized in terms of growth kinetics, eGFP fluorescence, and cytotoxicity in HEK293T cells (Figure 28).

The mutation of the phosphoprotein caused a loss of the P4 start codon and therewith probably a loss of the transcription variant P4. However, eGFP fluorescence, growth kinetics, and cytotoxicity were comparable with the parental SAD eGFP virus. Since it is already known that the P4 isoform is not essential for the virus life cycle these findings are not surprising (Brzozka et al., 2005). The first mutation within the L-gene caused a mutation of hydrophilic Ile into the hydrophobic Thr. However, SAD L(I30T) eGFP exhibited the same growth kinetics, eGFP fluorescence and cytotoxicity as the parental SAD eGFP, suggesting that the point mutation within

the RNA-dependent RNA polymerase does not affect neither the viral transcription nor the viral replication. The second mutation within the L-gene led to an introduction of an in frame stop codon within the L-gene. However, SAD L(stop) eGFP exhibited the same growth kinetics as the non-passaged SAD eGFP virus, but SAD L(stop) eGFP was defect for eGFP expression, such that the identity and the sequence of the virus has to be reexamined. As the virus grew as fast as the non-passaged virus, it is implausible that the virus had a defect concerning gene expression. However, since this virus was not of immediate interest for the purpose of this thesis, it was not further addressed. The trailer-mutation was the most frequent mutation, which was present in 94 % of all NGS reads. It exhibited a comparable eGFP fluorescence, grew as fast as the parental virus, and was as cytotoxic as the parental SAD eGFP in HEK293T cells.

Notably, the recombinant viruses SAD mut52/54 eGFP and SAD mut52/54/12845 eGFP exhibited a milder cytotoxicity in HEK293T cells and slower viral growth kinetics, which was associated with a reduced eGFP fluorescence. These observations might be explained by a reduced transcription and/or replication activity of these two viruses. Since the triple mutant SAD mut52/54/12845 eGFP behaves like SAD mut52/54 eGFP, it seems like the mutations in the leader region are dominant, since the trailer-mutation alone does not change the phenotype of the virus. Since the trailer-mutation is the most prominent mutation, it might be interesting to investigate whether the trailer-mutation supported the evolution of the less frequently mutated leader region.

Final investigations of the cytotoxicity of the recombinant viruses in mESC-derived neurons revealed that SAD mut52/54 eGFP and SAD mut52/54/12845 eGFP infected neurons lived as long as non-infected neuronal cultures and thus much longer than mESC-derived neurons infected with the parental SAD eGFP. The eGFP expression levels of SAD mut52/54 eGFP and SAD mut52/54/12845 eGFP infected neurons were up to five days post infection slightly reduced (data not shown), indicating that the two recombinant viruses exhibited also in neurons a reduced viral transcription and probably a reduced viral replication rate.

In summary, SAD mut52/54 and SAD mut52/54/12845 exhibited compared to parental SAD eGFP a strongly reduced cytotoxicity in non-neuronal HEK293T cells as well as in mESC-derived neurons. The low cytotoxicity of SAD mut52/54 eGFP and SAD mut52/54/12845 eGFP in neurons and HEK293T cells might be attributed to their reduced gene expression, which is represented by their reduced eGFP protein level. Morimoto et al described a direct correlation between the induction of apoptosis and increasing amounts of RABV glycoproteins (Morimoto et al., 1999). It would be imaginable that the reduced gene expression rate leads to a reduced glycoprotein level, which might act in an anti-apoptotic fashion.

Another theory, which is supported by data from Alexander Ghanem, might be that the reduced cytotoxicity of the two viruses in HEK293T cells and mESC-derived neurons might be due to a

reduced synthesis of viral RNAs and the reduced production of RNA products. Thereby, less cytosolic 5´triphosphate dsRNAs would be present within the cell. The 5´triphosphate dsRNAs is usually recognized by RIG-I that in turn leads to the induction of type I interferon genes or eventually programmed cell death in order to elimante severe infections (Hornung et al., 2006; Wang et al., 2016). Perhaps, the RNA levels of both leader mutants are too low, to induce the programmed cell death.

5.4.2 Future outlook

To characterize the exact effects of the leader mutations in terms of viral transcription, it would be necessary to evaluate and compare the transcription levels and RNA products of SAD mut52/54 eGFP or SAD mut52/54/12845 eGFP with the parental SAD eGFP virus using Northern blotting and RT-qPCR. In particular, the presence or enrichment of defective interfering particles and RNAs could be evaluated by these methods. Furthermore, knockout screens could be performed in order to identify how exactly RABV kills the cells and why the leader mutants exhibit a reduced neuronal toxicity.

Furthermore, the findings of this thesis imply the generation of a chimeric SAD virus comprising of SAD mut52/54 and the N2c matrix protein. The chimeric G-gene deficient SAD mut52/54 N2cM ΔG might be a tracer that is superior to SAD ΔG in transsynaptic transmission due to the N2c matrix protein and less toxic than SAD ΔG because of the leader mutations. In addition, SAD mut52/54 N2c M ΔG might be superior to N2c ΔG in terms of protein expression.

6 Appendix

6.1 List of oligonucleotide sequences

Name (numerical order)	Sequence (5´- 3´)
MEP6fw	ATAGCTAGCGCCACCATGGTGAGCAAGGGC
MEP6rv	ATATGCGGCC GCTTATTTCT TCTTCCTCGC
MEP7fw	ATAGCTAGCACCGCCATGGTGAGCAAGGGC
MEP7rev	ATAGCTAGCACCGCCATGGTGAGCAAGGGC
MEP8rev	TATGCGGCCG CCTATTTCTT CCGGCGCGCC
MEP25rv	TATGCGGCCG CTTATTATAT AATGATCTAC C
MEP27fw	ATAGCGGCCGCTGTGAAAAAAACTATTAACATCCCTCAAAAGACTCAAGGAAA GGCTAGCGCCACCATGAAGGACCGTCTGGAGCAGC
MEP27rv	TATCCGCGGTTACTGACTCTGGTATTTCACAGC
MEP31fw	ATAGCTAGCGCCACCATGGTGAGCAAGGGCG
MEP43fw	ATAGAATTCGCCACCATGGTTCCTCAGGC
MEP43rv	TATCTCGAGT TACAGTCTGG TCTC
MEP46fw	GTGTCTTCTACCTACTGCTCCACTAACCACGATAGACCCAAGCCTCAGCAGTTCT TTGGATTAATGGGGATGTCTTGTGACATTTTTACCAATAGTAGAG
MEP46rv	CTCTACTATTGGTAAAAATGTCACAAGACATCCCCATTAATCCAAAGAACTGCT GAGGCTTGGGTCTATCGTGGTTAGTGGAGCAGTAGGTAGAAGACAC
MEP47fw	CCTACTGCTCCACTAACCACGATGGGATGTCTTGTGACATTTTTACC
MEP47rv	GGTAAAAATGTCACAAGACATCCCATCGTGGTTAGTGGAGCAGTAGG
MEP-59fw	ataATCGATCAGAACCTACGCAACAC
MEP60fw	CCATTGTCCCCAACACCTTGAGGAACTCTG
MEP60rv	CAGAGTTCCTCAAGGTGTTGGGGACAATGG
MEP62fw	CGAGAGGACTTTCAGAGAGATGAAGGAGAGGATCC
MEP62rv	GGATCCTCTCCTTCATCTCTCTGAAAGTCCTCTCG
MEP64fw	GCTCCCAAGAGTCCTAGATTCACGCGTTGTGTC
MEP-64rev	GACACAACGCGTGAATCTAGGACTCTTGGGAGC
MEP69fw	ctgaGCGGCCGCCACCGCG
MEP69rv	ATCGAAAGTGCATTCCTTGATATTCTCTCC
ME70fw	TCAAGGAATGCACTTTCGATATACAGAGCC
ME70rv-	GAGCACCGGTTGCCCACTGAAC

MEP80fw	CCCAAGCCTCAGCAGTTCTTTGGATTAATGggcagcggaCTCCCTTCAAAAGGGtgtttaag
MEP80rv	AATCCAAAGAACTGCTGAGGCTTGGGTCTgcttccggagccGTAGTGAGCATCGGcttcc
MEP83fw	GCCGATGCTCACTACCTCCCTTCAAAAGGG
MEP83rv	CCCTTTTGAAGGGAGGTAGTGAGCATCGGC
MEP88fw	TATAACCCTAGGAAAGGCTCCCG
MEP103fw	ataGAATTCgccaccATGAACCTCCTACGTAAGATAG
MEP103rv	ataGCTAGCTTATTCTAGAAGCAGAGAGG
MEP108rv	GtcccaTtccagAttTgtaccaatcgcactgtcatcccactccaggttggtAGATCCCAGGCTCAGTCTGGTCTCACCCCCAC
MEP109rv	tatGCTAGCTTAaatcgcactgtcatcccactccaggttggttccGAtTgcGGAAtcGtcccaTtccagAttTgtaccaatcg
MEP110Afw	ataGCATGCAAACTCAAGTTATGTGG
MEP110Brv	cccactccaggttggtAGATCCCAGGCTACAACATGTCATCAGG
MEP110Crv	tccGAtTgcGGAAtcGtcccaTtccagAttTgtaccaatcgcactgtcatcccactccaggttggt
MEP110Drv	tatGCTAGCTTACAGTCTGGTCTCACCC
MEP110Efw	gtgggatgacagtgcgattAGAAGAGTCAATCGATCAG
MEP110Ffw	ggaAtgggaCgaTTCCgcAaTCggaaccaacctggagtgggatgacagtgcgattAG
ME111Afw	ataACTCGAGGGTCTTCCCTAGCG
ME111Brv	tatATCGATTGACTCTTCTaatcg
MEP112rv	tatgctagcCAGATCCGAAAGGAG
MEP115Afw	ataGGCGCGCCTAATACGACTCAC
MEP115Brv	CAGCGGGACATATTCcgctgcagcAAGCCACAGGTCATCGMEP
MEP115Cfw	CGATGACCTGTGGCTTgctgcagcgGAATATGTCCCGCTG
MEP115Drv	TTTGTATACCCAGTTCATGCCCTCAGG
ME120Arv	CTTGCGTAGAACGTTCATTTTATCAGTGGTGTTGCCTGTTTTTTTC
MEP120B fw	GAAAAAAACAGGCAACACCACTGATAAAATGAACGTTCTACGCAAGATA
MEP120B rv	GTGATAAATTTGCGGGATATAATCTGATTATTCTAGAAGCAGAGAAGAGTCTTTG
ME120C fw	CAAAGACTCTTCTCTGCTTCTAGAATAATCAGATTATATCCCGCAAATTTATCAC
ME120C rv	GAAGACCCTCGAGTGAAGGGATCTGTC

6.2 Cloning strategies of plasmids produced in this thesis

Plasmid (alphabetical order)	Description
pCAGGS-M34AAA	M34AAA was amplified from pSAD M34AAA and prolonged by adequate restriction sites using primer MEP103fw and MEP103rv. The PCR product and the pCAGGS vector were digested with EcoRI and NheI and subsequently ligated.
pCAGGS-M35AA	M35AA was amplified from pSAD M35AA and prolonged by adequate restriction sites using primer MEP103fw and MEP103rv. The PCR product and the pCAGGS vector were digested with EcoRI and NheI and subsequently ligated.
pCAGGS-SADG-ΔNAChbinding site	The glycoprotein sequence downstream of the nAChR binding site was amplified from pCAGGS G using primer MEP43fw and MEP47rv (product A). The sequence upstream of the nAChR binding site was amplified from pCAGGS G using primer MEP47fw and MEP43rv (product B). The PCR products were fused by a PCR using MEP43fw and MEP43rv. The PCR product AB and the pCAGGS G vector were digested with EcoRI and XhoI and subsequently ligated.
pCAGGS-SADG-ΔNAChbinding site-(SP)	The nAChR binding site was substituted with SP using an overlap PCR. The glycoprotein sequence downstream of site III was amplified from pCAGGS G and prolonged by the linker-SP-linker sequence using primer MEP43fw and MEP46rv (product A) and the sequence upstream of the nAChR binding site was amplified and prolonged by the linker-SP-linker sequence using primer MEP46fw and MEP43rv (product B). The PCR products were fused by a PCR using MEP43fw and MEP43rv. The resulting PCR product and the pCAGGS G vector were digested with EcoRI and XhoI and subsequently ligated.
pCAGGS-SADG-Δ-siteIII	The glycoprotein sequence downstream of the antigenic site III site was amplified from pCAGGS G using primer MEP43fw and MEP83rv (product A). The sequence upstream of the site III was amplified from pCAGGSG using primer MEP83fw and MEP43rv (product B). The PCR products were fused by a PCR using MEP43fw and MEP43rv. The PCR product AB and the pCAGGS

	G vector were digested with EcoRI and XhoI and subsequently ligated.
pCAGGS-SADG-Δ-siteIII [(GS)2-SP-(GS)2]	The antigenic site III was substituted with SP using an overlap PCR. The glycoprotein sequence downstream of the antigenic site III site was amplified from pCAGGS G and prolonged by linker-SP-linker sequence using primer MEP43fw and MEP80rv (product A). The sequence upstream of the site III was amplified from pCAGGS G and prolonged by linker-SP-linker using primer MEP80fw and MEP43rv (product B). The PCR products were fused by a PCR using MEP43fw and MEP43rv. The PCR product AB and the pCAGGS G vector were digested with EcoRI and XhoI and subsequently ligated.
pCAGGS-G-TM-3xKBS-RT	The transmembrane domain was amplified from pCAGGS G and prolonged with linker-3xKBS with MEP110Afw, MEP110Brv, MEP110Crv and ME109rv. The cytoplasmic tail was amplified and prolonged upstream of the C-tail with ME110Efw, MEP110Ffw and MEP110Drev. The two PCR products were fused by a PCR with MEP110Afw and MEP110Drv. The PCR product and the vector pCAGGS G were digested with SphI and NheI and subsequently ligated.
pCAGGS-SADG 3xKBS	The linker and the three KBS copies were inserted downstream of the cytoplasmic tail by amplification from pCAGGS G and prolonged with linker and three KBS copies using MEP43fw, MEP108rv and MEP109rv. The PCR product and the pCAGGS vector were digested with EcoRI and NheI and subsequently ligated.
Full-length RABV constructs	
pN2c M34AAA	N2c M34AAA was mutagenized with an overlap PCR using MEP115Afw and MEP115Brv for PCR A and MEP115Cfw and MEP115Drv for PCR B. The products were fused by PCR with oligos MEP115Afw and MEP115Drv. PCR product AB and vector pN2C were digested with AscI and BstZ17I and subsequently ligated.

pSAD eGFPStx4DN	eGFP-Stx4DN was amplified from eGFP Stx4 ΔTM (Ehlers) and prolonged with adequate restriction sites using MEP6fw and MEP6rv. PCR product and vector pSAD eGFP were digested with NheI and NotI and subsequently ligated.
pSAD eGFPStx4DN/Stx3DN	Stx3DN was amplified from pSAD-mChStx3DN and prolonged by the M/G gene border and adequate restriction sites using oligos MEP27fw and MEP27rv. The PCR product and the pSAD-eGFPStx4DN were digested with NotI and SacII and subsequently ligated
pSAD G-TM-3xKBS-RTeGFP	C-tail was amplified from pSAD eGFP and prolonged by adequate restriction sites using primer MEP59fw and MEP112rv (product B). Parts of the ecotdomain, TM and KBS were amplified and prolonged by adequate restriction sites from pCAGGS-SADG(1-480)-3KBS-RT (product A) with primer MEP111fw and MEP111rv. Product A was digested with PspXI and ClaI, product B with ClaI and NheI and the vector pSAD eGFP with PspXI and NheI, followed by ligation.
pSAD L(I30T) eGFP	pSAD eGFP was mutagenized to pSAD L(I30T) eGFP by an overlap PCR, using oligos MEP69fw/MEP60rv (PCR product A) and MEP60fw/MEP69rv(PCR product B). The PCR products were fused using MEP69fw and MEP69rv (PCR product AB). Vector pSAD eGFP and PCR product AB were digested with NotI and BsmI and subsequently ligated.
pSAD L(stop) eGFP	pSAD eGFP was mutagenized to pSAD L(stop) eGFP by an overlap PCR, using oligos MEP70fw/MEP64rv (PCR product A) and MEP64fw/MEP70rv(PCR product B). The PCR products were fused using MEP64fw and MEP64rv (PCR product AB). Vector pSAD eGFP and PCR product AB were digested with BsmI and AgeI and subsequently ligated.
pSAD mchStx1ADN	mCh-Stx1DN was amplified from mCherry Stx1 ΔTM (Ehlers) and prolonged with adequate restriction sites using MEP7fw and MEP8rv. PCR product and vector pSAD eGFP were digested with NheI and NotI and subsequently ligated.

pSAD mChStx3DN	mCh-Stx3DN was amplified from mCherry Stx3 ΔTM (Ehlers) and prolonged with adequate restriction sites using MEP7fw and MEP7rv. PCR product and vector pSAD eGFP were digested with NheI and NotI and subsequently ligated.
pSAD M34AAA eGFP	M34AAA was cut out from pCAGGS M34AAA with SnabI and BstZ17I and ligated with the digested pSAD eGFP vector.
pSAD N2CM	pSAD N2CM was generated by a triple fragment overlap PCR. pSAD L16 was the template for PCR A (MEP88fw/MEP120Arv) and PCR C (MEP120Cfw/MEP120Crv). N2CM was amplified from pN2C with MEP120Bfw and MEP120Brv. The fragments were fused by a PCR reaction with all three fragments using MEP88fw and MEP120Crv. The PCR product ABC and the vector pSAD L16 were digested with BstBI and subsequently ligated.
pSAD N2c M34AAA	pSAD N2c M34AAA was generated by a triple fragment overlap PCR. pSAD L16 was the template for PCR A (MEP88fw/MEP120Arv) and PCR C (MEP120Cfw/MEP120Crv). N2c M34AAA was amplified from pN2c M34AAA with MEP120Bfw and MEP120Brv. The fragments were fused by a PCR using oligos MEP88fw and MEP120Crv. The PCR product ABC and the vector pSAD L16 were digested with BstBI and subsequently ligated.
pSAD P(M83R) eGFP	Mutagenization of P(M83R) in a pCAGGS-N-P-part vector using oligos MEP62fw/MEP62rv. Subsequently, PCR product and pSAD L16 vector were digested with SnabI and NcoI, followed by ligation. P(M83R) were cut out with AvrII and SnabI and ligated with the digested pSAD eGFP vector.
Recombinant SAD deletion mutants	
pSAD ΔG eGFP-TeNT-LC	eGFP was amplified form pCAGGS eGFP and prolonged with adequate restriction sites and an overhang with 5´end of TeNT-LC using primer MEP31fw and MEP26rev. TeNT-LC was amplified from pCMV-TeNT-LC and prolonged with adequate restriction sites and an overhang with the 3´end of eGFP. Finally, the PCR products were fused by a PCR reaction using

	MEP31fw and MEP26rev, digested with NheI and NotI and ligated with the digested vector pSAD ΔG eGFP.
pSAD ΔM eGFP	The ΔM region was cut out from pSADΔM with AvrII and PspXI and ligated with digested pSAD eGFP vector.

6.3 List of abbreviations

In the following table, the abbreviations used in this thesis are listed.

Abbreviation	Description
%	per cent
2i	Two inhibitors
α	anti
Δ	delta-, deletion
5´-ppp	5´-triphosphate
A	adenine
Aa	amino acid
ABLV	Australian bat lyssavirus
ALIX	apoptosis-linked gene 2-interacting protein X
Amp	ampicllin
AMPA	α-amino-3-hydroxy-5-methyl-4-isoxazolepropionic acis
APS	ammonium persulfate
ATP	Adenosine triphosphate
BF	Bright field
BMP	bone morphogenetic protein
BoNT/A	Clostridium botulinum neurotoxin A
BoNT/C	Clostridium Botulinum neurotoxin C
bp	base pair
C	Cytosine
CDC	center of disease control and prevention
cDNA	complementary DNA
CNS	central nervous system
CNT	Clostridial neurotoxin
CPE	cytopathic effect
cRNA	Complementary RNA

C-tail	Cytoplasmic domain
CTD	C-terminal domain
C-terminal	carboxyterminal
CVS	Challenged virus
d	day
Da	dalton
ddH_2O	bidestilled water
DMSO	Dimethyl sulfoxid
DNA	Deoxyribonucleic acid
dNTP	deoxyribonucleotide
dsRNA	double stranded RNA
EBOV	Ebola virus
eGFP	Enhanced green fluorescent protein
EIAV	Equine infectious anemia virus
EM	electron microscopy
EMCV	Encephalomyocarditis virus IRES
EnvA	Envelope protein A
ESCRT	Endosomal sorting complexes required for transport
ERK	extracellular signal-related kinase
EV	empty vector
FCS	fetal calf serum
ffu	focus forming unit
FGF	fibroblast growth factor
G	glycoprotein
G	Guanine
GSK3	glycogen synthase kinase-3
h	hour
HC	Heavy chain
ICM	Inner cell mass
ICTV	International Committee on Taxonomy of Viruses
IGS	intergenic sequence
IRES	Internal ribosomal entry site
ISG	interferon-stimulated genes

HIV	Human immunodeficiency viurs
HRP	horseradish peroxidase
HTLV	Human T-lymphotropic virus
IF	immunofluorescence
JAK	Janus kinase
KBS	Kinesin-light chain binding sequence
L	Large protein
LC	Light chain
LD_{50}	Lethal dose, 50%
Le	leader
LIF	Leukemia inhibitory factor
LV	Lentiviral vector
M	Matrix protein
M	molar
mESC	Mouse embryonic stem cells
mEpiSCs	Mouse epiblast stem cells
MOI	multiplicity of infection
mRNA	messenger RNA
MVB	multivesicular bodies
N	nucleoprotein
nAChR	Nicotinic Acetylcholin receptor
NCAM	Neuronal Cell Adhesion Molecule
Nedd4	neuronal precursor cell-expressed developmentally gene 4
NGS	Next-generation sequencing
NMJ	Neuron Muscular Junction
NNSV	non-segmented negative strand RNA viruse
nt	nucleotide
N-terminal	aminoterminal
P	Phosphoprotein
p75NTR	p75 Nerve Growth Factor receptor
PNS	Peripheral nervous system
PSD	Postsynaptic density
RA	Retinoic acid

RNA	ribonucleic acid
RSV	Respiratory syncytial virus
SDS	Sodium dodecyl sulfate
SNARE	Soluble N-ehtlymaleimide-sensitive-factor attachment receptor
T	thymidine
TeNT	Tetanus neurotoxin
TM	Transmembrane domain
PEP	post exposure prophylaxis
p.i.	post infection
PAGE	polyacrylamide gel electrophoresis
PBS	phosphate buffered saline
PCR	polymerase chain reaction
PEI	polyethylenimine
PVDF	polyvinylidene fluoride
pH	Potential of hydrogen
RA	Retinoic acid
RABV	Rabies virus
RABV G	Rabies virus glycoprotein
RABV L	Rabies virus large protein
RABV M	Rabies virus matrix protein
RABV N	Rabies virus nucleoprotein
RABV P	Rabies virus phosphoprotein
RFP	Red fluorescent protein
RIG-I	Retinoic acid inducible I
RNP	ribonucleoprotein
RT	room temperature
SAD	Street Alabama Dufferin
SeV	Sendai virus
Snap25	synaptosome-associated protein of 25 kDa
SP	Substance P
SP	Signal peptide
ssRNA	single strand RNA
STAT	Signal transducer and activator of transcription

T7-Pol	T7 RNA polymerase
Tr	trailer
t-SNARE	target-membrane SNARE
U	unit
VAMP	Vesicle associated membrane protein
VPS4	vacuolar protein-sorting associated protein 4
v-SNARE	vesicular SNARE
VSV	Vesicular stomatitis virus
WB	Western blotting
wt	wildtype

7 List of figures and tables

7.1 List of figures

7.2 List of tables

8 References

Afonso, C.L., Amarasinghe, G.K., Banyai, K., Bao, Y., Basler, C.F., Bavari, S., Bejerman, N., Blasdell, K.R., Briand, F.X., Briese, T.*, et al.* (2016). Taxonomy of the order Mononegavirales: update 2016. Arch Virol *161*, 2351-2360.

Albertini, A.A., Baquero, E., Ferlin, A., and Gaudin, Y. (2012). Molecular and cellular aspects of rhabdovirus entry. Viruses *4*, 117-139.

Albertini, A.A., Schoehn, G., Weissenhorn, W., and Ruigrok, R.W. (2008). Structural aspects of rabies virus replication. Cellular and molecular life sciences : CMLS *65*, 282-294.

Albertini, A.A., Wernimont, A.K., Muziol, T., Ravelli, R.B., Clapier, C.R., Schoehn, G., Weissenhorn, W., and Ruigrok, R.W. (2006). Crystal structure of the rabies virus nucleoprotein-RNA complex. Science *313*, 360-363.

Antonucci, F., Corradini, I., Fossati, G., Tomasoni, R., Menna, E., and Matteoli, M. (2016). SNAP-25, a Known Presynaptic Protein with Emerging Postsynaptic Functions. Frontiers in synaptic neuroscience *8*, 7.

Astic, L., Saucier, D., Coulon, P., Lafay, F., and Flamand, A. (1993). The CVS strain of rabies virus as transneuronal tracer in the olfactory system of mice. Brain research *619*, 146-156.

Baker, R.W., and Hughson, F.M. (2016). Chaperoning SNARE assembly and disassembly. Nature reviews Molecular cell biology.

Baker, R.W., Jeffrey, P.D., Zick, M., Phillips, B.P., Wickner, W.T., and Hughson, F.M. (2015). A direct role for the Sec1/Munc18-family protein Vps33 as a template for SNARE assembly. Science *349*, 1111-1114.

Banerjee, A.K. (2008). Response to "Non-segmented negative-strand RNA virus RNA synthesis in vivo". Virology *371*, 231-233.

Bauer, A., Nolden, T., Schroter, J., Romer-Oberdorfer, A., Gluska, S., Perlson, E., and Finke, S. (2014). Anterograde glycoprotein-dependent transport of newly generated rabies virus in dorsal root ganglion neurons. Journal of virology *88*, 14172-14183.

Bennett, M.K., Calakos, N., and Scheller, R.H. (1992). Syntaxin: a synaptic protein implicated in docking of synaptic vesicles at presynaptic active zones. Science *257*, 255-259.

Bennett, M.K., Garcia-Arraras, J.E., Elferink, L.A., Peterson, K., Fleming, A.M., Hazuka, C.D., and Scheller, R.H. (1993). The syntaxin family of vesicular transport receptors. Cell *74*, 863-873.

Bibel, M., Richter, J., Lacroix, E., and Barde, Y.A. (2007). Generation of a defined and uniform population of CNS progenitors and neurons from mouse embryonic stem cells. Nature protocols *2*, 1034-1043.

Bibel, M., Richter, J., Schrenk, K., Tucker, K.L., Staiger, V., Korte, M., Goetz, M., and Barde, Y.A. (2004). Differentiation of mouse embryonic stem cells into a defined neuronal lineage. Nature neuroscience *7*, 1003-1009.

Biehl, J.K., and Russell, B. (2009). Introduction to stem cell therapy. The Journal of cardiovascular nursing *24*, 98-103; quiz 104-105.

Bieniasz, P.D. (2006). Late budding domains and host proteins in enveloped virus release. Virology *344*, 55-63.

Binz, T., Sikorra, S., and Mahrhold, S. (2010). Clostridial neurotoxins: mechanism of SNARE cleavage and outlook on potential substrate specificity reengineering. Toxins *2*, 665-682.

Blum, F.C., Przedpelski, A., Tepp, W.H., Johnson, E.A., and Barbieri, J.T. (2014). Entry of a recombinant, full-length, atoxic tetanus neurotoxin into Neuro-2a cells. Infect Immun *82*, 873-881.

Blumberg, B.M., Leppert, M., and Kolakofsky, D. (1981). Interaction of VSV leader RNA and nucleocapsid protein may control VSV genome replication. Cell *23*, 837-845.

Bobby, R., Medini, K., Neudecker, P., Lee, T.V., Brimble, M.A., McDonald, F.J., Lott, J.S., and Dingley, A.J. (2013). Structure and dynamics of human Nedd4-1 WW3 in complex with the alphaENaC PY motif. Biochimica et biophysica acta *1834*, 1632-1641.

Brzozka, K., Finke, S., and Conzelmann, K.K. (2005). Identification of the rabies virus alpha/beta interferon antagonist: phosphoprotein P interferes with phosphorylation of interferon regulatory factor 3. Journal of virology *79*, 7673-7681.

Brzozka, K., Finke, S., and Conzelmann, K.K. (2006). Inhibition of interferon signaling by rabies virus phosphoprotein P: activation-dependent binding of STAT1 and STAT2. Journal of virology *80*, 2675-2683.

Buchholz, U.J., Finke, S., and Conzelmann, K.K. (1999). Generation of bovine respiratory syncytial virus (BRSV) from cDNA: BRSV NS2 is not essential for virus replication in tissue culture, and the human RSV leader region acts as a functional BRSV genome promoter. Journal of virology *73*, 251-259.

Callaway, E.M., and Luo, L. (2015). Monosynaptic Circuit Tracing with Glycoprotein-Deleted Rabies Viruses. The Journal of neuroscience : the official journal of the Society for Neuroscience *35*, 8979-8985.

Ceccaldi, P.E., Gillet, J.P., and Tsiang, H. (1989). Inhibition of the transport of rabies virus in the central nervous system. Journal of neuropathology and experimental neurology *48*, 620-630.

Chen, B.J., and Lamb, R.A. (2008). Mechanisms for enveloped virus budding: can some viruses do without an ESCRT? Virology *372*, 221-232.

Coco, S., Raposo, G., Martinez, S., Fontaine, J.J., Takamori, S., Zahraoui, A., Jahn, R., Matteoli, M., Louvard, D., and Galli, T. (1999). Subcellular localization of tetanus neurotoxin-insensitive vesicle-associated membrane protein (VAMP)/VAMP7 in neuronal cells: evidence for a novel membrane compartment. The Journal of neuroscience : the official journal of the Society for Neuroscience *19*, 9803-9812.

Collins, P.L., Mink, M.A., and Stec, D.S. (1991). Rescue of synthetic analogs of respiratory syncytial virus genomic RNA and effect of truncations and mutations on the expression of a foreign reporter gene. Proceedings of the National Academy of Sciences of the United States of America *88*, 9663-9667.

Conzelmann, K.K., Cox, J.H., Schneider, L.G., and Thiel, H.J. (1990). Molecular cloning and complete nucleotide sequence of the attenuated rabies virus SAD B19. Virology *175*, 485-499.

Conzelmann, M.R.a.K.-K. (2011). Interferon in Rabies Virus Infection, Vol 79 (Elsevier).

Coulon, P., Ternaux, J.P., Flamand, A., and Tuffereau, C. (1998). An avirulent mutant of rabies virus is unable to infect motoneurons in vivo and in vitro. Journal of virology *72*, 273-278.

Curran, J., and Kolakofsky, D. (2008). Nonsegmented negative-strand RNA virus RNA synthesis in vivo. Virology *371*, 227-230.

Daste, F., Galli, T., and Tareste, D. (2015). Structure and function of longin SNAREs. Journal of cell science *128*, 4263-4272.

Davis, B.M., Rall, G.F., and Schnell, M.J. (2015). Everything You Always Wanted to Know About Rabies Virus (But Were Afraid to Ask). Annual review of virology *2*, 451-471.

De, B.P., and Banerjee, A.K. (1993). Rescue of synthetic analogs of genome RNA of human parainfluenza virus type 3. Virology *196*, 344-348.

Dulubova, I., Khvotchev, M., Liu, S., Huryeva, I., Sudhof, T.C., and Rizo, J. (2007). Munc18-1 binds directly to the neuronal SNARE complex. Proceedings of the National Academy of Sciences of the United States of America *104*, 2697-2702.

Etessami, R., Conzelmann, K.K., Fadai-Ghotbi, B., Natelson, B., Tsiang, H., and Ceccaldi, P.E. (2000). Spread and pathogenic characteristics of a G-deficient rabies virus recombinant: an in vitro and in vivo study. The Journal of general virology *81*, 2147-2153.

Fader, C.M., Sanchez, D.G., Mestre, M.B., and Colombo, M.I. (2009). TI-VAMP/VAMP7 and VAMP3/cellubrevin: two v-SNARE proteins involved in specific steps of the autophagy/multivesicular body pathways. Biochimica et biophysica acta *1793*, 1901-1916.

Farias, G.G., Guardia, C.M., Britt, D.J., Guo, X., and Bonifacino, J.S. (2015). Sorting of Dendritic and Axonal Vesicles at the Pre-axonal Exclusion Zone. Cell reports *13*, 1221-1232.

Fasshauer, D., Antonin, W., Margittai, M., Pabst, S., and Jahn, R. (1999). Mixed and non-cognate SNARE complexes. Characterization of assembly and biophysical properties. The Journal of biological chemistry *274*, 15440-15446.

Filippini, F., Rossi, V., Galli, T., Budillon, A., D'Urso, M., and D'Esposito, M. (2001). Longins: a new evolutionary conserved VAMP family sharing a novel SNARE domain. Trends in biochemical sciences *26*, 407-409.

Finke, S., and Conzelmann, K.K. (1997). Ambisense gene expression from recombinant rabies virus: random packaging of positive- and negative-strand ribonucleoprotein complexes into rabies virions. Journal of virology *71*, 7281-7288.

Finke, S., and Conzelmann, K.K. (2003). Dissociation of rabies virus matrix protein functions in regulation of viral RNA synthesis and virus assembly. Journal of virology *77*, 12074-12082.

Finke, S., Mueller-Waldeck, R., and Conzelmann, K.K. (2003). Rabies virus matrix protein regulates the balance of virus transcription and replication. The Journal of general virology *84*, 1613-1621.

Freed, E.O. (2002). Viral late domains. Journal of virology *76*, 4679-4687.

Garcia, I., Huang, L., Ung, K., and Arenkiel, B.R. (2012a). Tracing synaptic connectivity onto embryonic stem cell-derived neurons. Stem Cells *30*, 2140-2151.

Garcia, I., Kim, C., and Arenkiel, B.R. (2012b). Genetic strategies to investigate neuronal circuit properties using stem cell-derived neurons. Frontiers in cellular neuroscience *6*, 59.

Gaudin, Y. (2000). Rabies virus-induced membrane fusion pathway. J Cell Biol *150*, 601-612.

Gaudin, Y., Tuffereau, C., Benmansour, A., and Flamand, A. (1991). Fatty acylation of rabies virus proteins. Virology *184*, 441-444.

Ge, P., Tsao, J., Schein, S., Green, T.J., Luo, M., and Zhou, Z.H. (2010). Cryo-EM model of the bullet-shaped vesicular stomatitis virus. Science *327*, 689-693.

Ghanem, A., and Conzelmann, K.K. (2016). G gene-deficient single-round rabies viruses for neuronal circuit analysis. Virus research *216*, 41-54.

Ghanem, A., Kern, A., and Conzelmann, K.K. (2012). Significantly improved rescue of rabies virus from cDNA plasmids. European journal of cell biology *91*, 10-16.

Gluska, S., Zahavi, E.E., Chein, M., Gradus, T., Bauer, A., Finke, S., and Perlson, E. (2014). Rabies Virus Hijacks and accelerates the p75NTR retrograde axonal transport machinery. PLoS pathogens *10*, e1004348.

Gottlinger, H.G., Dorfman, T., Sodroski, J.G., and Haseltine, W.A. (1991). Effect of mutations affecting the p6 gag protein on human immunodeficiency virus particle release. Proceedings of the National Academy of Sciences of the United States of America *88*, 3195-3199.

Han, Z., Lu, J., Liu, Y., Davis, B., Lee, M.S., Olson, M.A., Ruthel, G., Freedman, B.D., Schnell, M.J., Wrobel, J.E.*, et al.* (2014). Small-molecule probes targeting the viral PPxY-host Nedd4 interface block egress of a broad range of RNA viruses. Journal of virology *88*, 7294-7306.

Hanna, J.H., Saha, K., and Jaenisch, R. (2010). Pluripotency and cellular reprogramming: facts, hypotheses, unresolved issues. Cell *143*, 508-525.

Harris, K.P., Zhang, Y.V., Piccioli, Z.D., Perrimon, N., and Littleton, J.T. (2016). The postsynaptic t-SNARE Syntaxin 4 controls traffic of Neuroligin 1 and Synaptotagmin 4 to regulate retrograde signaling. eLife *5*.

Harty, R.N., Brown, M.E., McGettigan, J.P., Wang, G., Jayakar, H.R., Huibregtse, J.M., Whitt, M.A., and Schnell, M.J. (2001). Rhabdoviruses and the cellular ubiquitin-proteasome system: a budding interaction. Journal of virology *75*, 10623-10629.

Harty, R.N., Paragas, J., Sudol, M., and Palese, P. (1999). A proline-rich motif within the matrix protein of vesicular stomatitis virus and rabies virus interacts with WW domains of cellular proteins: implications for viral budding. Journal of virology *73*, 2921-2929.

Hasan, N., Corbin, D., and Hu, C. (2010). Fusogenic pairings of vesicle-associated membrane proteins (VAMPs) and plasma membrane t-SNAREs--VAMP5 as the exception. PloS one *5*, e14238.

Hemachudha, T., Laothamatas, J., and Rupprecht, C.E. (2002). Human rabies: a disease of complex neuropathogenetic mechanisms and diagnostic challenges. The Lancet Neurology *1*, 101-109.

Henry, P.C., Kanelis, V., O'Brien, M.C., Kim, B., Gautschi, I., Forman-Kay, J., Schild, L., and Rotin, D. (2003). Affinity and specificity of interactions between Nedd4 isoforms and the epithelial Na+ channel. The Journal of biological chemistry *278*, 20019-20028.

Holt, M., Varoqueaux, F., Wiederhold, K., Takamori, S., Urlaub, H., Fasshauer, D., and Jahn, R. (2006). Identification of SNAP-47, a novel Qbc-SNARE with ubiquitous expression. The Journal of biological chemistry *281*, 17076-17083.

Hong, W. (2005). SNAREs and traffic. Biochimica et biophysica acta *1744*, 120-144.

Hong, W., and Lev, S. (2014). Tethering the assembly of SNARE complexes. Trends in cell biology *24*, 35-43.

Hornung, V., Ellegast, J., Kim, S., Brzozka, K., Jung, A., Kato, H., Poeck, H., Akira, S., Conzelmann, K.K., Schlee, M*., et al.* (2006). 5'-Triphosphate RNA is the ligand for RIG-I. Science *314*, 994-997.

Huang, M., Orenstein, J.M., Martin, M.A., and Freed, E.O. (1995). p6Gag is required for particle production from full-length human immunodeficiency virus type 1 molecular clones expressing protease. Journal of virology *69*, 6810-6818.

Hunt, C.A., Schenker, L.J., and Kennedy, M.B. (1996). PSD-95 is associated with the postsynaptic density and not with the presynaptic membrane at forebrain synapses. The Journal of neuroscience : the official journal of the Society for Neuroscience *16*, 1380-1388.

Hurley, J.H. (2015). ESCRTs are everywhere. The EMBO journal *34*, 2398-2407.

Hurley, J.H., and Hanson, P.I. (2010). Membrane budding and scission by the ESCRT machinery: it's all in the neck. Nature reviews Molecular cell biology *11*, 556-566.

Hussain, S., and Davanger, S. (2015). Postsynaptic VAMP/Synaptobrevin Facilitates Differential Vesicle Trafficking of GluA1 and GluA2 AMPA Receptor Subunits. PloS one *10*, e0140868.

Hussain, S., Ringsevjen, H., Egbenya, D.L., Skjervold, T.L., and Davanger, S. (2016). SNARE Protein Syntaxin-1 Colocalizes Closely with NMDA Receptor Subunit NR2B in Postsynaptic Spines in the Hippocampus. Frontiers in molecular neuroscience *9*, 10.

Irie, T., Licata, J.M., McGettigan, J.P., Schnell, M.J., and Harty, R.N. (2004). Budding of PPxY-containing rhabdoviruses is not dependent on host proteins TGS101 and VPS4A. Journal of virology *78*, 2657-2665.

Jackson, A.C. (2013). History of Rabies Research. In: Jackson AC (ed) Rabies: scientific basis of the disease and its managment. In Rabies: Scientific basis of the disease and its managment, A.C. Jackson, ed. (Elsevier).

Jackson, A.C., and Fu, Z.F. (2013). Pathgenesis. In Rabies: Scientific basis of the disease and its managment, A.C. Jackson, ed. (Elsevier).

Jackson, A.C., Ye, H., Phelan, C.C., Ridaura-Sanz, C., Zheng, Q., Li, Z., Wan, X., and Lopez-Corella, E. (1999). Extraneural organ involvement in human rabies. Laboratory investigation; a journal of technical methods and pathology *79*, 945-951.

Jurado, S., Goswami, D., Zhang, Y., Molina, A.J., Sudhof, T.C., and Malenka, R.C. (2013). LTP requires a unique postsynaptic SNARE fusion machinery. Neuron *77*, 542-558.

Kalamida, D., Poulas, K., Avramopoulou, V., Fostieri, E., Lagoumintzis, G., Lazaridis, K., Sideri, A., Zouridakis, M., and Tzartos, S.J. (2007). Muscle and neuronal nicotinic acetylcholine receptors. Structure, function and pathogenicity. The FEBS journal *274*, 3799-3845.

Kelly, R.M., and Strick, P.L. (2000). Rabies as a transneuronal tracer of circuits in the central nervous system. Journal of neuroscience methods *103*, 63-71.

Kennedy, M.J., Davison, I.G., Robinson, C.G., and Ehlers, M.D. (2010). Syntaxin-4 defines a domain for activity-dependent exocytosis in dendritic spines. Cell *141*, 524-535.

Kennedy, M.J., and Ehlers, M.D. (2011). Mechanisms and function of dendritic exocytosis. Neuron *69*, 856-875.

Klingen, Y., Conzelmann, K.K., and Finke, S. (2008). Double-labeled rabies virus: live tracking of enveloped virus transport. Journal of virology *82*, 237-245.

Koyuncu, O.O., Hogue, I.B., and Enquist, L.W. (2013). Virus infections in the nervous system. Cell host & microbe *13*, 379-393.

Lafon, M. (2005). Rabies virus receptors. Journal of neurovirology *11*, 82-87.

Lahaye, X., Vidy, A., Pomier, C., Obiang, L., Harper, F., Gaudin, Y., and Blondel, D. (2009). Functional characterization of Negri bodies (NBs) in rabies virus-infected cells: Evidence that NBs are sites of viral transcription and replication. Journal of virology *83*, 7948-7958.

Lentz, T.L. (1990). Rabies virus binding to an acetylcholine receptor alpha-subunit peptide. Journal of molecular recognition : JMR *3*, 82-88.

Lentz, T.L., Burrage, T.G., Smith, A.L., and Tignor, G.H. (1983). The acetylcholine receptor as a cellular receptor for rabies virus. The Yale journal of biology and medicine *56*, 315-322.

Lentz, T.L., Hawrot, E., and Wilson, P.T. (1987). Synthetic peptides corresponding to sequences of snake venom neurotoxins and rabies virus glycoprotein bind to the nicotinic acetylcholine receptor. Proteins *2*, 298-307.

Lentz, T.L., Wilson, P.T., Hawrot, E., and Speicher, D.W. (1984). Amino acid sequence similarity between rabies virus glycoprotein and snake venom curaremimetic neurotoxins. Science *226*, 847-848.

Lledo, P.M., Zhang, X., Sudhof, T.C., Malenka, R.C., and Nicoll, R.A. (1998). Postsynaptic membrane fusion and long-term potentiation. Science *279*, 399-403.

Lou, X., and Shin, Y.K. (2016). SNARE zippering. Biosci Rep *36*.

Lu, W., Man, H., Ju, W., Trimble, W.S., MacDonald, J.F., and Wang, Y.T. (2001). Activation of synaptic NMDA receptors induces membrane insertion of new AMPA receptors and LTP in cultured hippocampal neurons. Neuron *29*, 243-254.

Manning, S.E., Rupprecht, C.E., Fishbein, D., Hanlon, C.A., Lumlertdacha, B., Guerra, M., Meltzer, M.I., Dhankhar, P., Vaidya, S.A., Jenkins, S.R.*, et al.* (2008). Human rabies prevention--United States, 2008: recommendations of the Advisory Committee on Immunization Practices. MMWR Recommendations and reports : Morbidity and mortality weekly report Recommendations and reports *57*, 1-28.

Marschalek, A., Finke, S., Schwemmle, M., Mayer, D., Heimrich, B., Stitz, L., and Conzelmann, K.K. (2009). Attenuation of rabies virus replication and virulence by picornavirus internal ribosome entry site elements. Journal of virology *83*, 1911-1919.

Martello, G., and Smith, A. (2014). The nature of embryonic stem cells. Annual review of cell and developmental biology *30*, 647-675.

Martinez, A.N., and Philipp, M.T. (2016). Substance P and Antagonists of the Neurokinin-1 Receptor in Neuroinflammation Associated with Infectious and Neurodegenerative Diseases of the Central Nervous System. Journal of neurology & neuromedicine *1*, 29-36.

Mazarakis, N.D., Azzouz, M., Rohll, J.B., Ellard, F.M., Wilkes, F.J., Olsen, A.L., Carter, E.E., Barber, R.D., Baban, D.F., Kingsman, S.M.*, et al.* (2001). Rabies virus glycoprotein pseudotyping of lentiviral vectors enables retrograde axonal transport and access to the nervous system after peripheral delivery. Human molecular genetics *10*, 2109-2121.

Mebatsion, T. (2001). Extensive attenuation of rabies virus by simultaneously modifying the dynein light chain binding site in the P protein and replacing Arg333 in the G protein. Journal of virology *75*, 11496-11502.

Mebatsion, T., and Conzelmann, K.K. (1996). Specific infection of CD4+ target cells by recombinant rabies virus pseudotypes carrying the HIV-1 envelope spike protein. Proceedings of the National Academy of Sciences of the United States of America *93*, 11366-11370.

Mebatsion, T., Konig, M., and Conzelmann, K.K. (1996). Budding of rabies virus particles in the absence of the spike glycoprotein. Cell *84*, 941-951.

Mebatsion, T., Weiland, F., and Conzelmann, K.K. (1999). Matrix protein of rabies virus is responsible for the assembly and budding of bullet-shaped particles and interacts with the transmembrane spike glycoprotein G. Journal of virology *73*, 242-250.

Morimoto, K., Hooper, D.C., Carbaugh, H., Fu, Z.F., Koprowski, H., and Dietzschold, B. (1998). Rabies virus quasispecies: implications for pathogenesis. Proceedings of the National Academy of Sciences of the United States of America *95*, 3152-3156.

Morimoto, K., Hooper, D.C., Spitsin, S., Koprowski, H., and Dietzschold, B. (1999). Pathogenicity of different rabies virus variants inversely correlates with apoptosis and rabies virus glycoprotein expression in infected primary neuron cultures. Journal of virology *73*, 510-518.

Munster-Wandowski, A., Heilmann, H., Bolduan, F., Trimbuch, T., Yanagawa, Y., and Vida, I. (2017). Distinct Localization of SNAP47 Protein in GABAergic and Glutamatergic Neurons in the Mouse and the Rat Hippocampus. Frontiers in neuroanatomy *11*, 56.

Nichols, J., and Smith, A. (2009). Naive and primed pluripotent states. Cell stem cell *4*, 487-492.

Nichols, J., and Smith, A. (2012). Pluripotency in the embryo and in culture. Cold Spring Harbor perspectives in biology *4*, a008128.

Nikolic, J., Le Bars, R., Lama, Z., Scrima, N., Lagaudriere-Gesbert, C., Gaudin, Y., and Blondel, D. (2017). Negri bodies are viral factories with properties of liquid organelles. Nature communications *8*, 58.

Niwa, H., Yamamura, K., and Miyazaki, J. (1991). Efficient selection for high-expression transfectants with a novel eukaryotic vector. Gene *108*, 193-199.

Okumura, A., and Harty, R.N. (2011). Rabies virus assembly and budding. Advances in virus research *79*, 23-32.

Olson, A.L., Knight, J.B., and Pessin, J.E. (1997). Syntaxin 4, VAMP2, and/or VAMP3/cellubrevin are functional target membrane and vesicle SNAP receptors for insulin-stimulated GLUT4 translocation in adipocytes. Molecular and cellular biology *17*, 2425-2435.

Parent, L.J., Bennett, R.P., Craven, R.C., Nelle, T.D., Krishna, N.K., Bowzard, J.B., Wilson, C.B., Puffer, B.A., Montelaro, R.C., and Wills, J.W. (1995). Positionally independent and exchangeable late budding functions of the Rous sarcoma virus and human immunodeficiency virus Gag proteins. Journal of virology *69*, 5455-5460.

Park, J.K., Kim, H.S., Uh, K.J., Choi, K.H., Kim, H.M., Lee, T., Yang, B.C., Kim, H.J., Ka, H.H., Kim, H*., et al.* (2013). Primed pluripotent cell lines derived from various embryonic origins and somatic cells in pig. PloS one *8*, e52481.

Pattnaik, A.K., Ball, L.A., LeGrone, A.W., and Wertz, G.W. (1992). Infectious defective interfering particles of VSV from transcripts of a cDNA clone. Cell *69*, 1011-1020.

Peng, L., Liu, H., Ruan, H., Tepp, W.H., Stoothoff, W.H., Brown, R.H., Johnson, E.A., Yao, W.D., Zhang, S.C., and Dong, M. (2013). Cytotoxicity of botulinum neurotoxins reveals a direct role of syntaxin 1 and SNAP-25 in neuron survival. Nature communications *4*, 1472.

Pfaller, C.K., Cattaneo, R., and Schnell, M.J. (2015). Reverse genetics of Mononegavirales: How they work, new vaccines, and new cancer therapeutics. Virology *479-480*, 331-344.

Pirazzini, M., Rossetto, O., Eleopra, R., and Montecucco, C. (2017). Botulinum Neurotoxins: Biology, Pharmacology, and Toxicology. Pharmacological reviews *69*, 200-235.

Plachta, N., Bibel, M., Tucker, K.L., and Barde, Y.A. (2004). Developmental potential of defined neural progenitors derived from mouse embryonic stem cells. Development (Cambridge, England) *131*, 5449-5456.

Pornillos, O., Higginson, D.S., Stray, K.M., Fisher, R.D., Garrus, J.E., Payne, M., He, G.P., Wang, H.E., Morham, S.G., and Sundquist, W.I. (2003). HIV Gag mimics the Tsg101-recruiting activity of the human Hrs protein. J Cell Biol *162*, 425-434.

Prange, O., Wong, T.P., Gerrow, K., Wang, Y.T., and El-Husseini, A. (2004). A balance between excitatory and inhibitory synapses is controlled by PSD-95 and neuroligin. Proceedings of the National Academy of Sciences of the United States of America *101*, 13915-13920.

Prehaud, C., Coulon, P., LaFay, F., Thiers, C., and Flamand, A. (1988). Antigenic site II of the rabies virus glycoprotein: structure and role in viral virulence. Journal of virology *62*, 1-7.

Prehaud, C., Wolff, N., Terrien, E., Lafage, M., Megret, F., Babault, N., Cordier, F., Tan, G.S., Maitrepierre, E., Menager, P.*, et al.* (2010). Attenuation of rabies virulence: takeover by the cytoplasmic domain of its envelope protein. Science signaling *3*, ra5.

Puffer, B.A., Parent, L.J., Wills, J.W., and Montelaro, R.C. (1997). Equine infectious anemia virus utilizes a YXXL motif within the late assembly domain of the Gag p9 protein. Journal of virology *71*, 6541-6546.

Raingo, J., Khvotchev, M., Liu, P., Darios, F., Li, Y.C., Ramirez, D.M., Adachi, M., Lemieux, P., Toth, K., Davletov, B.*, et al.* (2012). VAMP4 directs synaptic vesicles to a pool that selectively maintains asynchronous neurotransmission. Nature neuroscience *15*, 738-745.

Rathore, S.S., Bend, E.G., Yu, H., Hammarlund, M., Jorgensen, E.M., and Shen, J. (2010). Syntaxin N-terminal peptide motif is an initiation factor for the assembly of the SNARE-Sec1/Munc18 membrane fusion complex. Proceedings of the National Academy of Sciences of the United States of America *107*, 22399-22406.

Raux, H., Flamand, A., and Blondel, D. (2000). Interaction of the rabies virus P protein with the LC8 dynein light chain. Journal of virology *74*, 10212-10216.

Reardon, T.R., Murray, A.J., Turi, G.F., Wirblich, C., Croce, K.R., Schnell, M.J., Jessell, T.M., and Losonczy, A. (2016). Rabies Virus CVS-N2c(DeltaG) Strain Enhances Retrograde Synaptic Transfer and Neuronal Viability. Neuron *89*, 711-724.

Roche, S., and Gaudin, Y. (2004). Evidence that rabies virus forms different kinds of fusion machines with different pH thresholds for fusion. Journal of virology *78*, 8746-8752.

Rohwedel, J., Guan, K., and Wobus, A.M. (1999). Induction of cellular differentiation by retinoic acid in vitro. Cells, tissues, organs *165*, 190-202.

Rungarunlert, S., Techakumphu, M., Pirity, M.K., and Dinnyes, A. (2009). Embryoid body formation from embryonic and induced pluripotent stem cells: Benefits of bioreactors. World journal of stem cells *1*, 11-21.

Rupprecht, C.E., Hanlon, C.A., and Hemachudha, T. (2002). Rabies re-examined. The Lancet Infectious diseases *2*, 327-343.

Schiavo, G., Benfenati, F., Poulain, B., Rossetto, O., Polverino de Laureto, P., DasGupta, B.R., and Montecucco, C. (1992). Tetanus and botulinum-B neurotoxins block neurotransmitter release by proteolytic cleavage of synaptobrevin. Nature *359*, 832-835.

Schiavo, G., Matteoli, M., and Montecucco, C. (2000). Neurotoxins affecting neuroexocytosis. Physiological reviews *80*, 717-766.

Schmidt, O., and Teis, D. (2012). The ESCRT machinery. Current biology : CB *22*, R116-120.

Schmitt, A.P., Leser, G.P., Morita, E., Sundquist, W.I., and Lamb, R.A. (2005). Evidence for a new viral late-domain core sequence, FPIV, necessary for budding of a paramyxovirus. Journal of virology *79*, 2988-2997.

Schnell, M.J., Foley, H.D., Siler, C.A., McGettigan, J.P., Dietzschold, B., and Pomerantz, R.J. (2000). Recombinant rabies virus as potential live-viral vaccines for HIV-1. Proceedings of the National Academy of Sciences of the United States of America *97*, 3544-3549.

Schnell, M.J., Mebatsion, T., and Conzelmann, K.K. (1994). Infectious rabies viruses from cloned cDNA. The EMBO journal *13*, 4195-4203.

Seif, I., Coulon, P., Rollin, P.E., and Flamand, A. (1985). Rabies virulence: effect on pathogenicity and sequence characterization of rabies virus mutations affecting antigenic site III of the glycoprotein. Journal of virology *53*, 926-934.

Sette, P., Jadwin, J.A., Dussupt, V., Bello, N.F., and Bouamr, F. (2010). The ESCRT-associated protein Alix recruits the ubiquitin ligase Nedd4-1 to facilitate HIV-1 release through the LYPXnL L domain motif. Journal of virology *84*, 8181-8192.

Sheng, M., and Kim, E. (2011). The postsynaptic organization of synapses. Cold Spring Harbor perspectives in biology *3*.

Shi, M., Zhang, Y.Z., and Holmes, E.C. (2018). Meta-transcriptomics and the evolutionary biology of RNA viruses. Virus research *243*, 83-90.

Silva, J., Barrandon, O., Nichols, J., Kawaguchi, J., Theunissen, T.W., and Smith, A. (2008). Promotion of reprogramming to ground state pluripotency by signal inhibition. PLoS biology *6*, e253.

Spruston, N. (2008). Pyramidal neurons: dendritic structure and synaptic integration. Nature reviews Neuroscience *9*, 206-221.

Steegmaier, M., Yang, B., Yoo, J.S., Huang, B., Shen, M., Yu, S., Luo, Y., and Scheller, R.H. (1998). Three novel proteins of the syntaxin/SNAP-25 family. The Journal of biological chemistry *273*, 34171-34179.

Stenmark, H., and Olkkonen, V.M. (2001). The Rab GTPase family. Genome biology *2*, Reviews3007.

Strack, B., Calistri, A., Craig, S., Popova, E., and Gottlinger, H.G. (2003). AIP1/ALIX is a binding partner for HIV-1 p6 and EIAV p9 functioning in virus budding. Cell *114*, 689-699.

Sudhof, T.C., and Rizo, J. (2011). Synaptic vesicle exocytosis. Cold Spring Harbor perspectives in biology *3*.

Sudhof, T.C., and Rothman, J.E. (2009). Membrane fusion: grappling with SNARE and SM proteins. Science *323*, 474-477.

Suh, Y.H., Terashima, A., Petralia, R.S., Wenthold, R.J., Isaac, J.T., Roche, K.W., and Roche, P.A. (2010). A neuronal role for SNAP-23 in postsynaptic glutamate receptor trafficking. Nature neuroscience *13*, 338-343.

Superti, F., Derer, M., and Tsiang, H. (1984). Mechanism of rabies virus entry into CER cells. The Journal of general virology *65 (Pt 4)*, 781-789.

Superti, F., Hauttecoeur, B., Morelec, M.J., Goldoni, P., Bizzini, B., and Tsiang, H. (1986). Involvement of gangliosides in rabies virus infection. The Journal of general virology *67 (Pt 1)*, 47-56.

Tan, G.S., Preuss, M.A., Williams, J.C., and Schnell, M.J. (2007). The dynein light chain 8 binding motif of rabies virus phosphoprotein promotes efficient viral transcription. Proceedings of the National Academy of Sciences of the United States of America *104*, 7229-7234.

Taylor, G.M., Hanson, P.I., and Kielian, M. (2007). Ubiquitin depletion and dominant-negative VPS4 inhibit rhabdovirus budding without affecting alphavirus budding. Journal of virology *81*, 13631-13639.

Teng, F.Y., Wang, Y., and Tang, B.L. (2001). The syntaxins. Genome biology *2*, Reviews3012.

Thongcharoen, P., Sureau, P., Wasi, C., Bourhy, H., Chaiprasithikul, P., and Puthavathana, P. (1990). Monoclonal antibody studies of rabies viruses isolated from Thailand. The Southeast Asian journal of tropical medicine and public health *21*, 129-133.

Thoulouze, M.I., Lafage, M., Schachner, M., Hartmann, U., Cremer, H., and Lafon, M. (1998). The neural cell adhesion molecule is a receptor for rabies virus. Journal of virology *72*, 7181-7190.

Tiffany, A.M., Manganas, L.N., Kim, E., Hsueh, Y.P., Sheng, M., and Trimmer, J.S. (2000). PSD-95 and SAP97 exhibit distinct mechanisms for regulating K(+) channel surface expression and clustering. J Cell Biol *148*, 147-158.

Tordo, N., Poch, O., Ermine, A., Keith, G., and Rougeon, F. (1986). Walking along the rabies genome: is the large G-L intergenic region a remnant gene? Proceedings of the National Academy of Sciences of the United States of America *83*, 3914-3918.

Totey, S. (2009). Stem Cells: Basics And Applications (McGraw-Hill Education (India) Pvt Limited).

Tuffereau, C., Benejean, J., Blondel, D., Kieffer, B., and Flamand, A. (1998). Low-affinity nerve-growth factor receptor (P75NTR) can serve as a receptor for rabies virus. The EMBO journal *17*, 7250-7259.

Ugolini, G. (2011). Rabies virus as a transneuronal tracer of neuronal connections. Advances in virus research *79*, 165-202.

Vaidyanathan, V.V., Yoshino, K., Jahnz, M., Dorries, C., Bade, S., Nauenburg, S., Niemann, H., and Binz, T. (1999). Proteolysis of SNAP-25 isoforms by botulinum neurotoxin types A, C, and E: domains and amino acid residues controlling the formation of enzyme-substrate complexes and cleavage. Journal of neurochemistry *72*, 327-337.

van den Bogaart, G., Lang, T., and Jahn, R. (2013). Microdomains of SNARE proteins in the plasma membrane. Current topics in membranes *72*, 193-230.

Van der Jeught, M., O'Leary, T., Ghimire, S., Lierman, S., Duggal, G., Versieren, K., Deforce, D., Chuva de Sousa Lopes, S., Heindryckx, B., and De Sutter, P. (2013). The combination of inhibitors of FGF/MEK/Erk and GSK3beta signaling increases the number of OCT3/4- and NANOG-positive cells in the human inner cell mass, but does not improve stem cell derivation. Stem cells and development *22*, 296-306.

Verderio, C., Rossetto, O., Grumelli, C., Frassoni, C., Montecucco, C., and Matteoli, M. (2006). Entering neurons: botulinum toxins and synaptic vesicle recycling. EMBO reports *7*, 995-999.

Vogel, K., and Roche, P.A. (1999). SNAP-23 and SNAP-25 are palmitoylated in vivo. Biochemical and biophysical research communications *258*, 407-410.

Vos, A., Neubert, A., Aylan, O., Schuster, P., Pommerening, E., Muller, T., and Chivatsi, D.C. (1999). An update on safety studies of SAD B19 rabies virus vaccine in target and non-target species. Epidemiology and infection *123*, 165-175.

Votteler, J., and Sundquist, W.I. (2013). Virus budding and the ESCRT pathway. Cell host & microbe *14*, 232-241.

Vyas, Y., and Montgomery, J.M. (2016). The role of postsynaptic density proteins in neural degeneration and regeneration. Neural Regen Res *11*, 906-907.

Wang, C.C., Shi, H., Guo, K., Ng, C.P., Li, J., Gan, B.Q., Chien Liew, H., Leinonen, J., Rajaniemi, H., Zhou, Z.H.*, et al.* (2007). VAMP8/endobrevin as a general vesicular SNARE for regulated exocytosis of the exocrine system. Molecular biology of the cell *18*, 1056-1063.

Wang, W., Wang, W.H., Azadzoi, K.M., Su, N., Dai, P., Sun, J., Wang, Q., Liang, P., Zhang, W., Lei, X.*, et al.* (2016). Activation of innate antiviral immune response via double-stranded RNA-dependent RLR receptor-mediated necroptosis. Scientific reports *6*, 22550.

Wheeler, A., and Smith, H.S. (2013). Botulinum toxins: mechanisms of action, antinociception and clinical applications. Toxicology *306*, 124-146.

Whelan, S.P. (2008). Response to "Non-segmented negative-strand RNA virus RNA synthesis in vivo". Virology *371*, 234-237.

Whitt, M.A., Buonocore, L., Prehaud, C., and Rose, J.K. (1991). Membrane fusion activity, oligomerization, and assembly of the rabies virus glycoprotein. Virology *185*, 681-688.

Wickersham, I.R., Finke, S., Conzelmann, K.K., and Callaway, E.M. (2007a). Retrograde neuronal tracing with a deletion-mutant rabies virus. Nature methods *4*, 47-49.

Wickersham, I.R., Lyon, D.C., Barnard, R.J., Mori, T., Finke, S., Conzelmann, K.K., Young, J.A., and Callaway, E.M. (2007b). Monosynaptic restriction of transsynaptic tracing from single, genetically targeted neurons. Neuron *53*, 639-647.

Wilkinson, L. (1977). The development of the virus concept as reflected in corpora of studies on individual pathogens. 4. Rabies--Two millennia of ideas and conjecture on the aetiology of a virus disease. Med Hist *21*, 15-31.

Willoughby, R.E., Jr., Tieves, K.S., Hoffman, G.M., Ghanayem, N.S., Amlie-Lefond, C.M., Schwabe, M.J., Chusid, M.J., and Rupprecht, C.E. (2005). Survival after treatment of rabies with induction of coma. The New England journal of medicine *352*, 2508-2514.

Wirblich, C., Tan, G.S., Papaneri, A., Godlewski, P.J., Orenstein, J.M., Harty, R.N., and Schnell, M.J. (2008). PPEY motif within the rabies virus (RV) matrix protein is essential for efficient virion release and RV pathogenicity. Journal of virology *82*, 9730-9738.

Wobus, A.M., and Boheler, K.R. (2005). Embryonic stem cells: prospects for developmental biology and cell therapy. Physiological reviews *85*, 635-678.

Wojczyk, B.S., Takahashi, N., Levy, M.T., Andrews, D.W., Abrams, W.R., Wunner, W.H., and Spitalnik, S.L. (2005). N-glycosylation at one rabies virus glycoprotein sequon influences N-glycan processing at a distant sequon on the same molecule. Glycobiology *15*, 655-666.

Wray, J., Kalkan, T., and Smith, A.G. (2010). The ground state of pluripotency. Biochemical Society transactions *38*, 1027-1032.

Wu, Y.J., Tejero, R., Arancillo, M., Vardar, G., Korotkova, T., Kintscher, M., Schmitz, D., Ponomarenko, A., Tabares, L., and Rosenmund, C. (2015). Syntaxin 1B is important for mouse postnatal survival and proper synaptic function at the mouse neuromuscular junctions. J Neurophysiol *114*, 2404-2417.

Wunner, W.H., and Conzelmann, K.-K. (2013). Rabies Virus. In Rabies: Scientific Basis of the disease and its managment, A.C. Jackson, ed. (Academic Press).

Wunner, W.H., Reagan, K.J., and Koprowski, H. (1984). Characterization of saturable binding sites for rabies virus. Journal of virology *50*, 691-697.

Xiang, Y., Cameron, C.E., Wills, J.W., and Leis, J. (1996). Fine mapping and characterization of the Rous sarcoma virus Pr76gag late assembly domain. Journal of virology *70*, 5695-5700.

Xu, J., Wang, H., Liang, T., Cai, X., Rao, X., Huang, Z., and Sheng, G. (2012). Retinoic acid promotes neural conversion of mouse embryonic stem cells in adherent monoculture. Molecular biology reports *39*, 789-795.

Yang, B., Gonzalez, L., Jr., Prekeris, R., Steegmaier, M., Advani, R.J., and Scheller, R.H. (1999). SNARE interactions are not selective. Implications for membrane fusion specificity. The Journal of biological chemistry *274*, 5649-5653.

Ye, Z., Sun, W., Suryanarayana, K., Justice, P., Robinson, D., and Wagner, R.R. (1994). Membrane-binding domains and cytopathogenesis of the matrix protein of vesicular stomatitis virus. Journal of virology *68*, 7386-7396.

Ying, Q.L., and Smith, A. (2017). The Art of Capturing Pluripotency: Creating the Right Culture. Stem cell reports *8*, 1457-1464.

Ying, Q.L., Wray, J., Nichols, J., Batlle-Morera, L., Doble, B., Woodgett, J., Cohen, P., and Smith, A. (2008). The ground state of embryonic stem cell self-renewal. Nature *453*, 519-523.

Zampieri, N., Jessell, T.M., and Murray, A.J. (2014). Mapping sensory circuits by anterograde transsynaptic transfer of recombinant rabies virus. Neuron *81*, 766-778.

Zeineddine, D., Hammoud, A.A., Mortada, M., and Boeuf, H. (2014). The Oct4 protein: more than a magic stemness marker. Am J Stem Cells *3*, 74-82.

Zhang, Y. (2017). Energetics, kinetics, and pathway of SNARE folding and assembly revealed by optical tweezers. Protein science : a publication of the Protein Society *26*, 1252-1265.